

Spring 10-26-2015

# Dynamic Building-To-Grid Integration Through Combined Building System Resources for Frequency Regulation Service

Peng Zhao

University of Colorado at Boulder, Peng.Zhao@colorado.edu

Follow this and additional works at: [https://scholar.colorado.edu/cven\\_gradetds](https://scholar.colorado.edu/cven_gradetds)



Part of the [Architectural Engineering Commons](#)

---

## Recommended Citation

Zhao, Peng, "Dynamic Building-To-Grid Integration Through Combined Building System Resources for Frequency Regulation Service" (2015). *Civil Engineering Graduate Theses & Dissertations*. 114.

[https://scholar.colorado.edu/cven\\_gradetds/114](https://scholar.colorado.edu/cven_gradetds/114)

This Dissertation is brought to you for free and open access by Civil, Environmental, and Architectural Engineering at CU Scholar. It has been accepted for inclusion in Civil Engineering Graduate Theses & Dissertations by an authorized administrator of CU Scholar. For more information, please contact [cuscholaradmin@colorado.edu](mailto:cuscholaradmin@colorado.edu).

**Dynamic Building-to-Grid Integration through Combined  
Building System Resources for Frequency Regulation  
Service**

by

**Peng Zhao**

B.S., Beijing Jiaotong University, 2008

M.S., Colorado School of Mines, 2010

A thesis submitted to the  
Faculty of the Graduate School of the  
University of Colorado in partial fulfillment  
of the requirements for the degree of  
Doctor of Philosophy

Department of Civil, Environmental, and Architectural Engineering

2014

This thesis entitled:  
Dynamic Building-to-Grid Integration through Combined Building System Resources for  
Frequency Regulation Service  
written by Peng Zhao  
has been approved for the Department of Civil, Environmental, and Architectural Engineering

---

Gregor P. Henze, Ph.D., P.E.

---

Frank S. Barnes, Ph.D.

---

Michael J. Brandemuehl, Ph.D., P.E.

---

Clemens Felsmann, Ph.D.

---

John Zhai, Ph.D.

Date \_\_\_\_\_

The final copy of this thesis has been examined by the signatories, and we find that both the content and the form meet acceptable presentation standards of scholarly work in the above mentioned discipline.

Zhao, Peng (Ph.D., Department of Civil, Environmental, and Architectural Engineering)

Dynamic Building-to-Grid Integration through Combined Building System Resources for Frequency  
Regulation Service

Thesis directed by Prof. Gregor P. Henze, Ph.D., P.E.

Frequency regulation (FR) is the electric grid service responsible for maintaining the system frequency at its nominal value of 60 Hz in the United States — an indicator of energy balance on the grid. In cases of mismatch between power supply and demand, frequency regulation resources either on the generation or the demand side, responding rapidly to restore system frequency to its nominal value. Due to the limited responsiveness of electric generators, fast and accurate demand side resources (DSR) have recently been encouraged to participate in frequency regulation. The tested DSR's include flywheels and battery banks. However, high initial equipment investment is typically required for these projects. Large commercial buildings dominating many urban cores have been shown to provide effective load shaping with little or no impact on occupants' comfort. This allows FR participation by manipulating the operation of heating, ventilating and air-conditioning (HVAC) systems. Commercial buildings are characterized by numerous interdependent HVAC subsystems and their controls. Therefore, a high-level supervisory control strategy is developed to take advantage of interactions between HVAC subsystems for FR with buildings' available capacity. This dynamically integrates building operations into grid operations (i.e., the ancillary services market) so that both parties know each other's capacities and constraints ahead of time. Unlike traditional demand response (DR) programs that engage only sporadically during times of grid stress, dynamic building-to-grid integration automatically and continuously provides solutions from the demand side maintaining energy balance on the grid. The benefit is expected to go beyond any current demand response programs.

## Dedication

To my grandparents, parents and my wife.

## Acknowledgements

It is my great pleasure to thank all who have helped and inspired me during my studies at the building systems program for my Ph.D. degree. In particular, I would like to thank my advisor, Dr. Gregor P. Henze for his patience and guidance during the completion of this work. His enthusiasm for research always motivate me to work harder on my research work. In addition, I would like to specifically thank Mr. Vincent J. Cushing, Jr. and Mr. Sandro Plamp of QCoefficient, Inc. for their encouragement, inspiration and guidance. I am grateful to Dr. Michael J. Brandemuehl for consistently offering advice. In the end, I greatly appreciate my fellow students Gregory Pavlak, Ryan Tanner and Saleh Al-Saadi for their technical discussions and friendship during my studies of the last a few years.

## Contents

| <b>Chapter</b> |   |           |
|----------------|---|-----------|
| <b>1</b>       | <b>Introduction</b>                                       | <b>1</b>  |
| 1.1            | Energy Balance of the Electric Power System . . . . .     | 1         |
| 1.2            | Frequency Regulation Resources . . . . .                  | 5         |
| 1.3            | The Need of Incorporating Demand Side Resources . . . . . | 7         |
| 1.4            | Dynamic Building-to-Grid Integration . . . . .            | 9         |
| 1.5            | Research Questions and Objectives . . . . .               | 10        |
| 1.6            | Scope . . . . .   | 12        |
| 1.7            | Organization of the Dissertation . . . . .                | 13        |
| <b>2</b>       | <b>Literature Review</b>                                  | <b>14</b> |
| 2.1            | Background Information of Frequency Control . . . . .     | 15        |
| 2.2            | Overview of FR Market within the PJM Territory . . . . .  | 16        |
| 2.2.1          | Traditional and Dynamic FR Signals . . . . .              | 17        |
| 2.2.2          | Requirements for Eligibility in PJM's FR Market . . . . . | 19        |
| 2.2.3          | FR Data Transfer . . . . .                                | 20        |
| 2.2.4          | Performance Score Calculation . . . . .                   | 22        |
| 2.2.5          | Regulation Market Clearing Process . . . . .              | 23        |
| 2.2.6          | Settlement . . . . .                                      | 26        |
| 2.3            | Recent Field Tests Work . . . . .                         | 28        |

|          |   |    |
|----------|---|----|
| <b>3</b> | Modeling of A Commercial Building HVAC Systems and Low-Level Controls                       | 29 |
| 3.1      | Five-Zone Model . . . . .   | 29 |
| 3.2      | Airside System . . . . .  | 33 |
| 3.2.1    | Pressure-Dependent Airside System . . . . .   | 34 |
| 3.2.2    | Pressure-Independent Airside System . . . . .   | 41 |
| 3.2.3    | Economizer . . . . .  | 45 |
| 3.3      | Waterside System . . . . .  | 47 |
| 3.3.1    | Chilled Water Loop Storage . . . . .  | 47 |
| 3.3.2    | Chiller Sequencing . . . . .  | 48 |
| 3.4      | Power-Consuming Subsystems . . . . .  | 50 |
| 3.4.1    | Fan System Power Consumption . . . . .  | 50 |
| 3.4.2    | Chilled Water Loop Power Consumption . . . . .  | 53 |
| 3.5      | Model Validation . . . . .  | 54 |
| <b>4</b> | Frequency Regulation Through Supervisory Control  | 57 |
| 4.1      | FR Signal Injection Methods . . . . .   | 57 |
| 4.2      | Supervisory Control Method . . . . .  | 59 |
| <b>5</b> | Results   | 66 |
| 5.1      | Case Study 1: Single Injection Results . . . . .  | 68 |
| 5.1.1    | $P_{\text{static}}$ Setpoint Injection . . . . .  | 70 |
| 5.1.2    | $T_{\text{zone}}$ Setpoint Injection . . . . .  | 71 |
| 5.1.3    | $T_{\text{DA}}$ Setpoint Injection . . . . .  | 74 |
| 5.1.4    | OAF Superposition . . . . .   | 81 |
| 5.2      | Summary of Single Injections . . . . .  | 83 |
| 5.3      | Case Study 2: Multiple Injection Results . . . . .  | 83 |
| 5.3.1    | Two Methods Combined: $P_{\text{static}}$ Setpoint and $T_{\text{zone}}$ Setpoint . . . . . | 86 |
| 5.3.2    | Two Methods Combined: $P_{\text{static}}$ Setpoint and $T_{\text{DA}}$ Setpoint . . . . .   | 87 |

|          |  |            |
|----------|--|------------|
| 5.3.3    | Two Methods Combined: $P_{\text{static}}$ Setpoint and OAF . . . . .                               | 90         |
| 5.3.4    | Three Methods Combined: $P_{\text{static}}$ Setpoint, $T_{\text{zone}}$ Setpoint and OAF . . . . . | 93         |
| 5.3.5    | Three Methods Combined: $P_{\text{static}}$ Setpoint, $T_{\text{DA}}$ Setpoint and OAF . . . . .   | 96         |
| 5.3.6    | All Four Methods Combined . . . . .  | 97         |
| 5.4      | Summary of Multiple Injections . . . . .   | 99         |
| <b>6</b> | <b>Conclusions and Future Work</b>   | <b>102</b> |
| 6.1      | Summary of Results and Contributions . . . . .   | 103        |
| 6.2      | Limitations of Current Methods . . . . .   | 108        |
| 6.3      | Future Work . . . . .  | 110        |
| 6.3.1    | Future Work Pertains to this Particular Research . . . . .   | 111        |
| 6.3.2    | Exploration of the Broader Impact to the Electric Power System . . . . .                           | 116        |
|          | <b>Bibliography</b>  | <b>118</b> |
|          | <b>Appendix</b>  |            |
| <b>A</b> | Results of $P_{\text{static}}$ Setpoint Injection  | 123        |
| <b>B</b> | Results of $T_{\text{zone}}$ Setpoint Injection  | 127        |
| <b>C</b> | Results of $T_{\text{DA}}$ Setpoint Injection  | 131        |
| <b>D</b> | Results of OAF Setpoint Superposition  | 135        |
| <b>E</b> | Results of Combined Injection: $P_{\text{static}}$ Setpoint and $T_{\text{zone}}$ Setpoint         | 139        |
| <b>F</b> | Results of Combined Injection: $P_{\text{static}}$ Setpoint and $T_{\text{DA}}$ Setpoint           | 143        |
| <b>G</b> | Results of Combined Injection: $P_{\text{static}}$ Setpoint and OAF                                | 147        |

|  |     |
|--|-----|
| <b>H</b> Results of Combined Injection: $P_{\text{static}}$ Setpoint, $T_{\text{DA}}$ Setpoint and OAF | 151 |
| <b>I</b> Results of Combined Injection: All Four Methods Combined                                      | 155 |

## Tables

### Table

|     |   |    |
|-----|---|----|
| 3.1 | Parameters of duct system design . . . . .  | 43 |
| 5.1 | Summary of $P_{\text{static}}$ setpoint injection . . . . .   | 70 |
| 5.2 | Summary of $T_{\text{zone}}$ setpoint injection . . . . .   | 73 |
| 5.3 | Summary of $T_{\text{DA}}$ setpoint injection . . . . .   | 77 |
| 5.4 | Summary of OAF superposition . . . . .  | 80 |
| 5.5 | Summary of two methods combined: $P_{\text{static}}$ setpoint and $T_{\text{zone}}$ setpoint . . . . .    | 86 |
| 5.6 | Summary of two methods combined: $P_{\text{static}}$ setpoint and $T_{\text{DA}}$ setpoint . . . . .      | 89 |
| 5.7 | Summary of two methods combined: $P_{\text{static}}$ setpoint and OAF . . . . .                           | 92 |
| 5.8 | Summary of three methods combined: $P_{\text{static}}$ setpoint, $T_{\text{zone}}$ setpoint and OAF . . . | 95 |
| 5.9 | Summary of three methods combined: $P_{\text{static}}$ setpoint, $T_{\text{DA}}$ Setpoint and OAF . . .   | 96 |

## Figures

### Figure

|     |  |    |
|-----|--|----|
| 1.1 | North American balancing authorities and regions . . . . .   | 2  |
| 1.2 | Importance of maintaining system frequency at its nominal value . . . . .  | 3  |
| 1.3 | Energy price equilibrate at a lower price with the introduction of demand elasticity<br>from demand side resources . . . . . | 8  |
| 2.1 | Regulation data transfer process of PJM . . . . .  | 21 |
| 2.2 | FR market clearing process in PJM . . . . .  | 25 |
| 2.3 | RMCCP distribution of summer weekdays in 2013 . . . . .  | 27 |
| 2.4 | RMPCP distribution of summer weekdays in 2013 . . . . .  | 27 |
| 3.1 | Commercial building HVAC system and its low-level controls . . . . .   | 30 |
| 3.2 | 3R2C model representation of heat transfer through opaque multilayer construction<br>element . . . . .                       | 31 |
| 3.3 | Block diagram of the pressure-dependent airside system . . . . .   | 35 |
| 3.4 | Fan performance curve for demonstrating the impacts of varying the static pressure<br>setpoint . . . . .                     | 37 |
| 3.5 | Pressure-dependent airside system with two zones . . . . .   | 38 |
| 3.6 | VAV system with N branches . . . . .   | 39 |
| 3.7 | Pressure-independent airside system with two zones . . . . .   | 41 |
| 3.8 | Duct system design based on the 5-zone geometry . . . . .  | 42 |

|      |  |    |
|------|--|----|
| 3.9  | Static pressure balance of the duct system . . . . .   | 44 |
| 3.10 | Open-loop outside air damper control strategy . . . . .  | 46 |
| 3.11 | Waterside system with chilled water storage . . . . .  | 47 |
| 3.12 | Sequencing of two chillers . . . . .   | 49 |
| 3.13 | Variable frequency drive topology of the open-loop V/Hz control . . . . .                                    | 51 |
| 3.14 | Supply fan motor power map . . . . .   | 52 |
| 3.15 | Validation of the baseline simulation results against the EnergyPlus Surrogate . . . . .                     | 55 |
| 4.1  | Supervisory control for single and multiple setpoints of FR injection . . . . .                              | 61 |
| 4.2  | Comparison of online and offline model-based controls . . . . .  | 64 |
| 5.1  | Outside dry-bulb temperature, baseline zone setpoint and FR prices of July 10 <sup>th</sup> , 2013 . . . . . | 66 |
| 5.2  | Hourly composite performance scores of the single injection methods . . . . .                                | 69 |
| 5.3  | Hourly frequency regulation capacities of the single injection methods . . . . .                             | 69 |
| 5.4  | Hourly revenue of the single injection methods . . . . .   | 69 |
| 5.5  | Performance score of $P_{\text{static}}$ setpoint injection of a selected hour . . . . .                     | 71 |
| 5.6  | System dynamics of HVAC components of $P_{\text{static}}$ setpoint injection . . . . .                       | 72 |
| 5.7  | Terminal damper positions of $P_{\text{static}}$ setpoint injection . . . . .                                | 72 |
| 5.8  | Air properties along the duct system of $P_{\text{static}}$ setpoint injection . . . . .                     | 73 |
| 5.9  | Performance score of $T_{\text{zone}}$ setpoint injection of a selected hour . . . . .                       | 75 |
| 5.10 | System dynamics of HVAC components of $T_{\text{zone}}$ setpoint injection of a selected hour . . . . .      | 75 |
| 5.11 | Performance score of $T_{\text{zone}}$ setpoint injection of a selected hour . . . . .                       | 76 |
| 5.12 | Terminal damper positions of $T_{\text{zone}}$ setpoint injection of a selected hour . . . . .               | 76 |
| 5.13 | Performance score of $T_{\text{DA}}$ setpoint injection of a selected hour . . . . .                         | 78 |
| 5.14 | System dynamics of HVAC components of $T_{\text{DA}}$ setpoint injection . . . . .                           | 79 |
| 5.15 | Air properties along the duct system of $T_{\text{DA}}$ setpoint injection . . . . .                         | 79 |
| 5.16 | Performance score of OAF superposition of a selected hour . . . . .  | 81 |
| 5.17 | System dynamics of HVAC components of OAF superposition . . . . .  | 82 |

|      |   |     |
|------|---|-----|
| 5.18 | Air properties along the duct system of OAF superposition . . . . .   | 82  |
| 5.19 | Hourly composite performance scores of the multiple injection methods . . . . .   | 84  |
| 5.20 | Hourly frequency regulation capacities of the multiple injection methods . . . . .  | 85  |
| 5.21 | Hourly composite performance scores of the multiple injection methods . . . . .   | 85  |
| 5.22 | Performance score of $P_{\text{static}}$ setpoint and $T_{\text{zone}}$ setpoint injection . . . . .                              | 87  |
| 5.23 | System dynamics of $P_{\text{static}}$ setpoint and $T_{\text{zone}}$ setpoint injection . . . . .                                | 88  |
| 5.24 | Terminal damper positions of $P_{\text{static}}$ setpoint and $T_{\text{zone}}$ setpoint injection . . . . .                      | 88  |
| 5.25 | Performance score of $P_{\text{static}}$ setpoint and $T_{\text{DA}}$ setpoint injection . . . . .                                | 90  |
| 5.26 | System dynamics of $P_{\text{static}}$ setpoint and $T_{\text{DA}}$ setpoint injection . . . . .                                  | 91  |
| 5.27 | Terminal damper positions of $P_{\text{static}}$ setpoint and $T_{\text{DA}}$ setpoint injection . . . . .                        | 91  |
| 5.28 | Air properties of $P_{\text{static}}$ setpoint and $T_{\text{DA}}$ setpoint injection . . . . .                                   | 92  |
| 5.29 | Performance score of $P_{\text{static}}$ setpoint injection and OAF superposition . . . . .                                       | 94  |
| 5.30 | System dynamics of $P_{\text{static}}$ setpoint injection and OAF superposition . . . . .   | 94  |
| 5.31 | Air properties of $P_{\text{static}}$ setpoint injection and OAF superposition . . . . .  | 95  |
| 5.32 | Air properties of $P_{\text{static}}$ setpoint injection and OAF superposition . . . . .  | 98  |
| 5.33 | The participation levels of two selected methods of their single injections and in their<br>multiple injection packages . . . . . | 100 |
| 6.1  | Two-step approach of training forward prediction model . . . . .  | 112 |
| 6.2  | Possible FR capacity calculated by the current method and the proposed method . .   | 114 |

# Chapter 1

## Introduction

### 1.1 Energy Balance of the Electric Power System

Electricity supply is provided by many sources of diverse technologies in order to track the aggregated load profile throughout the day. In the absence of effective grid-scale storage, electricity must be generated, distributed and consumed in real time. This poses a challenging task for the grid operators to dispatch vast amounts of power from various sources to meet the substantial variations from load valleys to load peaks on any day. In addition, renewable energy sources (RES), such as wind and solar, are increasingly introduced to the grid. These sources are intermittent, variable and introduce more volatility to grid operations at higher levels of penetration [9, 68]. Aside from balancing generation and load through economic dispatch on an hour-to-hour basis, grid operators also face small-scale levels of mismatch of generation and load that require short-term reserves called frequency regulation (FR) resources on second-to-second basis. In order to allocate appropriate amounts of generating resources for the demand, the independent system operators (ISO) and regional transmission organizations (RTO) make day-ahead predictions for the planned load of the next day. However, there are always deviations between the planned and the actual load. In addition, the slow response, inaccurate automatic generation control (AGC) and forced outages of power plants all could result in fluctuations on the system [50]. Therefore, FR resources are needed to track those small-scale demand variations and correct unintended fluctuations of supply in order to maintain the energy balance on the grid [49].

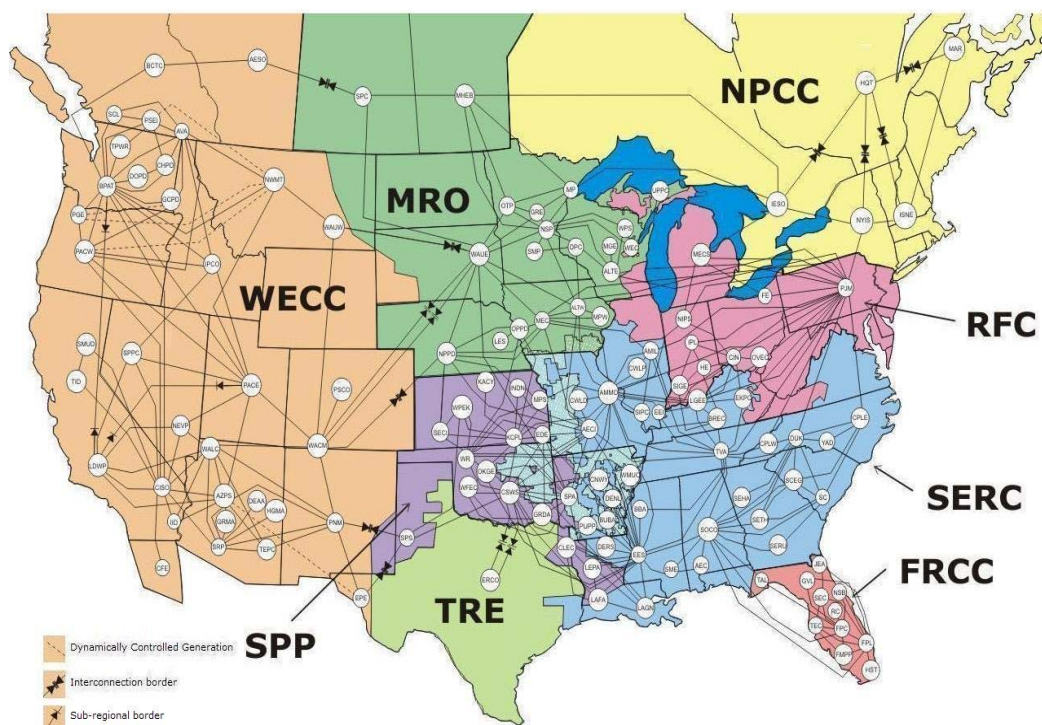


Figure 1.1: North American balancing authorities and regions [18]

The balance of supply and demand is handled by over 100 balancing authorities in the North America in measuring system frequency [18]. These balancing authorities are connected through tie-lines and are overseen by reliability coordinators [18]. The supply can be generated by generators and also be imported from the neighboring interconnected areas; whereas, the demand can be consumed in loads, losses on transmission lines and be exported to the neighboring interconnected areas [18, 37]. If the demand is greater than the supply, the frequency drops below the nominal value (i.e., 60 Hz in the U.S.); if the demand is less than the supply, the frequency rises above the target value [18]. The frequency rate of change is determined by the inertia of all generators and rotating loads on the grid [18]. Referring to Figure. 1.1, the Pennsylvania-New Jersey-Maryland (PJM) Interconnection serves not only the regional transmission organization (RTO) but also the balancing authority for its territory.

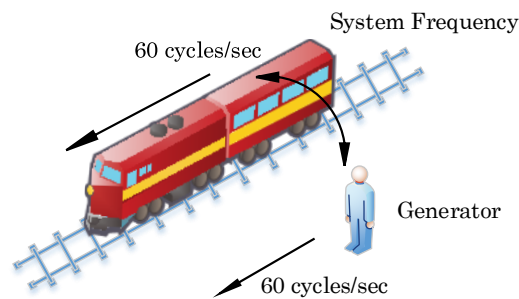


Figure 1.2: Importance of maintaining system frequency at its nominal value

Maintaining system frequency at its nominal value is crucial for power system reliability. Off-nominal frequency could damage equipments along the entire electric power supply chain, degrade the power quality delivered to end customers, impact energy market efficiency and the worst case would result in collapse of the power system [50]. The importance of maintaining system frequency can be illustrated by the example depicted in Figure. 1.2. Assuming a train called System Frequency is operated at constant speed of 60 cycles/second moving forward. The person called Generator needs to get onto the train but the train won't stop for him; so he has to run at the same speed, 60 cycles/second, in order to get onto the train. As long as Mr. Generator is running at 60

cycles/second, he could get on or off the train when he is asked to. Assume the system frequency was operated slower than its nominal speed for some unexpected reasons, it would not only be difficult for offline generators to go back online but could also trigger online generators' protective actions [50]. The under-frequency protection could trip the generator to avoid its speed close to the natural frequency of any of the turbine blades [21]. In such situations, the imbalance of generation and load is exacerbated and could lead to system collapse [50]. Thus, balancing supply and demand from both sides is the most effective way for maintaining the reliable power system operation.

FR is the ancillary service that provides continuous, rapid, and automatic corrections for frequency control on a second-to-second basis [49]. Typically, FR uses certain amount of generators (e.g., about 1% of total generation) equipped with AGC and the information gathered through the supervisory control and data acquisition (SCADA) system to continuously track the demand variations [18, 37]. However, when the frequency deviation is out of the controllable range of FR, system operators may also manually change the setpoint of all generation units synchronized on the grid for balancing the demand [37]. The frequency must be strictly maintained within a very narrow range in order to comply with the control performance standards (CPS) and the balancing authority area control error Limit (BAAL) reliability criteria [32]. A real-time value, area control error (ACE), is used to quantify the energy balance at each moment [18, 37]. Area control error is measured in MW and is calculated by the mismatch between the actual and scheduled power interchange between the neighboring interconnected areas along with the frequency bias caused by generators governor control and the reactive load response [37]. The balancing authorities must monitor and carefully control area control error in a limited range in order to fulfill their obligations to the North American Electric Reliability Corporation (NERC) for system reliability [46, 37]. Therefore, FR fine-tunes area control error and is the most important ancillary service for maintaining energy balance [37].

## 1.2 Frequency Regulation Resources

FR is a “zero electric energy” service because of the symmetrical responses towards positive and negative directions; thus, the long-term integral value of a FR resource’s electric power output is zero. Nonetheless, it does require significant amounts of fossil fuel input if provided by generators. Traditionally, FR is supplied by directing dedicated generators in response to a signal derived from area control error [37]. Research estimated that integrating renewable energy resources at the current pace would exceed both ramping rate and capacity of traditional FR resources can compensate [53, 55]. Thus, demand side resource (DSR) participation presents an attractive avenue for energy efficiency improvement in balancing generation and load. A recent report found that an ideal FR resource (i.e., unlimited capacity and instant response) can be two times more efficient than traditional slow-ramping resources in general [56]. Thus, fast-ramping demand side resources are encouraged to participate in FR [15, 39]. In recent years, three types of demand side resources have emerged that increasingly participate in the FR service [78]. 1) Grid-scale storage, such as flywheels, batteries, compressed-air energy storage (CAES) and pumped-hydro; these resources do not generate electricity as generators do but can draw and store electricity from the grid and then release it when needed [73, 51, 3]. 2) Heating systems, such as electric boilers and resistance heaters; these resources vary the heater electric consumption (i.e., adjusting the heating capacity) in response to the FR signal [75]. 3) Independent systems with variable frequency drives (VFD), such as wastewater treatment pumps and supply fans in air-handling units (AHU); these resources vary the motor electric consumption (i.e., adjusting the motor rotating speed) in response to the FR signal [52, 24]. These three types of resources typically have smaller capacity than generators but can ramp much faster and respond to the FR signal more accurately and thereby offer better performance. In October 2011, the U.S. Federal Electric Regulatory Commission (FERC) issued the final rule of Order 755, which directs the independent system operators (ISO) and regional transmission organizations (RTO) to evaluate and compensate FR services provided based on resources’ actual performance instead of their expected FR capacity [15]. PJM launched their

performance-based regulation (PBR) rule in October 2012 in response to FERC order No. 755. This rule compensates FR resources based on two parts of offers, capacity and performance, that are market-based and derived from bidding offers with uniform clearing price [39, 41]. In July 2013, FERC launched Order No. 784 [16]. This rule further expands upon Order 755 and emphasizes the accuracy and speed of FR resources [16].

Large commercial office buildings are equipped with flexible, often thermostatically controlled loads (e.g., air-conditioning systems, heating systems and water heaters), VFD-controlled motor loads (e.g., supply fan, return fan and chillers) and lighting loads. These loads are able to adjust their power consumption along with the dynamic FR signal thus provide commercial buildings the potential to participate in FR [78, 24, 13]. In addition, the thermal mass inherent in commercial buildings, such as concrete, insulation, drywall, carpet and furniture can be used to manipulate heating and cooling loads. Utilizing thermal mass for load shifting and cost reduction has been successfully implemented in commercial buildings in the summer season and is known as building thermal mass control or pre-cooling [62]. This has shown significant effect on peak load and cost reduction [10, 70, 62]. Typically, a supervisory optimal controller is needed to properly harness the thermal mass storage for maximum benefit such as cost savings [12, 30, 17]. A recent study proposed a model predictive control (MPC) framework to determine the optimal operating strategy considering energy cost, peak demand and FR revenue through simulations based on PJM's rules and pricing data [67].

As building thermal mass has demonstrated to be effective grid-scale storage, we argue that commercial building HVAC systems can provide FR similar to other prevailing storage devices such as batteries and flywheels while maintaining occupants' comfort. However, the question arises whether a commercial building is ramp-limited or a capacity-limited resource? According to PJM's performance-based regulation rule, the signal RegA is designed for ramp-limited resources that are typically rich in FR capacity but ramp slowly [40]. In contrast, signal RegD is designed for capacity-limited resources that feature typically less available capacity but ramp quickly [40]. Therefore, the question can be paraphrased as: "Are commercial building HVAC systems a RegA-following or

a RegD-following resource?” The answer is both, depending on the number of buildings controlled for FR. If a single building is utilized for FR, it should be a RegD-following resource because of the well-tuned control systems and the smaller moment of inertia of VFD-controlled motors. In addition, following RegA signal potentially requires maintaining FR at a high level in a single direction (either regulation up or down) for an extended time; this may exhaust the thermal storage and impact occupants’ comfort. However, if bundling buildings with different but complementary HVAC components and differing performance characteristics into a portfolio, the magnitude and performance of the FR service may be improved by taking advantage of the temporal diversity of capacity limits and part load ratios. Under such situation, a relatively constant FR capacity can be committed over the course of the day. Therefore, a building portfolio should follow the RegA signal and paid mostly for its near constant FR capacity. This research does not model portfolios and only focuses on RegD-following capability of a single building. The purpose is to provide readers insights as to how FR signals can be used in different scenarios and the usefulness of commercial buildings for FR.

### **1.3 The Need of Incorporating Demand Side Resources**

The aggregated load profile consists of three components in the stack: base load, intermediate load and peak load. Base load is satisfied by generation units with higher capital cost but lower operating cost (e.g., nuclear, hydro and coal-fired steam power plants) [74]. Conversely, peak load is satisfied by generation units with lower capital cost but higher operating cost (e.g., gas turbines and diesel generators) [74]. Generation units with variable costs that fall in between are employed to serve the intermediate load [74]. Although peak load generation units are not frequently used, the capacity is required to satisfy demand at all times [10]. Thus, outdated, inefficient and usually expensive generation units are adopted for the peak load since they are only needed for couple hours per year [10]. However, utilities and power plants are penalized for their emissions and these penalties are passed down to consumers in rates costing millions of dollars each year [74]. In addition, demand spikes cause transmission congestions because of either physical limitations of

transmission lines or the grid reliability requirements [64]. Though the wholesale energy market seeks to buy from the least expensive resources available, transmission congestion limits the amount of power to be delivered to areas where demand is high and renders power purchase from expensive resources more often [64]. This not only results in high prices for consumers but also impacts grid reliability and makes the area more vulnerable to unexpected outages of generators and transmission lines [64].

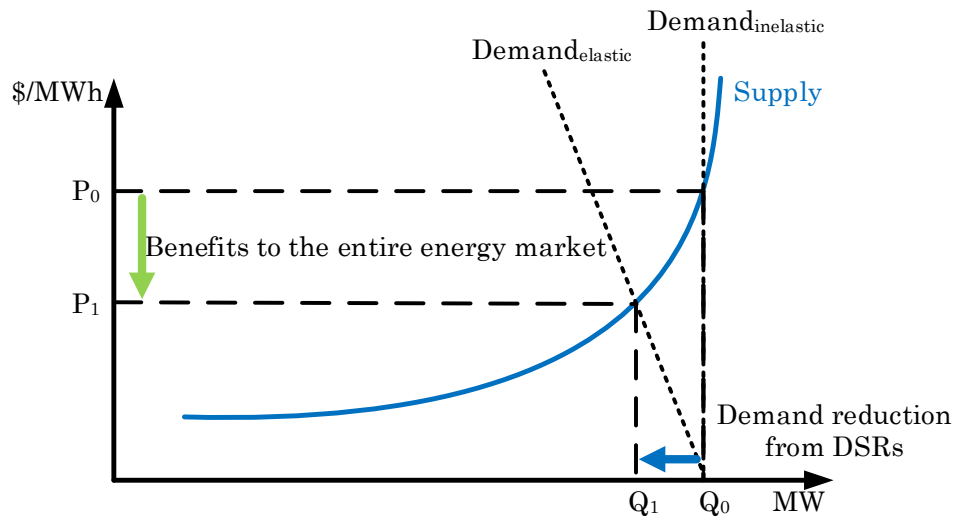


Figure 1.3: Energy price equilibrate at a lower price with the introduction of demand elasticity from demand side resources [47]

Therefore, the most effective solution is to introduce demand elasticity to reduce peak demand and thus reduce prices and price volatility. This is typically done through demand response (DR) programs that requires end-users to shed their load in response to the changes in the price of electricity [2]. Demand response programs are typically classified into two groups: 1) incentive-based programs and 2) price-based programs [2]. The end-users shift or shed their loads in responding to the dynamic pricing rates or for the financial incentives [2]. The goals of demand response programs include flattened demand curves, alleviated congestions, reduced price volatility, improved reliability through diversified resources, reduced cost for consumers and higher market efficiency [2, 47]. The introduction of demand elasticity through incorporation of small group of demand side

resources allow the energy supply and demand to equilibrate at a lower price in avoiding the steepest section of the supply curve (shown in Figure. 1.3 that generation cost curve increase exponentially when generation capacity is near its maximum) thus benefits the entire market [47].

In addition to the energy market stated above, demand side resources are also important for the FR market. Traditional FR resources (i.e., generators) are typically rich in capacity but ramp slowly. In contrast, dynamic FR resources (i.e., mostly are demand side resources) feature less capacity but ramp quickly. Both of these two types of resources are valuable for maintaining the grid reliability [15]. Thus, PJM's performance-based regulation rule established a two-part payment system that awards both capacity (i.e., reservation of power for FR) and performance (i.e., movement of power for FR) in incenting more dynamic resources to participate [39]. Meanwhile, it also retains the traditional resources in the market to reach the proper balance [39]. The result of incorporating dynamic demand side resources has already shown significant benefits after performance-based regulation rule's operation during the first year [22]. System reliability was improved as measured by improved control performance standards (CPS) and balancing authority area control error Limit (BAAL) scores with FR requirement kept constant [22]. Thus, it was suggested that FR requirements be lowered in order to determine the impact to system reliability by allocating less FR resources [22]. PJM lowered the requirement from 1% of total generation to 0.7% in 2013 (total generation in PJM is approximated from 80,000 MW valley load to 140,000 MW peak load) [22, 37]. In spite of this significant change in FR requirements, CPS and BAAL scores remained high and even increased in summer months with the introduction of about 490 MW of dynamic FR resources (i.e., batteries and flywheels) [22]. Thus, incorporating dynamic demand side resources proved to increase the energy efficiency on the entire power system.

#### **1.4 Dynamic Building-to-Grid Integration**

Buildings as the largest load on the grid have significant potential for participating as demand side resources. Typically, commercial buildings participate through demand response programs that shed loads during critical periods and receive financial incentives for the amount of load shed or

for simply being available. However, building managers usually found lack of transparency to the energy markets for energy cost and benefits analysis [10]. Energy consumption rebounds are typically found right after demand response events so that demand response programs are about load shifting and short-term shedding but not about energy efficiency or energy saving [58][57]. In addition, the rebound creates a new peak demand that is problematic for the energy balance and impacts grid reliability. Thus, traditional demand response programs have not met the expectations stated in section 1.3. Since traditional demand response programs are only focused on peak periods in the energy market, the emerging demand response programs aim at continuously integrating end-users in ancillary services markets during both peak and off-peak hours [57].

Dynamic building-to-grid integration seamlessly integrates building operations into grid operations so that both parties know each other's capacities and constraints ahead of time. Thus, building operation could be adjusted through model predictive control (MPC) algorithms for the optimum operation strategy. On the other hand, grid operators would make more accurate predictions of the planned load and work collaboratively with demand side resources to avoid peak demand. Unlike traditional demand response programs that engage only sporadically during times of grid stress, dynamic building-to-grid integration automatically and continuously provides solutions from the demand side maintaining energy balance on the grid. It systematically integrates the available capacity of building HVAC systems, the thermal mass of building structures and the comprehensive performance characteristics of a building portfolio into an expanded demand response package. The benefit is expected to go beyond any current demand response programs.

## 1.5 Research Questions and Objectives

The hypothesis of this research is that commercial buildings can provide demand side participation in FR markets by effectively manipulating the operation of large HVAC systems during summer cooling periods on a second-by-second time basis. Drilling down the proposed hypothesis yields four major questions that need to be answered in this research:

- (1) Can commercial building HVAC systems be used as demand side frequency regulation resources?
- (2) If yes, what are the possible methods that can be adopted to vary the HVAC system power consumption with the FR signal? Which methods are more effective in stimulating building HVAC systems for FR participation? What are the interaction and counteraction effects when several FR methods are adopted simultaneously?
- (3) How to model a commercial building HVAC system and its controls that allow evaluations of HVAC system interactions and counteractions on a second-by-second time basis?
- (4) How to design a high-level supervisory control that directs the building power deviation from the baseline for FR participation?
- (5) How to evaluate/quantify the FR service provided by commercial buildings?

These questions were investigated through the following primary objectives:

- (1) Develop simulation models that enable evaluation of short-term dynamic response of the building HVAC systems with FR signal injection every 2-4 seconds. The model should be developed in the technical environment specialized for modeling, simulating and analyzing of controls and dynamic systems (i.e., Matlab/Simulink). The developed model should allow us to evaluate the proposed FR signal injection methods both individually and simultaneously.
- (2) With the developed model of commercial HVAC system and its low-level controls, a high-level supervisory control is needed to direct the building power deviation from baseline for FR service. This supervisory control method should capture the capacity limits of the interdependent HVAC subsystems, maintain occupants' comfort while providing FR, and ensure the minimum requirement of performance score from the ISO/RTO is met.

- (3) Quantify the building models response to the injected FR signal. This work currently adopts the performance-based regulation rules proposed by the PJM, which is the first RTO that launched such rules.
- (4) Estimates on expected FR capacity and revenue by FR injection method adopted on a unit building area basis in order for building owners to roughly assess the potential revenue for FR participation.

## 1.6 Scope

The scope of this dissertation covers: 1) Motivation, hypothesis, questions and objectives of this research; 2) Background information and a summary of PJMs performance-based regulation rule; 3) Four proposed methods for FR signal injection; 4) Methods of modeling a commercial building HVAC system and its low-level controls that allow evaluations of second-to-second system dynamic response to the FR signal injection; 4) A supervisory control method to overcome the challenges of using commercial building HVAC system for FR; 5) Simulation results of single and multiple FR signal injection methods; and, 6) Analysis of the results observed and estimations for FR capacity and revenue of a typical high-rise commercial building.

However, this dissertation does not cover: 1) Summary or comparison of other ISOs or RTOs official FR rules. Thus, evaluation metrics and results analysis are limited to PJMs performance-based regulation rule only; 2) Methods of estimating hourly FR capacity in day-ahead based on a given peak demand limit and the estimated real-time pricing information; 3) A portfolio of buildings participate in FR for a relative constant capacity by taking the advantage of the temporal diversity of capacity limits and part load ratios; and, 4) Field testing results. For example, the illuminance variations and the associated internal heat gain variations with FR signal injection into the lighting power modulator must be tested in an actual building for occupants' acceptance.

## 1.7 Organization of the Dissertation

The organization of the dissertation is in the following sections: Chapter 2 presents a literature review and relevant background information. Chapter 3 describes the methods of modeling a commercial HVAC system and its low-level controls for baseline evaluation. Chapter 4 introduces four FR signal injection methods and a supervisory control method. Chapter 5 presents and evaluates the simulation results and provides an analysis of the results. Chapter 6 offers conclusion.

## Chapter 2

### Literature Review

The federal energy regulatory commission (FERC) issued the final rule of FERC order No. 755 on Oct. 10, 2011, where “*the commission finds that the current frequency regulation compensation practices of RTOs and ISOs result in rates that are unjust, unreasonable, and unduly discriminatory or preferential. Specifically, current compensation methods for regulation service in RTO and ISO markets fail to acknowledge the inherently greater amount of frequency regulation service being provided by faster-ramping resources. In addition, certain practices of some RTOs and ISOs result in economically inefficient economic dispatch of frequency regulation resources*” [15]. The new rule is usually referred to as pay-for-performance since it requires RTOs and ISOs to compensate the FR resources based on their actual amount of FR provided instead of FR expectation. The new rule requires the compensation to be based on two parts: 1) capacity, including lost opportunity cost (LOC), and 2) performance, which quantifies the performance of the resource following the FR signal [15, 44].

In addition to the performance-based regulation rule launched in PJM, California Independent System Operator (CAISO) and New York Independent System Operator (NYISO) also have launched their own pay-for-performance rules in responding to FERC order 755. However, either the requirement is set too high for buildings to participate (e.g., CAISO requires at least 0.5 MW of capacity and aggregation of demand side resources is not allowed) or the FR performance evaluation rules (i.e., the equivalent of performance score calculation rules of PJM) are not explicitly explained and the historical FR signal data (i.e., the equivalent of RegA and RegD signal of PJM

instead of area control error) is not disclosed to the public [25, 31, 45]. Yet, key concepts and nomenclatures are found similar across these pay-for-performance rules from different ISOs and RTOs (e.g., accuracy, mileage, performance index, prequalification test and settlement calculation rules) [31, 45]. Therefore, the summary of PJM's performance-based regulation rule represents the commonly shared methodologies in responding to FERC order 755. Employment of PJM's performance-based regulation rule for the evaluation of simulation results should not be viewed as biased or preferential to the PJM territory.

This Chapter includes two sections: 1) Background information of frequency control and an 2) Overview of FR market within the PJM territory as of October 2012. The overview not only provides a summary of performance-based regulation rules and the related technical background but also the analysis of the posted FR signal data and pricing data to assist the simulation results evaluations in Chapter 5.

## **2.1 Background Information of Frequency Control**

To a very large extent, the power system supplies electric power to meet the demand of commercial and residential buildings. However, the electric demand includes not only the power consumption on customer loads, but also the power exported to the adjacent control areas and the power losses on transmission lines [18]. The power supply must meet the anticipated demand at each period of time. This requires not only the hour-to-hour economic dispatch that enable the power system to follow the substantial variations between load valleys and peaks throughout any given day; but also seconds-to-seconds and minutes-to-minutes regulations that adjust the power generation for ongoing demand variations [18]. The supply resources include all generators synchronized within the control area and the power imported from the adjacent control areas [37]. The power supply must balance the power demand due to strict reliability standards; otherwise, serious reliability problems will occur. When the supply is greater than the demand, the frequency rises above 60 Hz and generators momentarily speed up due to inertial response until the generators governor control reduces the inputs into the prime mover [37]. When the supply is less than the

demand, the opposite happens [18].

Balancing supply and demand requires the frequency control continuum of time by adopting different resources; which includes: 1) Primary control. It includes governor control and load response and takes less than 5 seconds [18]. 2) Secondary control. It uses short-term reserves to provide frequency regulation through AGC based on the information gathered by the supervisory control and data acquisition (SCADA) systems [18]. It takes more than 30 seconds but less than 5 minutes [18]. 3) Tertiary control. It is the manual change of dispatching reserves in cases that the secondary control does not manage the imbalance; and takes from minutes up to hours [18]. 4) Time control. It is employed to overcome the errors accumulated over time from inaccurate meters, transducers and communications that cause a non-zero net area control error and deviate the average frequency from exactly 60 Hz [18, 37]. The errors are usually corrected automatically by software and the timeframe is usually hours [37].

## **2.2 Overview of FR Market within the PJM Territory**

PJM launched the final rule with the name performance-based regulation (PBR) on Oct 1, 2012 [39]. New concepts, including performance score, benefits factor, and mileage are developed in order to calculate market clearing prices [39, 41]. These prices are then used for selecting the most economical resources to provide FR and then for calculating the settlement payment to such resources [39, 41]. There are four major changes in the performance-based regulation rule: 1) Resources submit two- part of offers on capacity and performance [39]. 2) Two-part of clearing prices from PJM's market-based system called eMKT [39]. 3) Employment of intra-hour LOC as part of co-optimized clearing price for energy, synchronized reserve and FR [22]. 4) Resources' actual mileage is used for evaluation and market clearing [22]. A summary of the performance-based regulation rule is provided in the following sub-sections.

### 2.2.1 Traditional and Dynamic FR Signals

The performance-based regulation rule separates FR resources into two groups: ramp-limited and capacity-limited [19]. The typical ramp-limited resources include gas or coal-fired steam power plants which have large capacity but respond slowly to FR signals. Typical capacity-limited resources include batteries, flywheels, plug-in electric vehicles, and responsive loads which have small capacity but respond quickly to FR signals. To fully utilize these two types of resources, PJM developed two types of FR signals: the traditional regulation A signal (i.e., RegA) and the dynamic regulation D signal (i.e., RegD) [19]. Ramp-limited resource should follow the slower moving RegA signal and get paid mostly for capacity. By contrast, capacity-limited resources should follow the faster moving RegD signal and get paid mostly for performance [19].

The RegA and RegD signals are designed to complement each other. PJM hired a consulting firm to determine the impact of various percentage levels of RegA- and RegD-following resources to the whole FR market [48]. In response, a new concept called benefits factor was introduced that converts RegD-following resources into traditional RegA-following resources in terms of the value to the FR market and the payment to FR resources [39]. The benefits factor is approximated by Equation 2.1 [39]. Here,  $x$  represents the percentage of FR provided by RegD-following resources. When less than 41% of FR is provided by RegD-following resources, the benefits factor of each RegD-following resource is greater than unity. The FR offers of the RegD-following resources are then divided by the benefits factor; as a result, the adjusted FR offers become more competitive. However, the opposite occurs if there were too much FR provided by RegD-following resources. With the participation of fast moving RegD-following resources, the regulation requirement would be scaled down in achieving that less FR resources would be allocated but still maintaining the same level of grid reliability [48, 19].

$$\text{Benefits Factor} = \begin{cases} 2.9 - 4.634x & 0 \leq x \leq 62.5\% \\ 0 & 62.5\% < x \leq 100\% \end{cases} \quad (2.1)$$

$$\text{Mileage}_{\text{RegA}} = \sum_{i=0}^n |\text{RegA}_i - \text{RegA}_{i-1}| \quad (2.2)$$

$$\text{Mileage}_{\text{RegD}} = \sum_{i=0}^n |\text{RegD}_i - \text{RegD}_{i-1}| \quad (2.3)$$

As originally developed by New England independent system operator, PJM also employs the term mileage to describe the movement of FR signals, as defined in Equation 2.2 and Equation 2.3 [39]. Mileage is the sum of the absolute movement of the RegA or RegD signal and is calculated every hour [39]. Historical PJM data from January to June 2012 show that the RegD signal has a wider distribution of hourly mileage, ranging from 8 to 23 and centered at 16. The RegA signal has a narrower distribution of hourly mileage, ranging from 1.5 to 12 and centered at 6 [19]. Therefore, the average mileage of the RegD signal is about three times more than that of the RegA signal — a significantly greater burden. Where a resource is capable of following either FR signal, the resource owner may need to think twice before switching their FR resources from RegA to RegD. The wear and tear on the resource could result in a higher maintenance cost offsetting extra payment for performance.

PJM posted a sample of both types of signals of the same time period after the launch of performance-based regulation rule (i.e., from 12/18/2012 to 1/17/2012) [36]. The RegA signal is found biased to the negative direction; whereas, the RegD signal is found basically symmetrical. Then, the energy consumption between an ideal resource of 1 MW capacity that follow RegA and RegD exactly is compared to quantify how much extra energy would be consumed in providing FR. Given both RegA and RegD are with 2-second resolution, the energy consumed in each 2-second interval can be calculated in Equation 2.4. Here, FR Signal can be either RegA or RegD signal. So, summing up the FR Signal over a time period and then multiply 2/3600 would produce the amount of energy consumed by following the FR Signal. If that summation equals to zero, that means the signal is symmetrical during that selected period, otherwise, it is biased to either directions.

$$\text{Energy}_{2\text{-sec}}[\text{MWh}] = 1[\text{MW}] \cdot \text{FR Signal} \cdot \frac{2}{3600} \quad (2.4)$$

The extra energy consumption of following RegA is found negative for all days of the observed month. This suggests a FR resource on the generation side would regulation down more often and consume less energy. However, a demand side resource following the RegA signal would consume more energy and the averaged amount of extra energy would be approximately 5 MWh per day and 2 MWh for 8 hours participation from 9 AM to 5 PM. By contrast, the extra energy consumption of a demand side resource following RegD is found close to zero and both negative or positive values are observed for the 32 days. The averaged amount of extra energy would be approximately 0.13 MWh per day and 0.036 MWh for the 8 hours from 9 AM to 5 PM. Thus, the sample data suggests that demand side resources should participate through RegD-following only; otherwise, a significant energy penalty would be occurred if bidding into the RegA market.

The reason for the negative direction biased RegA is potentially two-fold: 1) the data posted is during the winter season during which over-generation occurred more often on the grid so that regulation down was allocated more frequently. The opposite could occur more often during the summer seasons since the peak electric demand of the summer seasons should be greater than that of the winter seasons. 2) PJM designed RegA and RegD in this way so that generators provide the capacity (i.e., reservation of power for FR) part of FR and demand side resources provide the performance (i.e., movement of power for FR) part of FR. The reason for the negative direction biased RegA signal would be clearer if PJM disclosed RegA data of the summer months. Based on the FR signal data available, this dissertation is focused on RegD signal following only.

### **2.2.2 Requirements for Eligibility in PJM's FR Market**

To be eligible for providing FR, a FR resource must meet the following requirements:

- (1) The resource must be able to provide at least 100 kW of FR capability [39]. Although not listed in the requirements, PJM expects symmetrical response for FR up and down. The performance score is penalized if a resource performs better in one direction than the other [20].

- (2) The resource must be able to receive FR signals sent by PJM and make FR response data available for PJM to poll [39].
- (3) Any new resource wishing to participate must score at least 0.75 for the initial performance test [39, 40]. The initial test signals for both RegA-following resource and RegD-following resource are available at [42].
- (4) The resource must maintain a minimum average performance score of 0.4 for the last 100 rolling hours in order to maintain eligibility; otherwise, the resource must reapply for participation [40].
- (5) For each participating hour, the resource must score at least 0.25 to receive credit for that hour [19].

### 2.2.3 FR Data Transfer

FR participation involves multi-step data transfer that is established based on the DNP 3.0 protocol, which is primarily used for communications in the supervisory control and data acquisition (SCADA) system [77]. The DNP 3.0 protocol supports single master to multiple slaves topology but only the single master to single slave scenario is used as an example to explain the regulation data transfer. For simplicity, the single master to slave scenario (shown in Figure. 2.1) is used as an example to explain the regulation data transfer process in PJM.

- (1) PJM sends the assigned FR signal (AReg) for the fleet to the FR resource every 10 seconds [43].
- (2) The resource owner determines the maximum FR capability for each resource (TReg) every 2 seconds and makes that value available for PJM to poll [43]. TReg sets the maximum regulation capability that the owners resource could possibly provide [43].
- (3) PJM sends the appropriate FR signal (either RegA or RegD) back to the resource every 2 seconds [43].

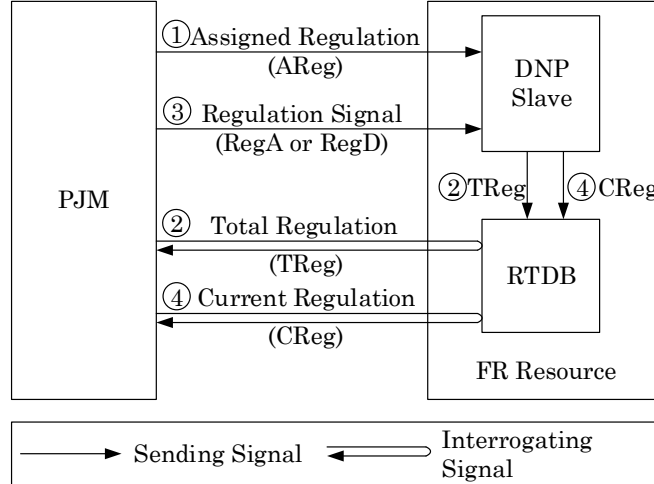


Figure 2.1: Regulation data transfer process of PJM

- (4) After the FR signal is sent to the FR resource, the FR transaction between PJM and the resource owner is established. The resource owner is responsible for making the current regulation (CReg) data available every 2 seconds for PJM to poll [43]. Here, CReg is calculated by subtracting the baseline power (i.e., the EcoBasepoint) from the resources actual power [43].

It is worth noting that in the masterslave topology used in PJM, only the master (i.e., PJM) can telemeter data to the slaves (i.e., FR resources); unsolicited messages from the slaves are not supported. Therefore, the regulation data generated by a FR resource (i.e., TReg and CReg) must be stored in a local real-time database (RTDB), where it is available for the master (i.e., PJM) to poll.

PJM mandates that the status for participation, TReg and FR maximum and minimum values must be submitted or changed up until 60 minutes ahead of the actual FR hour [39]. This provides opportunity for demand side resources have a day-to-day varying TReg or basepoint of power consumption (e.g., buildings) to participate. Predictions of the basepoint and TReg can be much more accurate in hour-ahead compare to day-ahead due to many factors impact energy calculation, such as weather, occupants and cooling loads. Similar requirements are found in the

equivalent rule of NYISO that the FR capacity and bidding prices of capacity and movement must be submitted to NYISO 75 minutes before the actual FR hour [45].

#### 2.2.4 Performance Score Calculation

PJM calculates the performance score for each resource for each hour as a composite score of accuracy, delay, and precision. Key equations of calculating these three components are listed in Equation 2.5, Equation 2.6 and Equation 2.7, respectively and the detailed definitions are available at [40].

Accuracy score is the maximum correlation between the FR signal and the FR resources response [40]. Here,  $r$  is the correlation coefficient of the two time series, recalculated with time shift  $\delta$  from 0 to 5 minutes in 10 second increments [40].

$$\text{Accuracy Score} = \max_{\delta=0 \text{ to } 5 \text{ min}} r(\text{FR Signal, Resource Response}) \quad (2.5)$$

Delay score is based on the delay in time between the FR signal and the point of maximum correlation as obtained in the process of calculating the accuracy score [40]. Therefore, the accuracy score and delay score are achieved at the same time [40].

$$\text{Delay Score} = \left| \frac{5 \text{ min} - \delta}{5 \text{ min}} \right| \quad (2.6)$$

Precision score is a function of the difference between the FR signal and the FR resource response [40].

$$\text{Precision Score} = 1 - \frac{1}{n} \sum \left| \frac{\text{Response} - \text{FR Signal}}{\text{Hourly Avg. FR Signal}} \right| \quad (2.7)$$

The calculation of the precision score is straightforward [40, 38]. However, a more detailed description of correlation and delay scores calculation process was found beneficial for better understanding these results [38]. Responses of FR resources are sampled every 10-second interval for performance score calculation [40]. Correlation and delay scores of each interval are determined at

the same time by finding the highest coincident scores [40]. Thus, a Score Scale in Equation 2.8 is introduced by PJM for finding such highest scores [38]. To calculate these two scores of each 10-second interval, data series of Signal (i.e.,  $T_{Reg} \cdot RegD$ ) and Response (i.e.,  $Power_{FR} - Power_{Baseline}$ ) are calculated first [38]. Then, this two series of data are compared to find the highest correlation coefficient between each 5-minute stationary window of Signal and 5-minute moving window of Response [38]. With the position of that highest correlation score determined, a delay score of each 10-second interval is determined on Score Scale [38]. The hourly average of each 10-second interval results in the hourly score [40]. As part of the design of Score Scale calculation, PJM allow 10 seconds latency of response without impacting performance score [40].

$$\text{Score Scale} = \min((1 - (\text{interval shift} - 1)/30), 1) \quad (2.8)$$

The performance score of the resource in that hour is calculated as the weighted average of the three individual scores [40]. PJM currently employs equal weights for the three items; therefore, each individual score accounts for 1/3 of the composite performance score [40]. A performance score of 1 is the maximum value that an ideal resource can achieve by following the FR signal perfectly. The performance score of each resource is applied to the regulation credit in each regulating hour. Therefore, performance score is the key that enables PJM to evaluate resources actual performance and transforms PJM from paying for regulation expectation to actual performance [19, 20]. In addition, performance score is also part of resources' offer evaluation, market clearing and settlement [22]. Thus, performance score is important to the entire process of the performance-based regulation rule [22].

### 2.2.5 Regulation Market Clearing Process

The sale and purchase of regulation in PJM is handled through a market-based system called eMKT [39]. The resource owners submit their specific regulation capability offer and regulation performance offer to the eMKT before 6:00 pm of day ahead [39]. Then, PJM processes these offers together with energy offers and resource schedules as submitted to the eMKT in the market clearing

engine (MCE) [39]. MCE co-optimizes regulation, synchronized reserve and energy in order to find the set of lowest cost resources for those services in each hour during the day [39]. For the regulation service, MCE first recalculates the adjusted regulation capability cost, the adjusted regulation performance cost, and the adjusted lost opportunity cost (LOC) for each unit of resource [39, 19]. Adjusted costs are computed using specific capability offers and performance offers as provided by resource owners, historic performance scores, specific benefits factors of the units, and regulation capabilities [39]. MCE then ranks resources in an ascending order in terms of the adjusted total offer cost per MW of capability [39]. Here, the adjusted total offer cost is the sum of the adjusted regulation capability cost, the adjusted regulation performance cost, and the adjusted LOC [39]. The unit with the highest rank in the merit order of the selected set of lowest cost resources sets the regulation market clearing price (RMCP) which is in turn used to derive the regulation market clearing performance price (RMPCP) and the regulation market clearing capability price (RMCCP) for each regulating hour [39, 20]. These two hourly prices are posted along with the locational marginal price (LMP) on PJM's website [35]. Each FR resource receives two parts of regulation credit that are calculated based on RMCCP and RMPCP capability and performance [39, 41]. The sum of the RMPCP credit and the RMCCP credit is the payment that a selected FR resource receives [41]. The specific benefits factor of the last selected resource, i.e., the most expensive one, determines the marginal benefits factor of the set of resources. The marginal benefits factor should be used for calculating the regulation credit for each participating unit. [39, 41]. The process of pay-for-performance in the PJMs regulation market is illustrated in Figure. 2.2 based on equations and rules defined in [39, 41].

Referring to Figure. 2.3 and Figure. 2.4, the distribution charts of the FR prices of the summer season (June to September) indicate that the RMCCP (i.e., the price in awarding resources' capacity contribution) is much greater than RMPCP (i.e., the pricing in awarding resources' movement contribution) on average. Here, each graph is plotted with minimum and maximum hourly pricing values as the lowest and the highest dashed lines, respectively. The dashed lines in between represents each 10th percentile increment. The solid line in the middle represents the average.

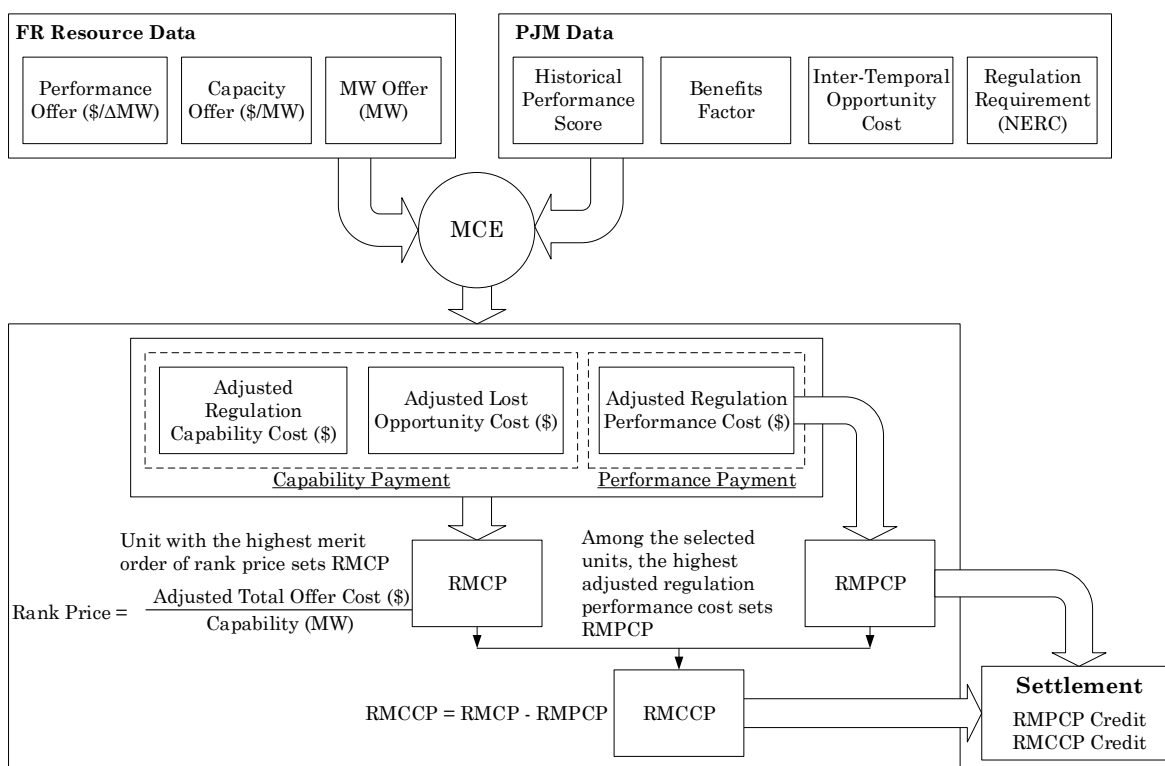


Figure 2.2: FR market clearing process in PJM [39, 41]

The distribution charts are only focused on the summer season because the commercial buildings' participation for FR in the summer cooling season is the focus of this dissertation. Winter heating season is also important for FR participation as long as the building is equipped with electric heating systems.

After the first year operation of performance-based regulation rule, the use of marginal benefits factor as the multiplier was found under compensate the contribution of RegD-following resources [22]. Thus, PJM introduced mileage ratio (MR) factor that compensate based on the mileage traveled [22]. MR is defined as the hourly mileage of the FR signal that the participating FR resource is following (RegA or RegD) over the hourly mileage of RegA signal [22]. The mileage of RegD signal in 2013 was 3.1 times greater than that of RegA signal [22]. Thus, RegD-following resources are awarded the “performance” part of payment multiplied by 3.1 on average starting from the second year of performance-based regulation rule [22]. A strong incentive for resources of fast-moving capability to participate.

### **2.2.6 Settlement**

The hourly payment for a participating FR resource would be the sum of the regulation market clearing capacity price (RMCCP) credit and regulation market clearing performance price (RMPCP) credit with equations calculated by Equation 2.9, 2.10 as shown in Figure. 2.2 [41]. The performance score achieved in each participating hour quantifies the FR resource's contribution in correcting area control error thus directly impacts its hourly payment. In cases that performance scores calculated less than 0.25, the payment would be forfeited for that hour [39]. According to the definition of MR factor, RegA-following resources are awarded with a factor of constant 1 and RegD-following resources are awarded with a greater value (i.e., around 3) for their additional contributions with dynamic movement [22].

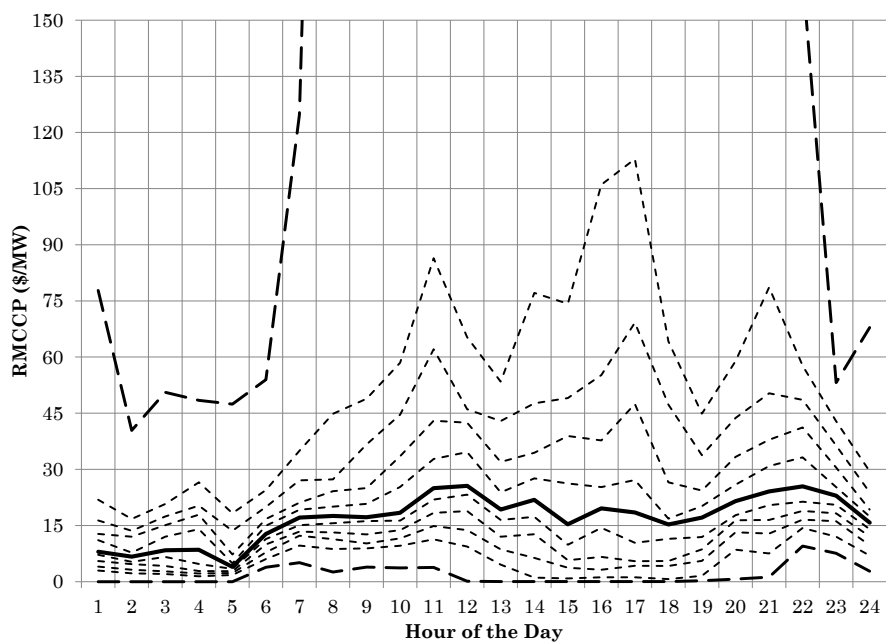


Figure 2.3: RMCCP distribution of summer weekdays in 2013

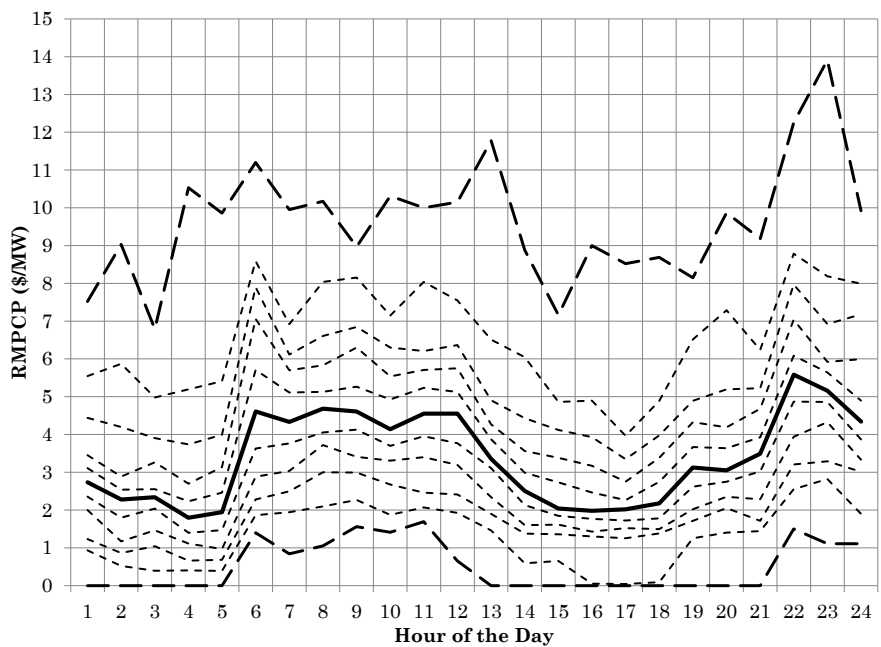


Figure 2.4: RMPCP distribution of summer weekdays in 2013

$$\text{RMCCP Credit} = \text{TReg} \cdot \text{Performance Score} \cdot \text{RMCCP} \quad (2.9)$$

$$\text{RMPCP Credit} = \text{TReg} \cdot \text{Performance Score} \cdot \text{MR} \cdot \text{RMPCP} \quad (2.10)$$

$$\text{FR Payment} = \text{RMCCP Credit} + \text{RMPCP Credit} \quad (2.11)$$

### 2.3 Recent Field Tests Work

Exploration of using demand side resources for FR is a dynamic research field. At the time of writing this dissertation, a successful test involving two-way communications of RegD signal was announced [61], which allows “near real-time telemetry” and translation of the RegD signal into executable commands to demand side resources through internet [61]. Thus, the technical barrier of implementing the supervisory control methods developed in this dissertation has been significantly reduced. Another field test has evaluated the response of injecting a 15 min artificial square wave into the zone temperature setpoint of a large commercial building [8]. The reason of adopting a 15 min artificial signal profile because that was the fastest changes that the hardware could take [8]. But, the test results have demonstrated that FR signal injections into the zone temperature setpoint can result in a building-wide participation for FR. This dissertation does not include results from field tests. However, these relevant research work have provided important information that guide this research to the phase of implementation.

## Chapter 3

### Modeling of A Commercial Building HVAC Systems and Low-Level Controls

To evaluate building HVAC systems for FR, a simulation model of commercial building with well-tuned controls is needed. This section introduces methods of modeling a scalable simulation model in the technical computing environment of Matlab/Simulink (Figure. 3.1) that allows second-to-second evaluations of its power in responding to the FR signal injection. The model is described in four sections: 1) five-zone model; 2) airside system; 3) waterside system and 4) power-consuming subsystems. Local PI controllers are modeled; however, a building automation system (BAS) is assumed that can supervise these controllers.

#### 3.1 Five-Zone Model

The five-zone model is measured of 44 m by 30 m (i.e., aspect ratio of 1.5) and is composed of one core zone and four perimeter zones (Figure. 3.8). The trapezoidal shaped perimeter zones surround the rectangular shaped core zone located in the center; thus, the dimensions of the perimeter zones are defined with the dimension of core zone is defined as 30 m long, 16 m wide and 3 m high. The South zone faces due South and has the longer base measured of 30 m. A resistance-capacitance (RC) circuit of two capacitors and three resistors, a 3R2C model, is employed to represent transient heat transfer through any opaque multilayer construction element (i.e., exterior walls, interior walls and floors) [26]. Referring to Figure. 3.2, Here,  $T_i$  and  $T_o$  are the ambient temperature nodes of the inside and outside of the element;  $C_i$  and  $C_o$  are the capacitance terms to represent the energy stored at the respective nodes;  $R_i$ ,  $R_m$  and  $R_o$  are the resistance terms to

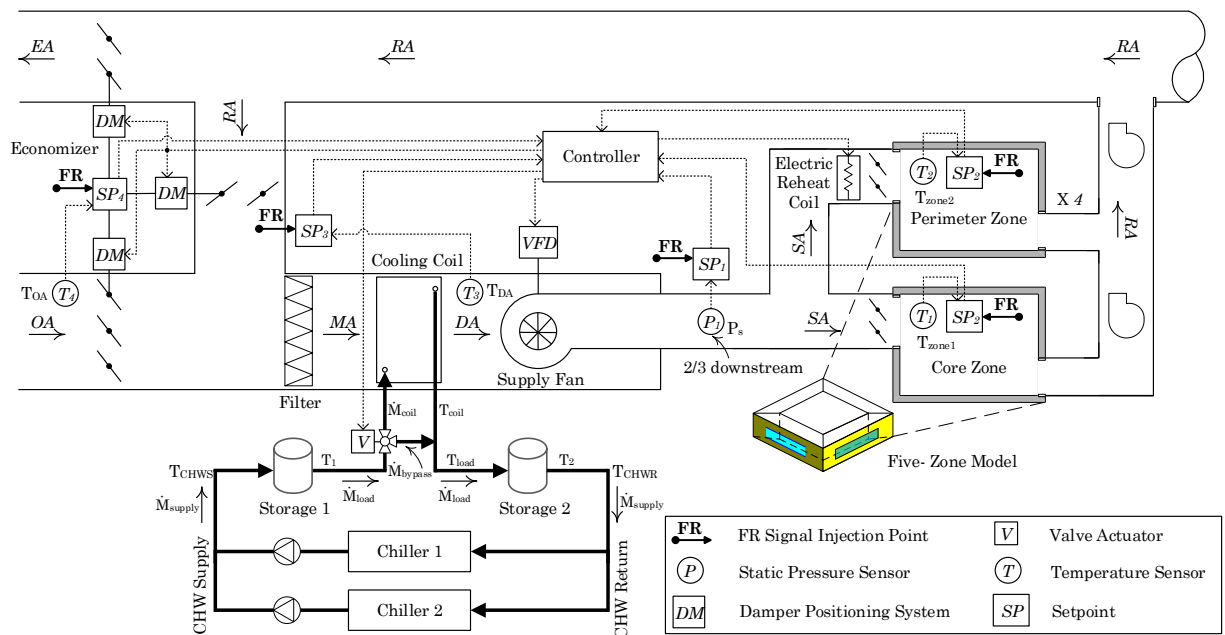


Figure 3.1: Commercial building HVAC system and its low-level controls

represent the thermal conductivity between the temperature nodes;  $T_s$  and  $T'_s$  are the temperature of the surfaces of the element. Typically, the resistance and capacitance of the RC circuit are found to obey the fraction ratio in Equation 3.1 and Equation 3.2 [26]. Here,  $R_T$  and  $C_T$  are the lumped resistance and capacitance for the construction element, respectively. With the construction materials of each layer given, the lumped R and C values can be calculated based on data listed in the ASHRAE Handbook of Fundamentals [5]. The hourly solar radiation measurement from weather stations is typically the global horizontal values [27]. Then, the global horizontal solar data is split into direct and diffuse parts and corrected regarding the azimuth and tilt angles of the exterior walls [27].

$$R_i = 0.1R_T, \quad R_m = 0.4R_T, \quad R_o = 0.5R_T \quad (3.1)$$

$$C_i = 0.15C_T, \quad C_o = 0.85C_T \quad (3.2)$$

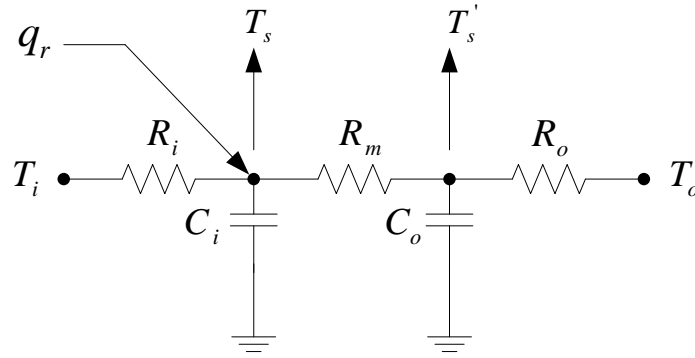


Figure 3.2: 3R2C model representation of heat transfer through opaque multilayer construction element [26]

The energy balance equations can be established regarding to temperature nodes  $T_s$  and  $T'_s$  based on the Kirchoffs current law [26]. Here,  $\dot{T}_s = \frac{dT_s}{dt}$ ,  $\dot{T}'_s = \frac{dT'_s}{dt}$  and  $q_r$  represents the solar radiation transmitted to the room [27]. Hourly solar radiation data is transmitted through windows and is assumed to be uniformly distributed to all opaque surfaces; therefore, the transmitted

solar radiation is dealt as heat flux directly fed into the 3R2C construction element models [26]. The dynamics of heat transfer through the multilayer element is modeled in Equation 3.3 and Equation 3.4 [26]. This model can be used to represent all opaque surfaces in a zone, (e.g., exterior walls, interior walls, and floors).

$$0.15C_T\dot{T}_s = q_r + \frac{T_i - T_s}{0.1R_T} - \frac{T_s - T'_s}{0.1R_T} \quad (3.3)$$

$$0.85C_T\dot{T}'_s = \frac{T_s - T'_s}{0.4R_T} - \frac{T'_s - T_o}{0.5R_T} \quad (3.4)$$

A simple window model is adopted in Equation 3.5 [27]. Here, window surface area  $A_g$  takes 60% of exterior wall area of each perimeter zones and have glass transmissivity  $\tau_g$  of 0.4 and the corrected solar radiation to the plane of window  $q_{r-surf}$ . The window is a typical double insulated glazing with argon filling with U-value  $U_g$  of  $1.1 \text{ Wm}^{-2}\text{K}^{-1}$  [33].

$$q_r = A_g\tau_g q_{r-surf} \quad (3.5)$$

The measured weather input data also includes hourly wind speed ( $vw$ ), exterior air temperature ( $T_o$ ) and exterior air relativity humidity ( $RH_o$ ). The hourly air change rate (ACH)  $N_i$  of each perimeter zone is refined with  $vw$ ,  $T_o$ , and interior air temperature ( $T_i$ ) for infiltration heat transfer [26]. Here, the building is assumed tightly insulated with standard ACH of  $1.0 \text{ h}^{-1}$ . The infiltration rate is turned off to zero during HVAC system's operating hours (i.e., 6:00 to 18:00) because of pressurization and mechanical ventilation rate  $Nv_i$  is applied to the zones.

In each zone, both a sensible heat balance and a latent heat balance (i.e., moisture-driven) are calculated. Assuming each zone has air thermal capacity  $C_i$  and volume  $V_i$ , convective internal heat gain  $q_{cc}$ , convective HVAC plant heat input  $q_{cp}$ ; any of the five opaque surfaces (i.e., four walls and one floor) has area of  $A_s$ , temperature of  $T_s$  and internal surface resistance  $R_i$  of its 3R2C model; and the supply air temperature of  $T_{SA}$ . The internal temperature of each perimeter zone can be determined by Equation 3.6. The temperature of the core zone is calculated without the infiltration term. Here, it is worth noting that the air thermal capacity  $C_i$  is the product of the

room air mass multiplied by specific heat capacity of air  $C_{p,a}$  and an air thermal mass multiplier  $k$  (i.e., a term to represent the thermal storage characteristics of interior objects). The latent balance is modeled by neglecting surface absorption and desorption. Assuming each zone has room air mass of  $M_i$ , humidity ratio of  $g_i$ , latent heat gain from people of  $q_l$  and standard latent heat of vaporization of water in air defined as  $h_{fg}$ . The supply air humidity  $g_{SA}$  is calculated based on the outside air conditions (i.e.,  $T_o$  and  $RH_o$ ) and air properties calculated through the air-side duct system, which includes return air (RA) mixed with outside air (OA) and passes through the cooling coil for discharge air (DA), and then adds up fan heat for supply air (SA). The humidity ratio ( $\frac{kg}{kg}$ ) of each zone can be formed in Equation 3.7.

$$C_i \frac{dT_i}{dt} = q_{cc} + q_{cp} - \left[ \sum \left( \frac{A_s(T_i - T_s)}{R_{i,s}} \right) + A_g U_g (T_i - T_{SA}) + \frac{N_i V_i (T_i - T_{SA})}{3} \right] \quad (3.6)$$

$$M_i \frac{dg_i}{dt} = 1.2 \frac{N_i V_i (g_{SA} - g_i)}{3600} \Big|_{\text{non-HVAC Hrs}} + 1.2 \frac{N_{vi} V_i (g_{SA} - g_i)}{3600} \Big|_{\text{HVAC Hrs}} + \frac{q_l}{h_{fg}} \quad (3.7)$$

Here, the internal sensible heat gain ( $q_{cc}$ ) and the latent heat gain from people ( $q_l$ ) are defined as event-driven loads with nominal values of  $20 \text{ Wm}^{-2}$  and  $4 \text{ Wm}^{-2}$  for occupied hours from 8:00 to 18:00, respectively. In addition, a Gaussian random variation with variance of 1% of the nominal internal gain values is added.

### 3.2 Airside System

Two approaches are developed to design the airside system: 1) pressure-dependent and 2) pressure-independent. The pressure-dependent system uses the thermostat controller (i.e., PI controller) directly controls the terminal damper position in order to regulate the volume flow rate of air into the zone for maintaining zone temperature. This works well if the duct static pressure is not disturbed in a wide range. However, this research found that injecting FR signal to the static pressure setpoint an effective way to manipulate the HVAC system operation for FR service. In the simulation environment, the static pressure setpoint was deviated as large as 70% from the baseline setpoint. Under such conditions, a pressure-independent airside system is needed to

maintain zone temperature stable regardless the significant disturbances on duct static pressure. The pressure-independent airside system is only possible through cascade PI controllers, which is designed with an outer zone temperature control loop and an inner air volume flow rate control loop. The temperature controller sets a floating setpoint of the volume flow rate controller; then, the volume flow controller determines the damper position regarding the duct static pressure variations. Thus, the zone temperature is decoupled from duct pressure variations by more active moving dampers. Both approaches can be extended from one zone to multiple zones for the variable air volume (VAV) system.

### 3.2.1 Pressure-Dependent Airside System

A single zone pressure-dependent air side system is designed in Figure. 3.3. When the static pressure setpoint is varied by the FR signal injection and the zone temperature setpoint is maintained as constant, the static pressure setpoint is compared with the static pressure at the sensor. The difference of the two quantities is denoted as  $P_{\text{error}}$  and is fed into a PID controller for calculating the command frequency  $f$  input to the VFDmotorfan system. The system then produces the correct amount of volume flow rate  $\dot{V}$  according to the command frequency  $f$  in order to vary the static pressure at the sensor for minimizing  $P_{\text{error}}$  to zero. As soon as  $P_{\text{error}}$  is stabilized at zero, the system has reached steady-state of the new static pressure setpoint. In this process, the power consumption is expected to vary with the FR signal in terms of both magnitude and direction in a positive correlation according to the fan affinity laws in Equation 3.8 [6]. Here,  $N$  is the rotating speed of the fan, and  $W$  is the power consumed by the fan.

$$\frac{\dot{V}_1}{\dot{V}_2} \propto \frac{N_1}{N_2}, \quad \frac{\dot{W}_1}{\dot{W}_2} \propto \left(\frac{N_1}{N_2}\right)^3 \quad (3.8)$$

To demonstrate this, an actual commercial fan (SWB-349-AF) is selected and its performance curve is employed to analyze the fan power consumption with the reset of static pressure setpoint as shown in Figure. 3.3 [23]. The fan only operates at the intersecting points of the fan total pressure  $P_t$  and the duct pressure  $P_d$ ; therefore, a solver is employed in the simulation model that

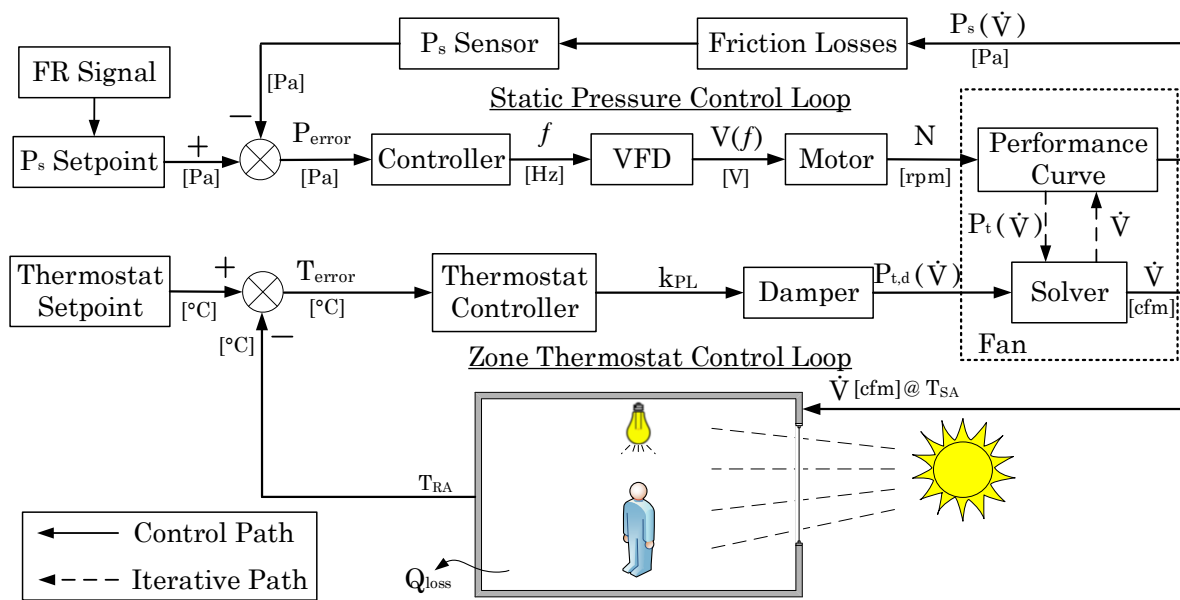


Figure 3.3: Block diagram of the pressure-dependent airside system

continuously finds the operating points of the fan with the given command frequency  $f$ . In a fan-duct system, the total pressure  $P_t$  is the sum of static pressure  $P_s$  and velocity pressure  $P_v$  as shown in Equation 3.9 [7]. The velocity pressure  $P_v$  can be calculated by Equation 3.11 with the selected duct cross-sectional area  $A_{\text{duct}}$  and the assumption of constant air density  $\rho_{\text{air}}$ . The total pressure  $P_t$  curves from the manufacturer are re-plotted as second order regression curves with  $\dot{V}$  as the independent variable. Thus, the static pressure curves  $P_s$  can be plotted as second order polynomials since both of the total pressure  $P_t$  and velocity pressure  $P_v$  curves are of second order. The duct pressure  $P_d$  typically only depends on the design parameters of the duct; however, it varies with the damper position in a VAV system. Therefore, the part-load coefficient (i.e.,  $K_{\text{PL}}$ ) is defined to represent the dynamics of the movement of damper in Equation 3.11. When the volume flow rate  $\dot{V}$  is varied by the fan for maintaining the static pressure setpoint, the damper adjusts its position to allow only the right amount of air into the zone for maintaining the zone temperature setpoint. Therefore, the value of  $K_{\text{PL}}$  can be used for identifying the damper position in a VAV system. The operating range of the damper position is from 25% of wide open (i.e.,  $K_{\text{PL}}$  is at minimum-load position  $K_{\text{ML}}$ ) to wide open (i.e.,  $K_{\text{PL}}$  is at full-load position  $K_{\text{FL}}$ ).

$$P_t = P_s + P_v \quad (3.9)$$

$$P_v = \frac{1}{2} \rho_{\text{air}} \left( \frac{\dot{V}}{A_{\text{duct}}} \right)^2 \quad (3.10)$$

$$P_d = K_{\text{PL}} \dot{V}^2 \quad (3.11)$$

Figure. 3.4 demonstrates how the solver would respond when the static pressure setpoint resets. Assuming the static pressure setpoint is reset from 1 in.wg (i.e., 250 Pa) to 1.1 in.wg (i.e., 275 Pa) at the sensor. This will result in the static pressure setpoint at the fan reset from 3 in.wg (i.e., 750 Pa) to 3.3 in.wg (i.e., 825 Pa) if we assume the static pressure sensor is located at 2/3 downstream of the duct and the friction losses is exactly 2/3 of the pressure developed at the fan. Now assume the original operation is at point 1 with  $\text{RPM} = 612$  and  $\dot{V} = 24.1 \times 10^3 \text{ cfm}$  (i.e.,  $11.25 \text{ m}^3/\text{s}$ ). When the static pressure setpoint at the fan is reset to 3.3 in.wg, the new operating point

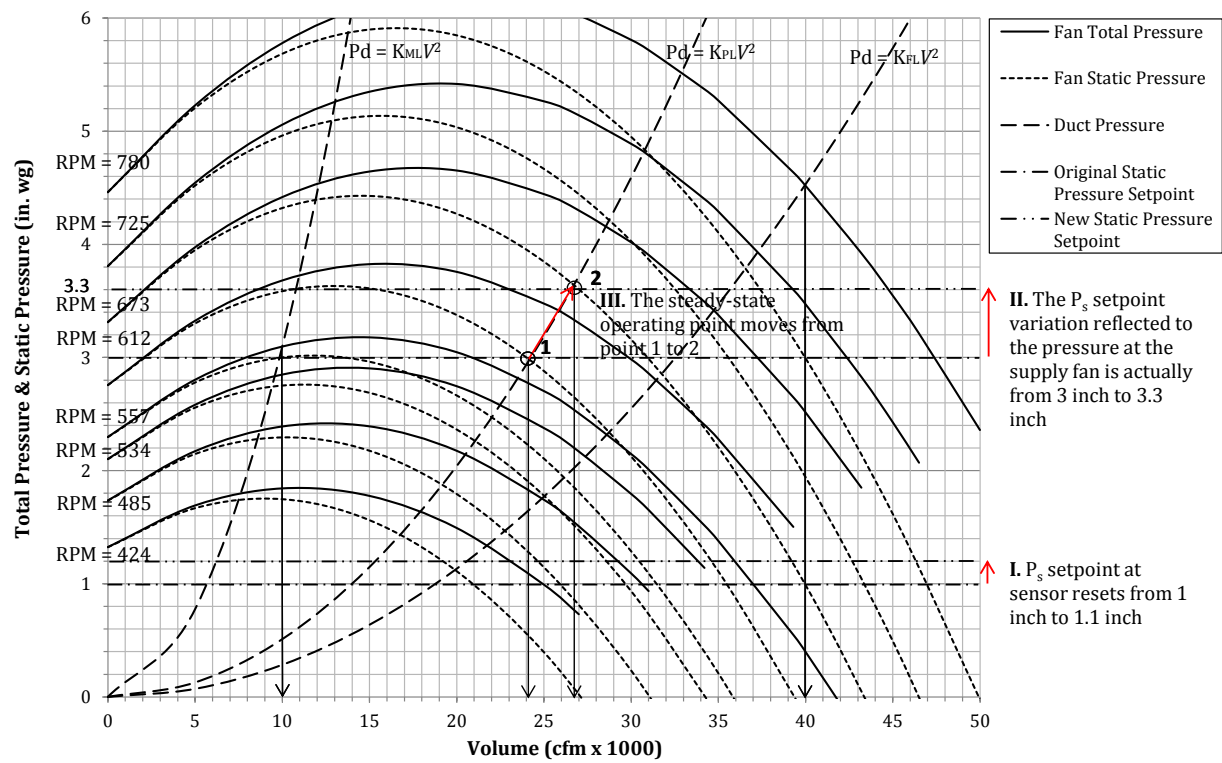


Figure 3.4: Fan performance curve for demonstrating the impacts of varying the static pressure setpoint

should stabilize on this horizontal pressure line. Assuming the damper position is maintained as constant (i.e., reflected by  $K_{PL}$  as constant) in this process, the fan should eventually operate at point 2 with  $RPM = 673$  and  $\dot{V} = 26.8 \times 10^3 \text{cfm}$  (i.e.,  $12.51 \text{ m}^3/\text{s}$ ).

Assuming a constant damper position can be true only when the static pressure setpoint reset happens very quickly so that the damper is not able to respond fast enough. In fact, the dampers response in the simulation model is assumed to have a travel time of 30 seconds and the AHU is subjected to a static pressure setpoint update every 2 seconds. While the dampers position can be approximated as constant in a 2 second period; that assumption does not hold true for a one-hour measurement period applicable to regulation. The continuous response over an hour with a changing damper position is important to RegD response.

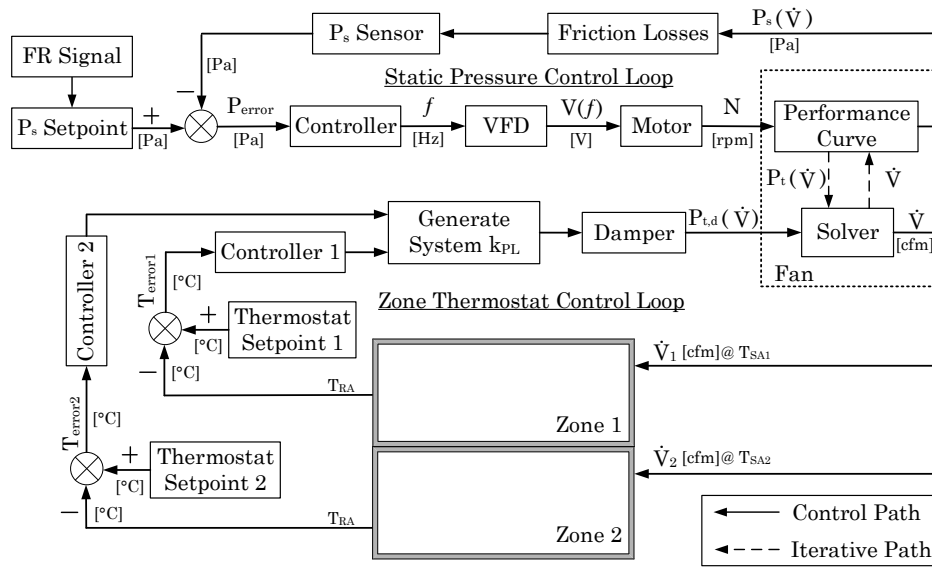


Figure 3.5: Pressure-dependent airside system with two zones

Based on the single zone design, multiple zone VAV system can be designed with ducts to each zone connected in parallel as shown in Figure. 3.5. Here, only two zones are shown for clarity but is scalable in the model easily. The static pressure control loop is maintained the same as in Figure. 3.3. However, the volume flow rate is split for each zone regarding the different cooling loads

of each zone caused by the individual solar radiation and internal heat gains. Based on the volume flow rate of each zone, the duct pressure variation is calculated from each zone's contribution (i.e.,  $K_{PL}$ ) to conclude the total changes to the main duct pressure variation (i.e.,  $K_{PL,sys}$ ). Thus, the key changes of expanding the design from an one-zone model to a multiple-zone model is twofold: 1) split the total volume flow rate of the supply fan for each zone based on their individual cooling loads (i.e., Equation 3.16); 2) generate  $K_{PL,sys}$  from  $K_{PL}$  of each zone to represent the duct total pressure variations (i.e., Equation 3.18). The step-by-step derivation are presented in the following.

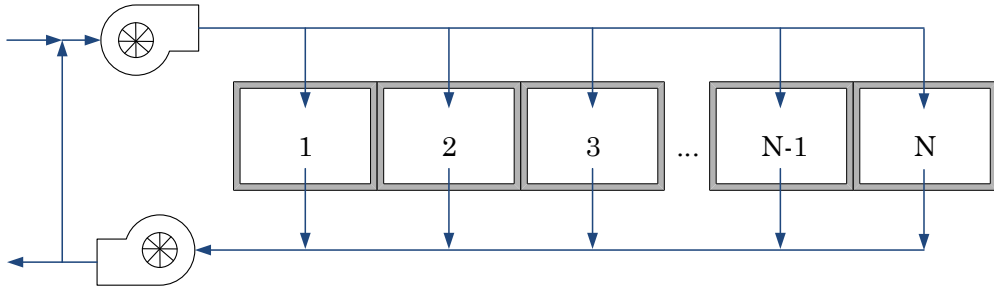


Figure 3.6: VAV system with N branches

Assume a VAV system with N branches connected in parallel as shown in Figure. 3.6, the pressure drop in each branch  $\Delta P_{zone,i}$  should be equal to the main duct pressure drop of the system  $\Delta P_{sys}$  as shown in Equation 3.12. Here,  $\Delta P_{zone,i}$  the  $\Delta P_{sys}$  can be calculated by Equation 3.14 and Equation 3.15, respectively.  $\dot{V}_{zone,i}$  is the supply air volume flow rate into the  $i^{th}$  zone and  $\dot{V}_{sys}$  is the supply air volume flow rate of the supply fan. Obviously,  $\dot{V}_{zone,i}$  and  $\dot{V}_{sys}$  obey the relationship in Equation 3.15.

$$\Delta P_{zone,i} = \Delta P_{sys} \quad i \in [1, N] \quad (3.12)$$

$$\Delta P_{zone,i} = K_{PL,i} \cdot \dot{V}_{zone,i}^2 \quad (3.13)$$

$$\Delta P_{sys} = K_{PL,sys} \cdot \dot{V}_{sys}^2 \quad (3.14)$$

$$\dot{V}_{sys} = \sum_{i=1}^N \dot{V}_{zone,i} \quad (3.15)$$

The fraction of volume flow rate into each zone can be calculated by dividing Equation 3.14 by Equation 3.15. The composite coefficient  $K_{PL,sys}$  can be solved by substituting Equation 3.12, Equation 3.14 and Equation 3.15 into Equation 3.15. The derivation is shown in two steps:

- (1) The fraction of supply air volume flow rate into the  $i^{\text{th}}$  zone can be derived as:

$$f_{zone,i} = \frac{\dot{V}_{zone,i}}{\dot{V}_{sys}} = \frac{\sqrt{\frac{\Delta P_{zone,i}}{K_{PL,i}}}}{\sqrt{\frac{\Delta P_{zone,i}}{K_{PL,sys}}}} \quad (3.16)$$

- (2) Then, adding the fraction of all  $N$  zones, the sum must equal to 1. Assume there are three zones (i.e.,  $N = 3$ ), the following equation can be established and the composite coefficient  $K_{PL,sys}$  is solved in the following:

$$\sum_{i=1}^N \sqrt{\frac{K_{PL,sys}}{K_{PL,i}}} = 1 \Rightarrow \sqrt{\frac{K_{PL,sys}}{K_{PL,1}}} + \sqrt{\frac{K_{PL,sys}}{K_{PL,2}}} + \sqrt{\frac{K_{PL,sys}}{K_{PL,3}}} = 1 \quad (3.17)$$

$$K_{PL,sys} = \left( \frac{\sqrt{K_{PL,1} \cdot K_{PL,2} \cdot K_{PL,3}}}{\sqrt{K_{PL,1} \cdot K_{PL,2}} + \sqrt{K_{PL,1} \cdot K_{PL,3}} + \sqrt{K_{PL,2} \cdot K_{PL,3}}} \right)^2 \quad (3.18)$$

Since  $f_{zone,i}$  and  $K_{PL,sys}$  are the requested information at the same timestep but are essentially derived from the same sets of equations (i.e., Equation 3.12 to Equation 3.15). Thus, a unit delay block is necessary that calculates the  $f_{zone,i}$  with  $K_{PL,sys}$  from the previous timestep but calculates the duct total pressure with the  $K_{PL,sys}$  from the current timestep. In this way, the multiple zone airside VAV system can be solved iteratively. In the model, each timestep is 1 second.

Although the airside system described in this section correctly captures the system dynamics in simulations [78]. The design is found not easy to explain to peers and difficult to adjust parameters. For example,  $K_{PL}$  is important to this design but is not a normal term to the HVAC design field. In addition,  $K_{PL}$  represents the lumped duct pressure drop; thus, the pressure drop of the designed values of components in the AHU and VAV boxes cannot be individually adjusted. Therefore, the airside system is remodeled with the standard HVAC system design method (i.e., the static regain method) and parameters of the designed values of components are adjustable. In addition, cascade controllers are adopted in each zone for steady zone temperature regardless of wide range variations of duct pressure.

### 3.2.2 Pressure-Independent Airside System

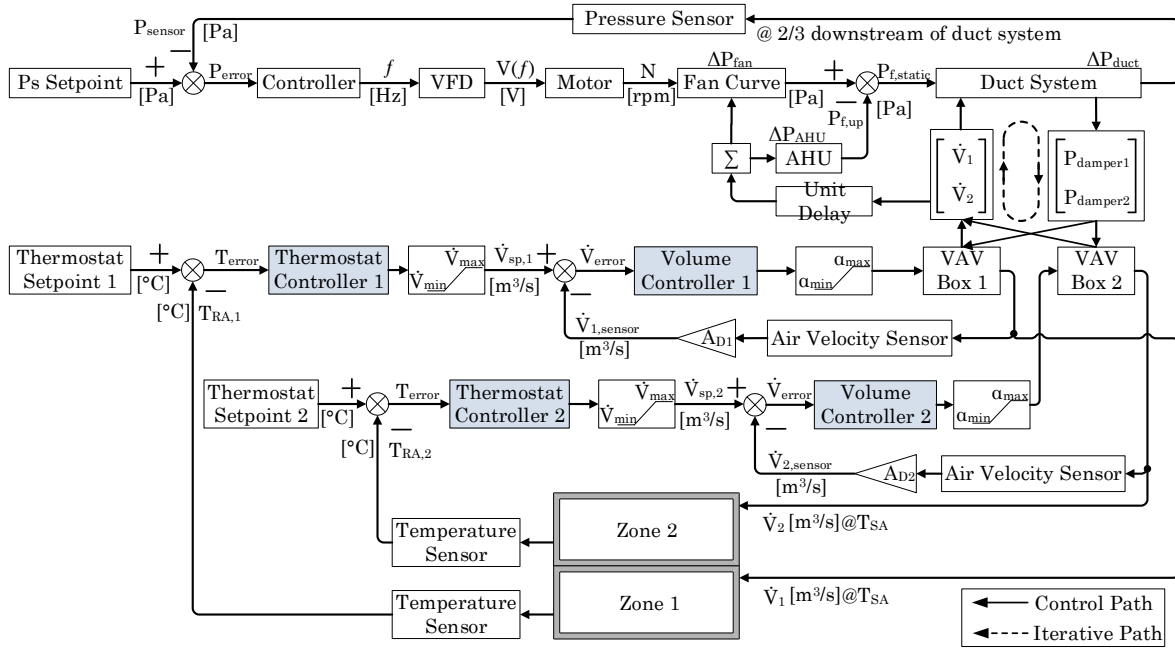


Figure 3.7: Pressure-independent airside system with two zones

The pressure-independent airside system can be modeled by adopting cascade controllers for less disturbed zone temperature while the duct pressure is disturbed in a significant range. A cascade controller is applied to each zone and is composed of two control loops: 1) inner-loop of volume flow rate control and 2) outer-loop of zone temperature control. The output of the outer-loop controller (i.e., temperature controller) determines a floating setpoint  $\dot{V}_{SP}$  for the inner-loop; whereas, the inner-loop controller (i.e., air flow rate controller) determines terminal damper position which reflects the amount of air delivered to each zone. Therefore, pressure variations in the duct system is balanced by active terminal dampers' movement instead of zone temperature drift, thus, leaving the zone temperature less disturbed. For illustration purpose, a simplified airside system is shown in Figure. 3.7 with only two zones. The cascade controllers are highlighted in blue.

The setpoint  $\dot{V}_{SP}$  for each perimeter zone is limited by the rule-of-thumb of  $1.0 \text{ cfm} \cdot \text{sf}^{-1}$  (i.e.,  $0.005 \text{ m}^3\text{s}^{-1}\text{m}^{-2}$ ) multiplied by the zone floor area; and 50% of that value for the core zone because

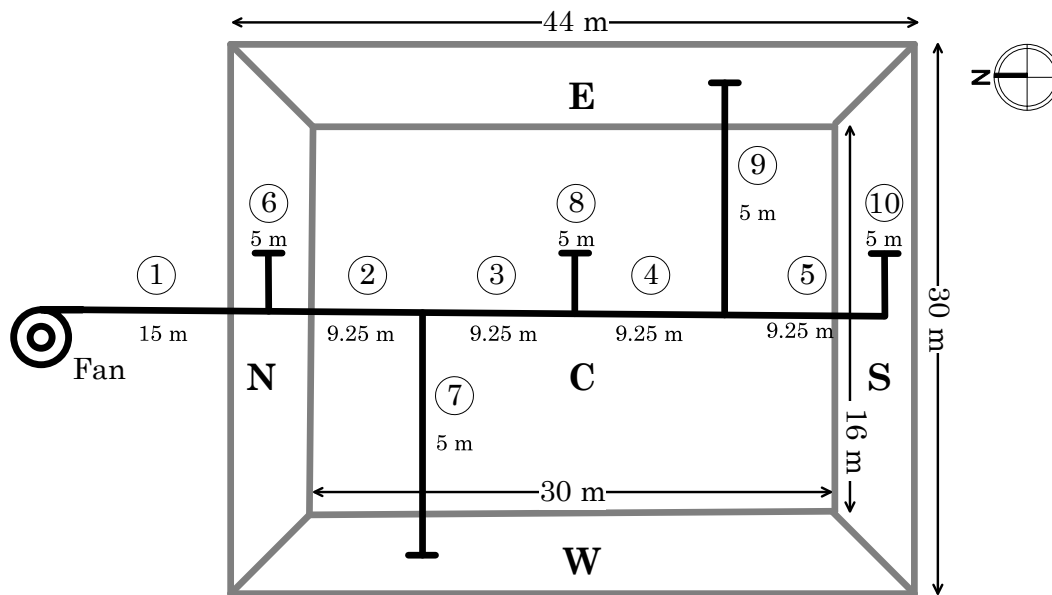


Figure 3.8: Duct system design based on the 5-zone geometry

no solar heat gains applied. These upper limit volume flow rate are the design values for each zone. Under design conditions of volume flow rate and the inlet air velocity from the supply fan set at 3,500 fpm (i.e.,  $17.78 \text{ ms}^{-1}$ ), a pressure balanced high-velocity duct system can be designed using the static regain method, achieving approximately the same static pressure at each takeoffs [60]. The duct system is designed based on the 5-zone geometry in its simplest fashion (i.e., only one VAV box for each zone and each branches are assumed to have the same length). Section ① to ⑤ are straight duct sections and ⑥ to ⑩ are branches. Based on the given length of straight duct sections and branches (in Figure. 3.8) and the designed volume flow rate of each zone, the diameter of duct sections and branches can be calculated through static regain method. Thus, the duct system is designed and the results are tabulated in Table 3.1.

Table 3.1: Parameters of duct system design

| Duct | Length [m] | Diameter [m] |
|------|------------|--------------|
| ①    | 15         | 0.79         |
| ②    | 9.25       | 0.78         |
| ③    | 9.25       | 0.72         |
| ④    | 9.25       | 0.59         |
| ⑤    | 9.25       | 0.40         |
| ⑥    | 5          | 0.51         |
| ⑦    | 5          | 0.51         |
| ⑧    | 5          | 0.51         |
| ⑨    | 5          | 0.46         |
| ⑩    | 5          | 0.39         |

Then, this duct system is used to calculate pressure losses in the duct system, in particular the static pressure at the sensor located at  $2/3$  downstream of the straight duct. This sensed static pressure is compared with the static pressure setpoint for their difference, which is denoted as  $P_{error}$ . This error term is then fed into a PID controller for the command frequency  $f$  input to the VFD-motor-fan system. The system then drives the supply fan to deliver the correct amount of air in order to vary the static pressure at the sensor, driving  $P_{error}$  to zero. According to the

ASHRAE Handbook of Fundamentals, the supply fan is the only source of pressure increase in the duct system [7]. Referring to Figure. 3.9, the static pressure balance of supply fan and the duct system is formulated in Equation 3.19 by neglecting the pressure drop in the zones  $P_{zone}$  and on the return path  $P_{RA}$ . Therefore, the static pressure developed by the supply fan  $\Delta P_{fan,static}$  must overcome the static pressure drop in the AHU  $\Delta P_{AHU,static}$  and static pressure drop in the straight duct from inlet to the sensor  $\Delta P_{duct,static(inlet \rightarrow sensor)}$ ; then, the remaining value equal to the static pressure setpoint  $P_{sensor}$ , which is usually set at 0.8 to 1.2 in.wg. (i.e., 200 to 300 Pa).

$$P_{sensor} = \Delta P_{fan,static} - \Delta P_{AHU,static} - \Delta P_{duct,static(inlet \rightarrow sensor)} \quad (3.19)$$

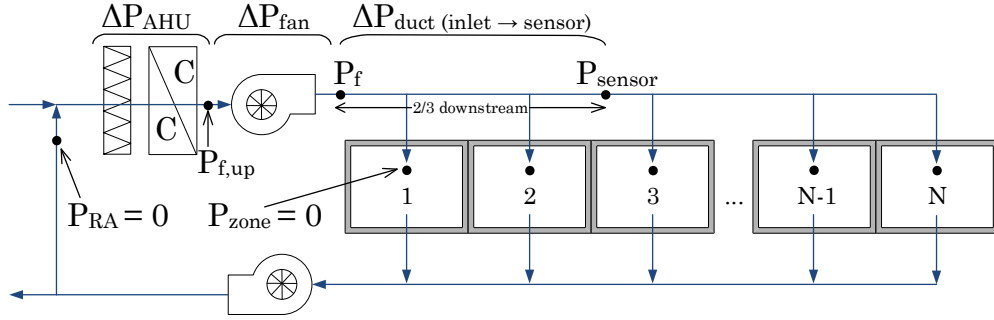


Figure 3.9: Static pressure balance of the duct system

Here,  $\Delta P_{duct,static(inlet \rightarrow sensor)}$  is calculated in the duct system through the balance of pressure drops in each VAV boxes, which houses reheat coils and terminal dampers with total pressure drop of  $\Delta P_{RHCoil}$  and  $\Delta P_{damper}$ , respectively. Each reheat coil is modeled as a quadratic curve as function of incoming air velocity and has a designed pressure drop of 0.1 in.wg. (i.e., 25 Pa). Each terminal damper has designed pressure drop of 0.3 in.wg. (i.e., 75 Pa) and its pressure drop is modeled by Equation 3.21 with air velocity  $v$  sensed by the velocity sensor and the variable  $C$  as function of damper position  $\alpha$  defined in Equation 3.22. Here,  $\alpha$  ranges from 0 to 1 (i.e., close to fully open) and the leakage coefficient  $\lambda$  equals to 0.01. Thus, the constant  $C_{open}$  can be calculated at the design condition when equals unity,  $\Delta P_{damper}$  equals to 0.3 in.wg. and the velocity  $v$  at its design value,

which can be calculated from Equation 3.22 with designed volume flow rate  $\dot{V}_{\text{zone}}$  and damper area  $A_D$ .  $\Delta P_{\text{AHU}}$  includes pressure drop of the filter  $\Delta P_{\text{filter}}$  and of the cooling coil  $\Delta P_{\text{CCoil}}$ ; both obey second order regression curves with incoming air velocity as the independent variable.  $\Delta P_{\text{filter}}$  and  $\Delta P_{\text{CCoil}}$  are zero when the inlet air velocity is zero and reaches their respective maximum values, 1 in.wg. (i.e., 250 Pa) and 1.5 in.wg. (i.e., 375 Pa), when the inlet air velocity reaches its designed value of 500 fpm (i.e.,  $2.54 \text{ ms}^{-1}$ ).  $\Delta P_{\text{fan}}$  is modeled based on an actual commercial fan (SWB-222-Belt Drive) [23]. Its performance curve provides the static pressure drop with the delivered air volume flow rate. Its power is developed as function of these two variables based on manufacturer's data in Figure. 3.14 [23].

$$\Delta P_{\text{damper}} = C\rho v^2/2 \quad (3.20)$$

$$C = C_{\text{open}}\lambda^{2\alpha-2} \quad (3.21)$$

$$\dot{V}_{\text{zone}} = A_D v \quad (3.22)$$

Referring to Figure. 3.7, there are two main control loops: the cascade controlled zone temperature loop and the static pressure loop. These two loops are linked through VAV boxes. With the pressure drop on each terminal dampers produced by the duct system and the damper position calculated by the cascade controllers, the VAV boxes request the supply fan to deliver the total amount of volume flow rate of air to the respective zones. Here, a unit delay block is necessary that delays the total volume flow rate to the supply fan for one simulation time step (i.e., 1 second); but, first calculates the individual volume flow rate for each zones in the cascade controlled loop with  $\Delta P_{\text{damper}}$  and  $\alpha$  from the previous simulation time step. In this way, this pressure-independent airside system can be solved iteratively.

### 3.2.3 Economizer

Referring to Figure. 3.10, a dry-bulb economizer system is modeled in Equation 3.23 that controls the outside air fraction (OAF) in order to use most of the cooler OA in summer mornings.

With the discharge air temperature setpoint set at  $13^{\circ}\text{C}$ , the mixed air temperature setpoint is also set at  $13^{\circ}\text{C}$  in order to minimize the cooling coil load. Thus,  $\text{MActrl}$  is the MA controller signal output generated based on the error term of  $13^{\circ}\text{C}$  setpoint and the sensed MA temperature.  $\text{minOAF}$  is the minimum OAF according to building code; here,  $\text{minOAF}$  equals to 20%.  $\text{GT}(T_{\text{RA}}, T_{\text{OA}})$  is a Boolean that ensures the  $\text{MActrl}$  and  $\text{minOAF}$  is compared only when the OA temperature  $T_{\text{OA}}$  is lower than the RA temperature  $T_{\text{RA}}$ ; otherwise, OAF is maintained at 20% for minimum amount of OA inlet. A wet cooling coil model is employed that cools and dehumidifies the incoming MA for outgoing DA [71]. Referring to Figure. 3.1, a PI controller is used to regulate the valve position to control the chilled water mass flow rate for the  $T_{\text{DA}}$  maintained at  $13^{\circ}\text{C}$ .

$$\text{OAF} = \max(\text{MActrl} \cdot \text{GT}(T_{\text{RA}}, T_{\text{OA}}), \text{minOAF}) \quad (3.23)$$

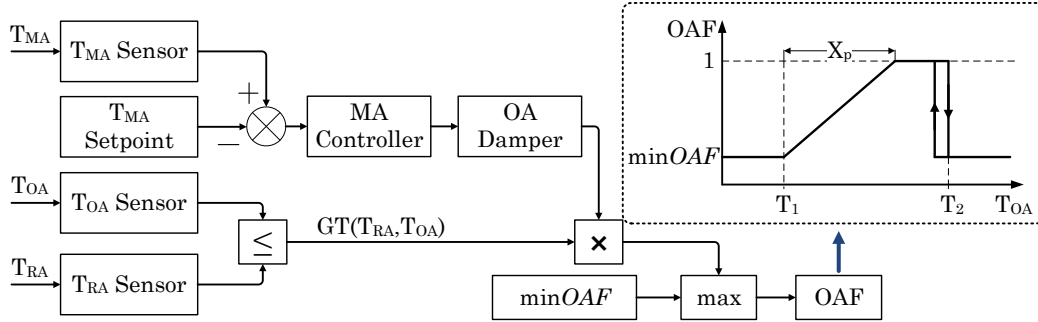


Figure 3.10: Open-loop outside air damper control strategy

Unlike close-loop controllers for other HVAC subsystems (e.g., static pressure control and zone temperature control), smaller proportional bands of controllers are preferred so that controllers are more sensitive to smaller error terms in order to launch corrections. Here, the proportional band  $X_p$  of the MA controller needs to be set as wide as possible so that the wider range of cooler OA can be utilized. Referring to Figure. 3.10,  $T_1$  is the base value that ensures the HVAC system is still in the cooling mode.  $6^{\circ}\text{C}$  is applied to  $T_1$ , which equals to the chilled water supply temperature setpoint.  $T_2$  is the temperature triggers OAF to its minimum position.  $25^{\circ}\text{C}$  is applied to  $T_2$ ,

which equals to the zone temperature setpoint. In addition, the hysteresis effect is defined to have a 1 K band. Thus,  $X_p$  is set as 18 K for the MA controller and thus the controller could allow as low as 6°C OA inlet, which would significantly reduce the cooling load of the coil.

### 3.3 Waterside System

The waterside system provides chilled water to the cooling coil. Often, large commercial buildings use more than one chiller to satisfy cooling demand; thus, properly modeling chiller sequencing is important to evaluate capacity limits of chillers. Simply employing one infinite-capacity chiller would introduce significant errors. In addition, storage effects in the piping system of chilled water loops is modeled as a first-order state-space model with an adjustable time constant of 10 min. Referring to Figure. 3.1, chilled water storage is modeled as storage tanks located in the middle of both supply and load paths.

#### 3.3.1 Chilled Water Loop Storage

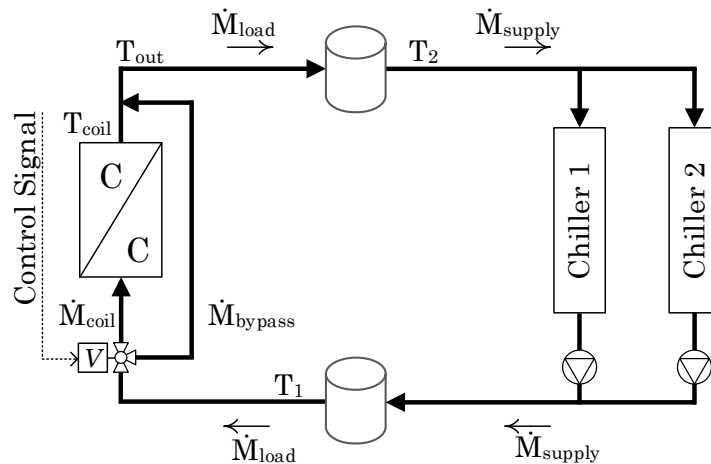


Figure 3.11: Waterside system with chilled water storage

The chilled water loop storage of Figure. 3.1 is provided in a more detailed drawing in Figure. 3.11 for clarity. The storage is assumed as fully mixed stirred tanks so that the temperature

inside is uniform and equals to the outlet temperature (i.e.,  $T_1$  and  $T_2$  of Storage 1 and Storage 2, respectively). Based on an energy balance,  $T_1$  and  $T_2$  can be formulated in Equation 3.25 and Equation 3.26 and rearranged in Equation 3.27 and Equation 3.27 with the assumption that water is incompressible. Here, state variables are  $T_1$  and  $T_2$ , chilled water supply temperature  $T_{chws}$  set at  $6^\circ\text{C}$ , storage tank volume  $V_1$  and  $V_2$  are both sized at  $60 \text{ m}^3$ , and volume flow rate on the supply side  $\dot{V}_{\text{supply}}$  and return side  $\dot{V}_{\text{load}}$  is set at  $0.1 \text{ m}^3/\text{s}$  when only one chiller is turned on and  $0.2 \text{ m}^3/\text{s}$  when both chillers are on.  $T_{\text{load}}$  is determined by the three-way valve and further based on conservation of mass that chilled water mass flow rate into the coil  $\dot{M}_{\text{coil}}$  and on the bypass  $\dot{M}_{\text{bypass}}$  is equal to the mass flow rate on the return path  $\dot{M}_{\text{load}}$ . In order to maintain DA temperature at its setpoint,  $\dot{M}_{\text{coil}}$  is actively regulated. Thus, the coil load variation is reflected to the supply side and varies the power of the chilled water loop. A state-space model is formulated for the storage effect in the chilled water loop in Equation 3.27 and Equation 3.27.

$$\rho_{\text{water}} V_1 \frac{dT_1}{dt} = \dot{M}_{\text{supply}} T_{\text{chws}} - \dot{M}_{\text{load}} T_1 \quad (3.24)$$

$$\rho_{\text{water}} V_2 \frac{dT_2}{dt} = \dot{M}_{\text{load}} T_{\text{load}} - \dot{M}_{\text{supply}} T_2 \quad (3.25)$$

$$\dot{T}_1 = \frac{\dot{V}_{\text{supply}}}{V_1} T_{\text{chws}} - \frac{\dot{V}_{\text{load}}}{V_1} T_1 \quad (3.26)$$

$$\dot{T}_2 = \frac{\dot{V}_{\text{load}}}{V_2} T_{\text{chws}} - \frac{\dot{V}_{\text{supply}}}{V_2} T_2 \quad (3.27)$$

### 3.3.2 Chiller Sequencing

The building's cooling load over the course of the day is satisfied by sequencing two chillers, Chiller 1 and Chiller 2. Chiller load  $\dot{Q}_{\text{ch}}$  and chiller capacity  $\dot{Q}_{\text{ch,max}}$  are normalized by dividing by the rated capacity  $\dot{Q}_{\text{ch,rated}}$  and are denoted as  $Q$  and  $Q_{\text{MAX}}$  in Equation 3.29 and Equation 3.30, respectively [29].  $\dot{Q}_{\text{ch,rated}}$  is achieved with ambient wet bulb temperature of  $24^\circ\text{C}$  and chilled water supply temperature of  $6^\circ\text{C}$  [29].  $Q_{\text{MAX}}$  is a function of  $T_{\text{chws}}$  and ambient wet bulb temperature  $T_{\text{wb}}$  [29]. Here,  $T_{\text{wb}}$  can be calculated with hourly  $T_o$  and  $\text{RH}_o$  [76]. In addition, power of a single chiller  $P_{\text{ch}}$  is normalized by the rated power  $P_{\text{ch,rated}}$  and denoted as  $P$  in Equation 3.31, which

is a function of  $Q$  and  $T$  [29]. Here,  $T$  is defined as the difference of the actual  $T_{wb}$  and  $T_{chws}$  over the difference of their rated values (i.e.,  $24^\circ\text{C}$  and  $6^\circ\text{C}$ , respectively) and denoted as  $T$  in Equation 3.31 [29].

$$Q = \frac{\dot{Q}_{ch}}{\dot{Q}_{ch,rated}} \quad (3.28)$$

$$Q_{MAX} = \frac{\dot{Q}_{ch,max}}{\dot{Q}_{ch,rated}} \quad (3.29)$$

$$P = \frac{\dot{P}_{ch}}{\dot{P}_{ch,rated}} \quad (3.30)$$

$$T = \frac{T_{wb} - T_{chws}}{T_{wb} - T_{chws}|_{rated}} \quad (3.31)$$

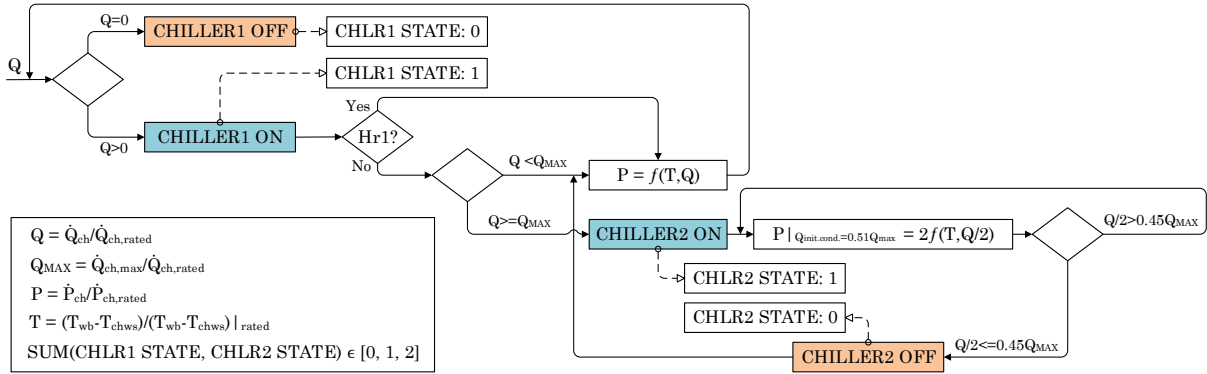


Figure 3.12: Sequencing of two chillers

Chiller sequencing rules are defined by the following five steps: 1) Chiller 1 starts when a non-zero  $Q$  is sensed. 2) In the first hour of operation, Chiller 2 is disabled and only Chiller 1 is enabled to minimize the peak demand that would be occurred for the first hour. 3) After the first hour, if  $Q$  is greater than  $Q_{MAX}$ , Chiller 2 is turned on; otherwise, only Chiller 1 is operating. 4) After Chiller 2 is turned on, Chiller 1 and Chiller 2 equally share load  $Q$  and both ramp up to serve the load from the same starting point (i.e., 51% of  $Q_{MAX}$ ). Therefore, turning on Chiller 2 requires extra time for Chiller 1 to ramp down and Chiller 2 to ramp up to the starting point; thus, frequent sequencing should be avoided. 5) To maintain both chillers operating, the equally shared

load by either chiller (i.e.,  $Q/2$ ) should be greater than 45% of  $Q_{MAX}$ ; otherwise, Chiller 2 is turned off and the sequencing logic return back to the scenario of only Chiller 1 is operating. The chiller on and off states are output as Boolean values. In addition, it also indicates what value should be applied to  $\dot{V}_{supply}$  and  $\dot{V}_{load}$  in Equation 3.27 and Equation 3.27.

### 3.4 Power-Consuming Subsystems

The power consumption of the modeled HVAC system includes the supply fan, return fan and the chilled water loop, which includes the power drawn from chillers, cooling tower fans and condenser water pumps [29]. The power consumption of the one floor model is multiplied by 70 for the power consumption of a 1 million square feet high-rise commercial building.

#### 3.4.1 Fan System Power Consumption

There are two types of fans used in commercial building: centrifugal and axial; most supply and return fans in high-rise commercial buildings are centrifugal type [65]. Supply and return fans equipped with VFDs can significantly reduce power consumption when the ventilation load is reduced since the fan power is proportional to the fan motor speed raised to the power of three as shown in Equation 3.8. Thus, demand controlled ventilation offers significant energy and cost savings that the payback period of installing VFDs is typically as short as two to three years. In this research, VFD controlled supply and return fans are required so that their power can follow the FR signal injections.

The AC induction motor is the working horse in commercial buildings. Supply fans, return fans, pumps, and elevators are all driven by induction motors. An induction motor can be viewed as a three-phase transformer; the only difference is that the secondary side is a short-circuited rotating rotor. The three-phase sinusoidal current on the stator creates a synchronously rotating magnetic field; thus, the rotating speed of the magnetic field is defined as the synchronous speed  $N_e$  [11].

$$N_e = 120f_e/N_p \quad (3.32)$$

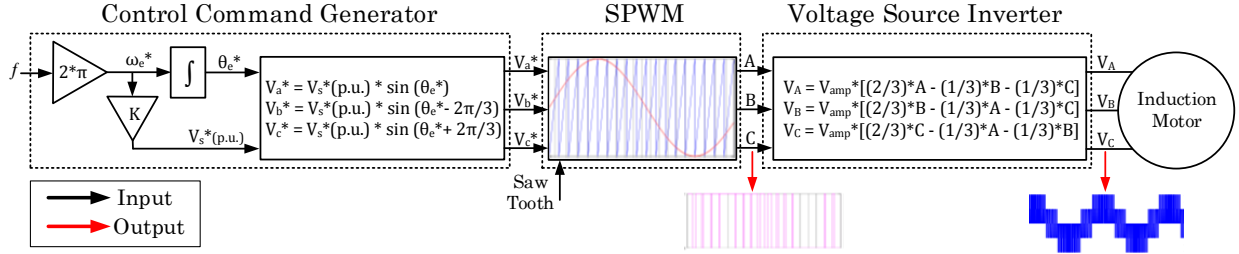


Figure 3.13: Variable frequency drive topology of the open-loop V/Hz control

Referring to Equation 3.32, the synchronous speed depends on the stator frequency  $f_e$  and the number of poles  $N_p$ . For a given induction machine, the number of poles does not change after manufactured; therefore, the synchronous speed only depends on the stator frequency. As the synchronously rotating magnetic field sweeps around the short-circuited rotor winding at speed  $N_e$ , current is induced on the rotor circuit [11]. According to Lenz's law, the rotor will move in the same direction as the rotating magnetic field. However, the rotor's rotating speed  $N_r$  will never reach the synchronous speed  $N_e$ . Therefore, the induction machine is also referred to as asynchronous. Thus, it is intuitive to vary the stator frequency by variable frequency drive (VFD) in order to vary the shaft speed referring to Equation 3.32. However, industrial practice shows that if  $V_s$  is kept constant while stator frequency is varied, the flux tends to saturate and causes excessive stator current and distortion of the flux wave [11]. Thus, the most prevailing VFD technology, V/Hz control, requires the stator voltage  $V_s$  to be varied proportionally with the stator frequency  $f$  for a constant air gap flux [11]. The VFD of V/Hz control is modeled based on the equations and descriptions of [11] and [66].

Referring to Figure 3.13, the VFD is composed of three major parts: 1) control command generator; 2) sinusoidal pulse width modulation (SPWM) controller; and 3) voltage source inverter [11, 66]. Referring to the static pressure control loop of Figure 3.3 and Figure 3.7, the controller

outputs the control signal  $f$  based on  $P_{\text{error}}$ ; this control signal is injected into the VFD for motor speed control. According to V/Hz control theory, control signal is translated into a sinusoidal control command carrying the command signal  $f$  based on a defined V/Hz constant [11]. This constant is typically maintained at the standard condition. For the commonly used 480Y/277V motor in commercial buildings, this constant  $K$  can be calculated with the standard frequency  $f$  of 60 Hz in Equation 3.33. Thus, a 3-phase sinusoidal control command is formulated in the Control Command Generator: 1) Magnitude  $V_s^*$  is the command frequency  $\omega_e$  multiplied by the constant (e.g., 1.725) for the stator voltage [11]. 2) Phase angle  $\theta_e^*$  is the integration of  $\omega_e$  [11]. Then, this 3-phase command signal directs the SPWM controller of the Voltage Source Inverter to generate a six-stepped voltage wave for motor speed control [11]. Note that the six-stepped voltage wave is different from typical sinusoidal waves from the utility. However, an induction motor is an inductive device that it prevents fast step changes of voltage and smoothies stepped waves just like sinusoidal waves.

$$K = \frac{V_s}{\omega_e} = \frac{460\sqrt{2}}{2 \cdot \pi \cdot 60} = 1.725 \quad (3.33)$$

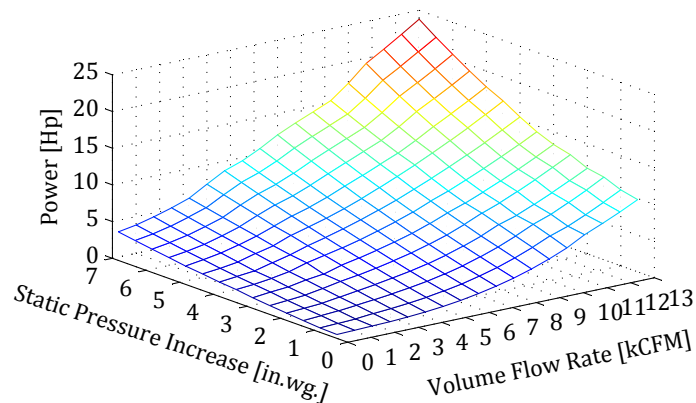


Figure 3.14: Supply fan motor power map

Referring to Figure. 3.14, the power consumption of a fan system is dependent not only 1) the volume flow rate of air (i.e., proportional to fan motor speed) but also 2) the static pressure

increase through the fan (i.e., determined by Equation 3.19 through the static pressure control loop of Figure. 3.7). Here, the power consumption map of a centrifugal fan is modeled based on manufacturer's data (SWB-222-Belt Drive), which is selected based on the total volume flow rate of the 5-zone model at the designed condition [23]. The VFD-controlled return fan power should follow the supply fan but on a smaller scale. A calibrated EnergyPlus model of a 1 million sq. ft high-rise commercial building is used to estimate the return fan power at 47% of the supply fan power consumption. The calculation results are converted to SI units in the simulation results.

### 3.4.2 Chilled Water Loop Power Consumption

The power consumption of the chilled water system is modeled based on an empirical model with parameters adjusted for the purpose of evaluating FR from a large commercial building [29]. The same EnergyPlus model is used as a surrogate for curve-fitting.  $Q_{MAX}$  and  $P$  are fitted based on the data generated from the EnergyPlus model simulation with a Chicago 2013 weather file converted to TMY3. The fitted  $Q_{MAX}$  and  $P$  are shown in Equation 3.34 and 3.35.  $Q_{MAX}$  is found to have a strong sensitivity to  $T_{chws}$  variations but only a very slight sensitivity to  $T_{wb}$ .  $P$  has a strong sensitivity to  $Q$  and the sensitivity to  $T_{chws}$  is dependent on the value of  $Q$ . When  $Q$  is less than 40%,  $P$  is found to be insensitive to  $T_{chws}$  variations.  $T_{chws}$  setpoint is maintained at 6 °C in simulations. The mean bias error (MBE) and the normalized root mean square error (NRMSE) of  $P$  is found equal to 0.00029376 and 0.0013, respectively for the 1699 hours of chiller operation of the simulated year of 2013.

$$Q_{MAX} = (6204.362 + 681.634T_{chws} - 19.497T_{chws}^2 + 1.843T_{wb} - 1.023T_{wb}^2 + 0.427T_{chws}T_{wb}) \cdot 10^{-4} \quad (3.34)$$

$$P_{MAX} = 0.1741901 + 0.0866872T - 0.4282460T^2 + 1.1601062Q - 0.5011509Q^2 + 1.4296213TQ \quad (3.35)$$

The combined power consumption of the supply fan, return fan and the chilled water loop is the aggregated power of the HVAC system. Therefore, the interactions between multiple HVAC

components and subsystems are considered in this aggregated value when setpoint of one particular subsystem is varied. The power components of the supply fan, return fan and CHW loop are scaled by a factor of 70 to represent the power response from a 1 million sq. ft. high-rise commercial building.

### 3.5 Model Validation

Validation is carried out in comparing the one-day simulation results of the Matlab/Simulink against a calibrated EnergyPlus model, which represents a 41-story skyscraper with total air-conditioned space area of 928,296 sq. ft. and is located in the loop of Chicago, IL. The EnergyPlus model was calibrated against the measured data of the actual building and it makes hour-to-hour real time optimized thermal mass control strategies for the actual building through online MPC. Thus, the simulation results of the EnergyPlus model should represent the actual building power consumption with high accuracy and is used as the surrogate for the Matlab/Simulink model to tune against. Model tuning is conducted by hand until good agreement between the two models is achieved in steady-state time periods. The tuning conducted include chiller sizing, duct system sizing, fan system sizing, adjustment of chiller sequencing point and adjustment of heat gains from people, light and plug loads. Simulation results of the two models are compared based on the weather of July 10<sup>th</sup>, 2013, whose outside dry-bulb temperature is plotted in Figure. 5.1. The simulated power consumption of both models are scaled up to represent that from a 1 million sq. ft. high-rise commercial building. Thus, a scaling factor of 70 is applied to the 5-zone model built in Matlab/Simulink and a scaling factor of 1.08 is applied to the EnergyPlus model.

Referring to Figure. 3.15, the simulated power consumption of the two building models are compared against each other with hourly average values. The hour showing on the horizontal axis is hour ending. Good agreement between the results of the two models is observed when both models reach steady-state (i.e., 11:00 to 18:00). The EnergyPlus surrogate model is observed to have the power consumption depressed in the first hour (6:00 to 7:00) but then rises much higher for the following three hours. On the other hand, the Matlab/Simulink model only spikes for the

first hour and steady-state is observed to start from the third hour. Two major reasons are found for mismatches between the two models:

- (1) The EnergyPlus model adopts a volume flow rate limit for the first hour to avoid fan power spikes for that hour. This limit is modeled according to the energy management system (EMS) rule implemented in the controlled building. However, the Matlab/Simulink does not have such a volume flow rate limit for the first hour, because it is not built on or calibrated against that actual building.
- (2) The EnergyPlus model has a complete condensing loop with two cooling towers included in the loop. However, the Matlab/Simulink employs the formula of an empirical model introduced in [29]. This model lumped the cooling tower efficiency into the chiller capacity and its power shown in Equation 3.34 and Equation 3.35, respectively

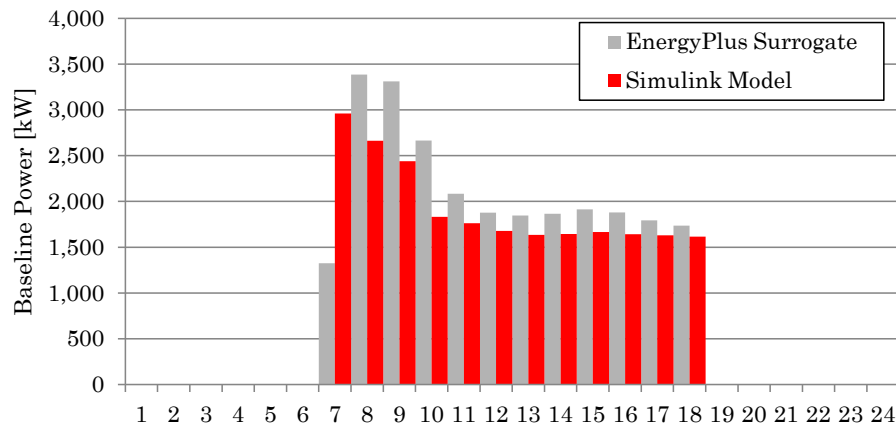


Figure 3.15: Validation of the baseline simulation results against the EnergyPlus Surrogate

Although the Matlab/Simulink model does not match well for the first a few hours after the HVAC system turned on in the baseline simulation, the hours that the EnergyPlus model operate in steady-state show good matches between the two models. This means the model in Matlab/Simulink gets the ballpark value of a 1 million sq. ft building correct when it reaches steady-state. Since frequency regulation (FR) from buildings are carried out during these steady-

state hours, the FR capacity estimation should also be in the correct range. Thus, the Matlab/Simulink is employed for exploring the potentials of commercial building HVAC systems for FR participation.

## Chapter 4

### Frequency Regulation Through Supervisory Control

The fast responsiveness of HVAC components and their controls enable commercial HVAC systems to provide FR from the demand side, if equipped with a high-level supervisory control that overrides the typical building operations in response to a FR signal. The supervisory control designed in this Chapter is based on PJM's performance-based regulation rules that are summarized in Chapter 2. Yet, key concepts and nomenclature are found similar across these pay-for-performance rules from different ISOs and RTOs as discussed in Chapter 2. Therefore, the supervisory control method developed in this Chapter should not be viewed as exclusively designed for or preferential to the PJM territory. The idea of the model-based supervisory control method is adaptable to other ISO and RTO regions with some adjustments.

#### 4.1 FR Signal Injection Methods

Four methods of FR signal injection are proposed that are believed to offer significant power responses from a whole-building participation: 1) static pressure ( $P_{\text{static}}$ ) setpoint, 2) zone temperature ( $T_{\text{zone}}$ ) setpoint, 3) discharge air temperature ( $T_{\text{DA}}$ ) setpoint and 4) outside air fraction (OAF) where the FR signal is superimposed on top of the OAF determined by the dry-bulb economizer. These four injection methods and their respective sensors are labeled in Figure. 3.1 and are varied in the fashion of Equation 4.1. Here,  $X$  is either the selected setpoints or the baseline OAF.  $\text{RegD}$  is in the range of 0 to 1 with 4-second resolution. The + sign applies to  $P_{\text{static}}$  setpoint and OAF (assuming  $T_{\text{OA}}$  is greater than the  $T_{\text{zone}}$  setpoint during FR hours but - sign is applied in the

economizer mode); whereas the - sign applies to  $T_{\text{zone}}$  setpoint and  $T_{\text{DA}}$  setpoint. The minimum requirement for selecting these methods is to provide at least  $\pm 100$  kW of total FR capability (TReg), achieving a performance score greater than 0.4 where the calculation rules are summarized in Chapter 2. TReg is affected by the range of setpoints deviation around the baseline setpoint along with the FR signal. This range is controlled by participation level (PL), a setpoint-specific value that is determined through simulations and is limited by the system physical characteristics and occupant comfort [78]. Taking the Pstatic setpoint for instance, the model would fail to converge if a participation level greater than 80% of baseline (i.e., baseline set at 250 Pa) was employed. Thus, 70% (i.e.,  $\pm 175$  Pa deviation range) is set as the maximum participation level for Pstatic setpoint. The same rationale holds true for participation levels of the other three setpoints. However, system capacity limits and thermal comfort are found to be the major limitations for those three PLs.

$$X_{\text{FR}} = X_{\text{baseline}} \pm \text{PL} \cdot \text{RegD} \quad (4.1)$$

The minimum and maximum OAF need to be adjusted for FR injection due to the minimum OAF (i.e., 20%) and the 100% OAF would both lockout the setpoint deviations. Therefore, the midpoint of OAF at the two extremes is adjusted in Equation 4.2 and Equation 4.3. Take 30% participation level for instance, the  $\text{OAF}_{\text{mid-min,FR}}$  is adjusted to 30% and  $\text{OAF}_{\text{mid-max,FR}}$  is adjusted to 70%. Thus, OAF is allowed to vary in the ranges of 0 to 60% and 40% to 100% at the two extremes. However, employing a participation level greater than 20% would result in greater HVAC power than the baseline on a hot summer day. Thus, a day-ahead simulation is required to set an hourly power consumption limit in order to avoid greater energy consumption and expenses from FR participation.

$$\text{OAF}_{\text{mid-min,FR}} = \max(20\%, \text{PL}) \quad (4.2)$$

$$\text{OAF}_{\text{mid-max,FR}} = 100\% - \text{PL} \quad (4.3)$$

A model based supervisory control method is proposed that predicts participation levels for

both singular and multiple setpoints following FR signal to direct the building operations in real-time for the highest revenue while comfort is maintained. Case studies of summer seasons are presented in Chapter 5. Similar control strategy can be employed for winter seasons if electric heating systems are employed in the controlled building. The supervisory control strategy provides a novel approach to dynamically integrate building operations into grid operations for FR.

## 4.2 Supervisory Control Method

Although a single building is a dynamic FR resource due to its faster ramping speed than generators as discussed in section 1.2, it is still different from typical capacity-limited resources. It does have many capacity limits or other types of limits that must be managed when providing FR. However, these limits are not as straightforward as design capacities shown on nameplates. Instead, these limits vary from day-to-day operations and are in many different forms. These include, for example, tenant comfort and air quality constraints, chiller and AHU sequencing protocols, capacity limits because of interdependent HVAC subsystems, and utility peak demand charges. To quantify the FR capability, building's baseline power is needed ahead of time for the submission to PJM at least one hour earlier [39]. Thus, a calibrated building simulation model is required to predict the baseline power and FR capacity in advance. In addition, the performance score requirement of PJM sets another limit that requires FR resources must score as high as possible; otherwise, the payment for FR participation would be reduced. Given the fact that the building HVAC system can receive FR signal injection from multiple methods (e.g., setpoints) and adoption of these methods would result in different responses. Thus, a model-based method is important that can simulate and evaluate the building's FR participation with many combinations of FR injection methods and various participation levels in advance. Then, based on the goal of pursuing the highest revenue or the highest performance score, the selected combination of FR injection methods and their respective participation levels are used to direct the HVAC system operation in the actual hour. Therefore, a model-based supervisory control method is proposed to 1) determine HVAC baseline power consumption and regulation capacity; 2) capture capacity limits of HVAC subsystems and

the interdependencies between these subsystems; and 3) determine the appropriate participation levels of employed FR methods in order to direct the HVAC system for FR in the actual hour. PJM's performance-based regulation rule mandates that resources' availability status, FR capacity and FR maximum and minimum information may be adjusted and submitted to PJM up until one hour ahead of the actual FR hour [39]. Therefore, simulations are conducted from two hours ahead of the actual FR hour by adopting the latest predictions of weather, pricing information and RegD signal to minimize economic penalties due to inaccurate predictions.

Referring to Figure. 4.1, the lower half of the figure shows how the supervisory control is carried out from hour to hour. The simulation of the baseline power consumption should start from beginning of the day to ascertain the thermal history based on the specific OA conditions and internal loads of that day. Simulations of supervisory control of each FR hour must be started at least two hours ahead of the FR hour considered. Because the building's baseline power consumption (i.e., EcoBasepoint) and its available regulation capacity (i.e., TReg) of the FR hour must be submitted to PJM at least one hour (60 min) ahead, at which the FR market closes for that hour [39]. Thus, this provides one hour period for 1) conducting simulations to determine the information for submission and 2) sending the information back to PJM. So simulation speed (i.e., time required for conducting simulations of one FR hour) is an important factor that affects the success of this method. In addition to the required information for PJM, another important outcome of the simulations the selected participation levels of each FR injection method must be recorded locally in order to direct the building operations in the actual FR hour. Then, based on the thermal history of the FR hour effected by the selected participation levels, simulations move on to the next FR hour, so on and so forth. Here, the FR period is selected from 9 AM to 5 PM because fairly steady-state response is observed during that period given the building HVAC system operation is scheduled from 6 AM to 6 PM and the occupied period is scheduled from 8 AM to 6 PM.

The upper half of Figure. 4.1 shows how the important information (for submission to PJM and directing building operation) are determined by supervisory control in each hour. Assume

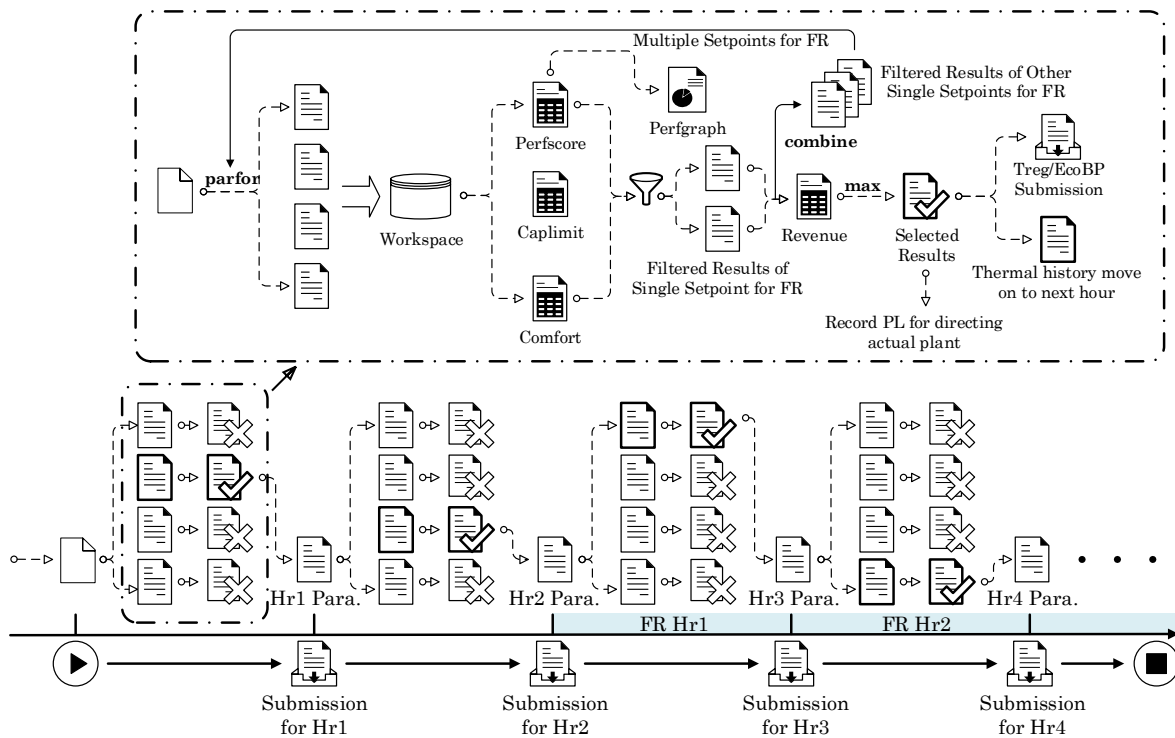


Figure 4.1: Supervisory control for single and multiple setpoints of FR injection

four participation levels are tested for a particular FR injection method, and only one of the four participation levels is selected through simulations; because it stimulates the building HVAC system more effectively and achieves the highest revenue as indicated by simulations. To find this particular participation level, the simulated results (i.e., building total power response) of the four participation levels need to be compared. In addition, three criteria are established to filter out the participation levels that would violate PJM's performance-based regulation rules, building operation codes or occupants' comfort. The three criteria are defined in the following:

- (1) **Performance score limit.** According to PJM's performance-based regulation rule, any FR resource must achieve an average performance score greater than 0.4 for the last 100 hours to maintain eligibility [40]. Thus, 0.4 is the lower limit to rule out participation levels that result in low performance scores. In addition, PJM also mandates that 0.75 is the lowest performance score for new resources that must score in initial tests [39]. Thus, the lowest performance score limit should be adjusted for different cases.
- (2) **Capacity limits.** participation levels that result in chillers sequencing more often than the baseline are ruled out. The rationale of limiting chiller sequencing is two-fold: 1) chiller sequencing takes extra time and energy. Referring to the description of chiller sequencing in section 3.3.2, sequencing requires both chillers engage and the entire process takes about 20 to 30 minutes in large buildings; 2) FR service provided by buildings are viewed as an add-on feature for FR participation with available capacity on top of the baseline HVAC operation schedules. Thus, two questions are of interest: Would the available capacity for FR meet the minimum requirement of performance-based regulation rule? What would be the extra revenue and benefit of a typical summer day? These two questions are answered with the simulation results in Chapter 5. If the building was operated with an optimized pre-cooling strategy, the cooling load would be shifted to early morning hours and the chiller capacity limit should be lifted up during the occupied hours; however, that is out of the focus of this research. It is worth noting that chiller sequencing is not must be

avoided. This research only focuses the FR market from the current day so it is important to limit the FR participation within the baseline operation schedules in order to avoid the possibility of triggering a higher peak demand charge. However, if a day-ahead simulation was conducted, the allowable FR capacity for each hour can be provided considering energy cost, peak demand limit and predicted FR revenue [67]. Thus, it reduces the possibility of triggering economic penalties by FR participation. In that case, the predicted hourly allowable FR capacity would be used to limit the range of FR participation and triggering of chiller sequencing would not be an issue any more. However, that is out of the focus of this research as well.

- (3) **Occupants' comfort zone.** The zone temperature  $T_i$  and relative humidity  $RH_i$  are compared with the ASHRAE 55 summer comfort zone to rule out participation levels that result in uncomfortable zone air conditions [4]. The baseline  $T_{zone}$  setpoint is set at 25 °C, allowing a  $\pm 1K$  maximum temperature deviation range that still resides inside the comfort zone.

These three filters rule out some of the participation levels but allowing the rest to proceed for revenue calculations with the PJM's hourly real time pricing data posted online. The participation level that can stimulate the building HVAC system to achieve the highest revenue is selected to direct the building's operation in the actual FR hour. For multiple injections, the filtered results from each single injections are combined as a participation level package, which is fed back to the model for simulations and filtering again. Since the system response from multiple FR injections is not simple additions from single injections due to the interactions and counteractions between HVAC subsystems.

In order to pursue the global objective (i.e., the highest revenue), single FR injections tend to drive the particular HVAC subsystem to its boundaries in order to stimulate a higher regulation capacity from building-wide participation. Multiple FR injections; however, stimulate several HVAC subsystems at the same time and thus each subsystem is less likely to be driven to its boundaries

in order to achieve the same level of regulation capacity. Thus, multiple injections may reduce the wear and tear of the HVAC systems for FR participation.

In addition, single FR injections tend to have less control on the counteractions between HVAC subsystems, such as counteractions between the airside and the waterside systems. When one particular subsystem is driven to respond to the FR signal, a comprehensive response of the HVAC system should be expected, which includes both interactions and counteractions between HVAC subsystems. If significant counteractions are resulted, the combined HVAC power response may be poor in terms of tracking the FR signal regardless how accurately the particular HVAC subsystem is. Multiple FR injections; however, stimulate HVAC subsystems simultaneously and thus more likely to direct the interconnected subsystems to the same direction with strengthened interactions and depressed counteractions. Thus, results of both single injections and multiple injections are presented in section V for comparison.

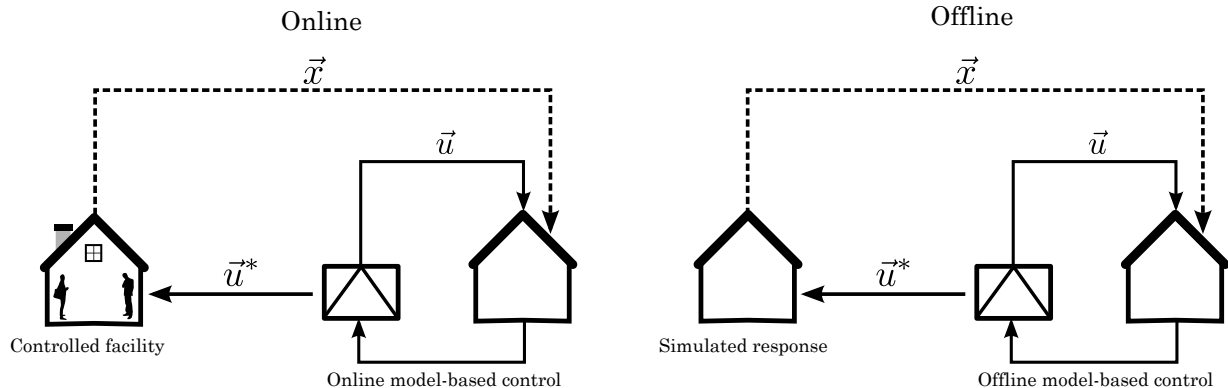


Figure 4.2: Comparison of online and offline model-based controls

Model-based supervisory controls can be evaluated either offline or online. Offline supervisory control has full knowledge of pricing and weather information and the physical characteristics of the modeled facility and its occupants. Thus, it makes “perfect” predictions and has no time constraints because it is essentially using an algorithm to make optimum operating strategies for a controlled model. Online supervisory control; in contrast, involves using a calibrated model simulated ahead of time to determine the optimum operation strategies of a controlled facility in

real time. Predictions are not perfect due to many unpredictable factors (e.g., controlled facility, weather, RegD data and pricing information) that impact energy consumption, FR capacity and performance score. Therefore, offline supervisory control provides an avenue to test the designed operation strategy and explore the system response in a cost effective way. Typically, model-based controls use optimization algorithms to find the optimum operation strategies. However, the supervisory control method proposed in this dissertation selects the best participation level packages from all simulated cases. Because of the complexity of the HVAC systems and the low-level controls of the modeled high-rise commercial building, adopting optimization algorithms is not an easy task and may not accelerate the computing time either. Therefore, section 6.3 proposes a potential solution for the online model-based controls by using forward predictions. The results presented in this dissertation will be focused on offline, so simulation speed is not that critical as online controls. However, accomplishing the simulation tasks of about one thousand simulations of one FR hour with various combinations of participation levels is attainable within one actual hour on a laptop computer. Here, a computer with i7-3632QM processor at 2.2 GHz and equipped with 12 GB memory and solid-state drive. Simulation of one FR hour takes only about 4 seconds. If parallel computing was used, the time consumed for simulations of many participation levels would be even shorter.

## Chapter 5

### Results

Simulation case studies are carried out based on a typical summer day of Chicago, IL and the real-time FR prices are in the middle range of the month (i.e., July 10<sup>th</sup>, 2013) as shown in Figure. 5.1. The weather file of Chicago is selected because it is a major metropolitan city in the PJM territory. The hourly clearing prices: RMCCP and RMPCP are posted online for payment calculations [41]. Simulations by offline supervisory control are conducted by assuming the controlled building is not bundled with other FR resources. In addition, FR market clearing and FR signal dispatching are not simulated but it is assumed that the controlled building is pre-selected in the FR market during the 8-hour scheduled period. Thus, the “hourly-integrated regulation MW” defined in PJM’s performance-based regulation manual equals the assigned regulation capacity (AReg) and also equals TReg under such conditions [78, 41, 19].

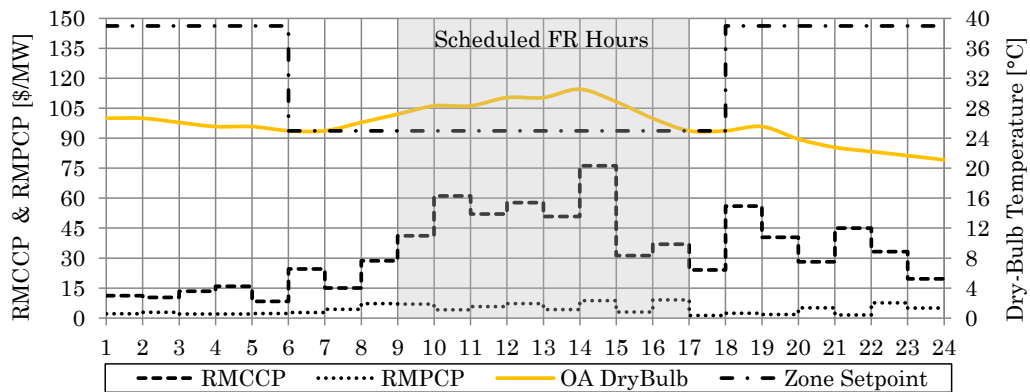


Figure 5.1: Outside dry-bulb temperature, baseline zone setpoint and FR prices of July 10<sup>th</sup>, 2013

As buildings are RegD following, the MR factor applies for the settlement calculation. An annual average of 3.1 is provided for the first year operation of performance-based regulation rule from October 2012 to October 2013 [22]. Thus, a value of 3.1 is adopted for all hours in the simulation of July 10<sup>th</sup>, 2013. Since November 2013, the hourly MR factor is posted on PJM's website along with the RMCCP and RMPCP pricing information [35]. The MR factor for April of 2014 indicates the average value of 2.9 and the maximum hourly value of 33.4 and a minimum hourly value of 1.3 [35]. Thus, simulations should be conducted again after the summer 2014 data is available in order to capture the dynamics of MR factor to the payment of FR.

The baseline setpoints are defined as the following:  $P_{\text{static}}$  setpoint is at 250 Pa,  $T_{\text{zone}}$  setpoint is at 25 °C,  $T_{\text{DA}}$  setpoint is at 13 °C and  $T_{\text{MA}}$  setpoint is at 13 °C to determine OAF based on  $T_{\text{RA}}$  and  $T_{\text{OA}}$  but limited to the range of 20% to 100%. Participation levels are selected for each FR injection method that are physically attainable but also large enough for significant system responses.  $P_{\text{static}}$  setpoint deviation is limited to  $\pm 175$  Pa for reliable responses from the model.  $T_{\text{zone}}$  setpoint deviation is limited to  $\pm 1$  K because any larger participation levels would not be deemed acceptable and significant variation of air volume flow rate in the duct system and zones is already observed.  $T_{\text{DA}}$  setpoint deviation is limited up to  $\pm 7$  K as suggested by a previous research on  $T_{\text{SA}}$  setpoint reset in a real building [72]. On this particular day with hot OA conditions, OAF deviation is limited to 20%. Thus, the OAF is allowed to vary from 0 to 40% and 60% to 100% at the two extremes. Adopting a participation level greater than 20% would allow more OA into the building than baseline on average and result in higher energy expenses. However, if a day with OA temperature falls below  $T_{\text{zone}}$  setpoint during the scheduled FR hours, a greater participation level of OAF could be potentially employed if the hourly FR capacity limit is provided from a day-ahead simulation. Here, the participation levels (PL) of all four methods are organized in the following vectors. The offline supervisory control determines the most profitable set of participation levels through simulations.

- PL of  $P_{\text{static}}$  setpoint: [25; 50; 75; 100; 125; 150; 175] Pa
- PL of  $T_{\text{zone}}$  setpoint: [0.1; 0.2; 0.3; 0.4; 0.5; 0.6; 0.7; 0.8; 0.9; 1] K
- PL of  $T_{\text{DA}}$  setpoint: [1; 2; 3; 4; 5; 6; 7] K
- PL of OAF setpoint: [16; 17; 18; 19; 20]

## 5.1 Case Study 1: Single Injection Results

An 8-hour (i.e., 9AM to 5PM) RegD signal profile with 4-second resolution from PJM's website is used for simulation. The results of performance score, FR capacity (i.e., TReg), revenue and response symmetry are all important to the evaluation of FR resource's response against FR signal. Single injection simulations allow evaluations of each methods individually thus provides the foundation of results analysis for the multiple injections conducted in section 5.3. Although RegD signal is injected into single setpoints, the combined response of interactions and counteractions between HVAC subsystems is important to the analysis.

For a one day simulation, the static pressure setpoint injection and the zone temperature setpoint injection can stimulate the building systems to achieve composite scores in the range of [0.8, 0.9]. These scores are very competitive compare to the scores achieved by the flywheels and batteries in PJM's market in 2012. The discharge air temperature setpoint injection and the outside air damper fraction superposition stimulate the building systems to achieve lower composite scores in the range of [0.6, 0.7].

The zone temperature setpoint injection can effectively stimulate the building systems for much higher FR capacities (and result in much higher revenue) because of the building-wide participation from both waterside and airside systems. The detailed analysis are provided in the following subsections.

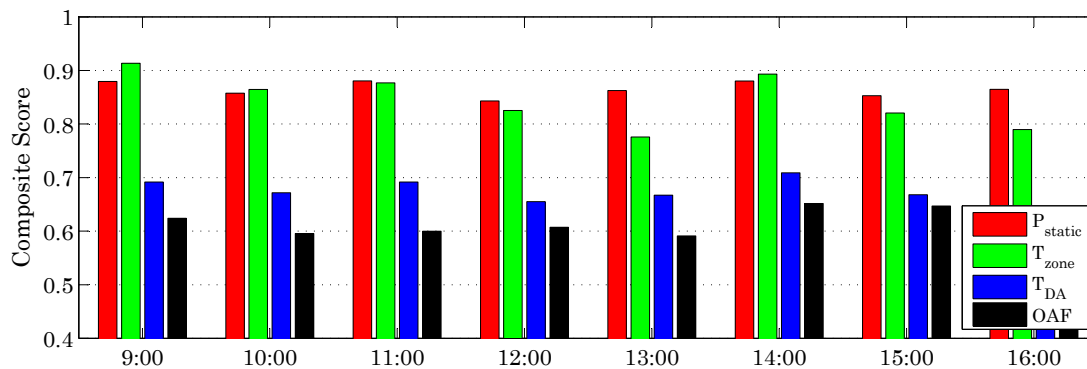


Figure 5.2: Hourly composite performance scores of the single injection methods

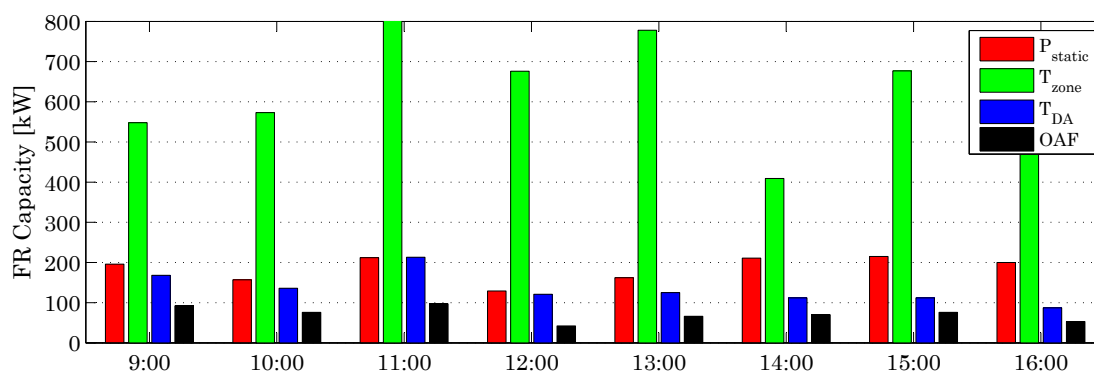


Figure 5.3: Hourly frequency regulation capacities of the single injection methods

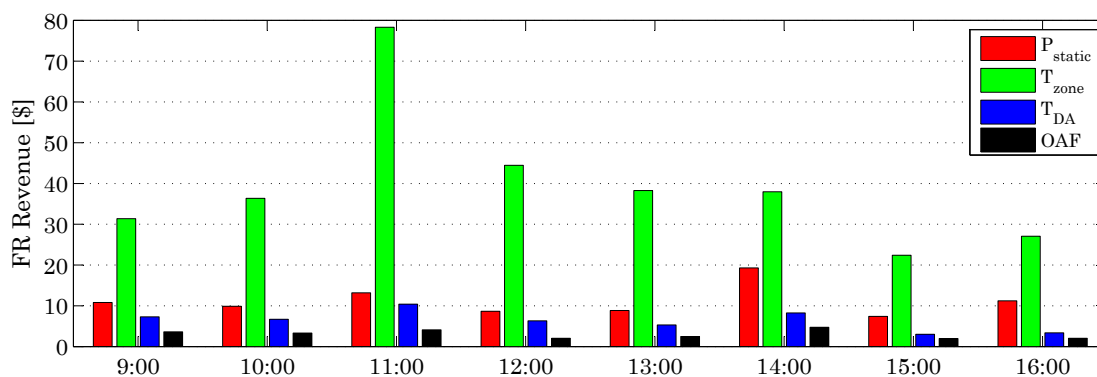


Figure 5.4: Hourly revenue of the single injection methods

Table 5.1: Summary of  $P_{\text{static}}$  setpoint injection

| Hour           | PL — $P_s$ | Performance Score |             |       | TReg<br>[kW] | Revenue<br>[\$] |           |
|----------------|------------|-------------------|-------------|-------|--------------|-----------------|-----------|
|                | [Pa]       | Composite         | Correlation | Delay |              |                 | Precision |
| 9              | 175        | 0.8795            | 0.9628      | 1     | 0.6758       | 196             | 10.81     |
| 10             | 175        | 0.8575            | 0.9567      | 1     | 0.6158       | 157             | 9.88      |
| 11             | 175        | 0.8804            | 0.9848      | 1     | 0.6564       | 212             | 13.18     |
| 12             | 175        | 0.8430            | 0.9901      | 1     | 0.5390       | 129             | 8.67      |
| 13             | 175        | 0.8624            | 0.9763      | 1     | 0.6108       | 162             | 8.86      |
| 14             | 175        | 0.8802            | 0.9530      | 1     | 0.6876       | 211             | 19.30     |
| 15             | 175        | 0.8528            | 0.8938      | 1     | 0.6647       | 215             | 7.39      |
| 16             | 175        | 0.8647            | 0.9669      | 1     | 0.6271       | 200             | 11.22     |
| Total Revenue: |            |                   |             |       |              |                 | \$89.30   |

### 5.1.1 $P_{\text{static}}$ Setpoint Injection

Table 5.1 summarizes the simulation results of the 8-hour FR participation. The results show that  $P_{\text{static}}$  setpoint injection directs the power of HVAC systems closely follow the injected RegD signal. This is revealed by the unity delay score and high composite scores of all FR hours. The combination of supply fan, return fan and the chilled water loop provides FR capacity greater than the minimum requirement of 100 kW and results in about \$90 revenue for the 8-hour of FR participation.

The hour of 14:00 to 15:00 is presented to show the system response in greater details. Figure. 5.5 shows the response of the combined output of the building (i.e., Response) versus the ideal response when following the FR signal exactly (i.e., Signal). A high performance score (i.e., 0.8802) indicates the  $P_{\text{static}}$  setpoint injection can effectively stimulate building HVAC systems to track the FR signal as revealed by high accuracy scores and precision scores. However, the Response tends to deviate from the Signal when the Signal is remained high at one direction for the time period from 14:52 to 14:58. Referring to Figure. 5.6, the supply and return fan power gradually decreases regardless of the Signal. Because the terminal damper's counteraction becomes significant when the static pressure setpoint is in a single direction for prolonged time period as shown in Figure. 5.7. The terminal dampers are regulated to reduce the volume flow rate of supply

air into zones to maintain steady zone temperature, which is revealed by the zone air (i.e., return air) plotted in Figure. 5.8. Referring to Figure. 5.6, the interaction with the chilled water loop becomes more significant with higher volume flow rate of supply air. Thus, when more supply air is requested for the five zones, the chilled water mass flow rate of the cooling coil also needs to be increased accordingly. This interaction results in both airside and waterside systems to participate and results in a FR capacity of  $\pm 211$  kW for this observed hour. The chilled water loop is observed to follow the Signal gradually due to the storage effect modeled with a time constant of 10 min.

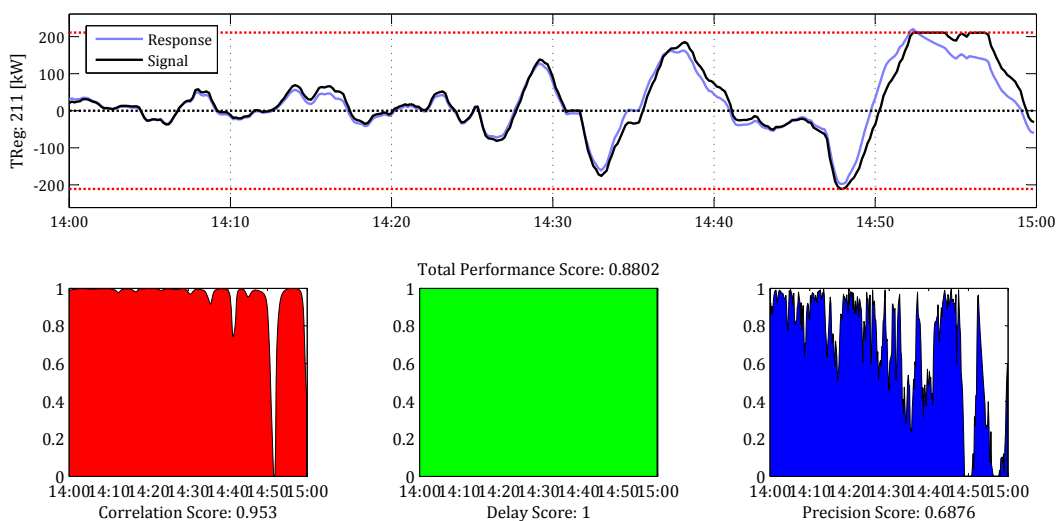


Figure 5.5: Performance score of  $P_{\text{static}}$  setpoint injection of a selected hour

### 5.1.2 $T_{\text{zone}}$ Setpoint Injection

Table 5.2 summarizes the simulation results of  $T_{\text{zone}}$  setpoint injection. The results show that this method can stimulate the HVAC system for significantly larger FR capacities of each hour and thus greatly increased revenue of \$316 for the same 8 hours of FR participation. Yet, the average composite score of the 8 hours is observed to be similar to that of the  $P_{\text{static}}$  setpoint injection. The participation levels are observed to be frequently limited by the chiller sequencing protocol and occupant's comfort.

The system response of the hour from 14:00 to 15:00 shows that the Response follows the

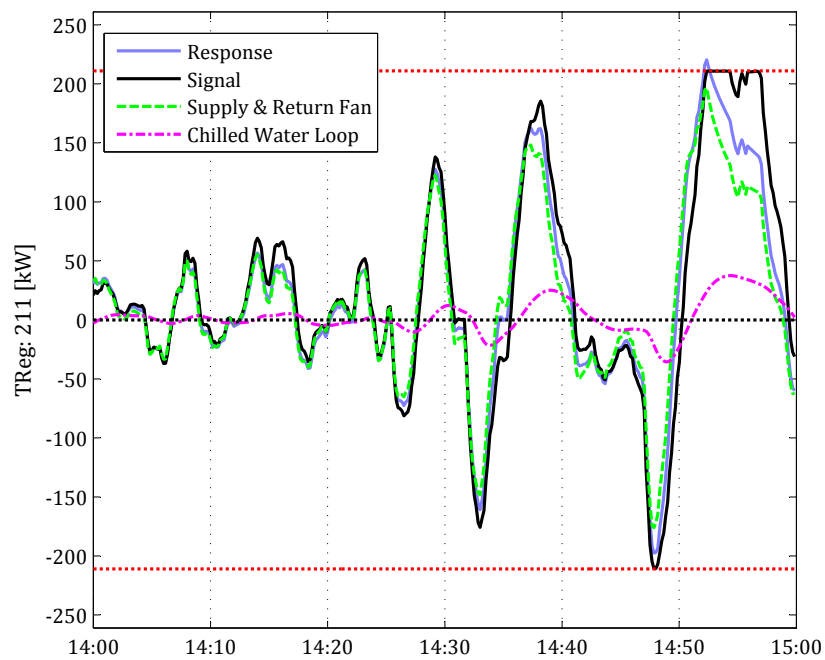


Figure 5.6: System dynamics of HVAC components of  $P_{\text{static}}$  setpoint injection

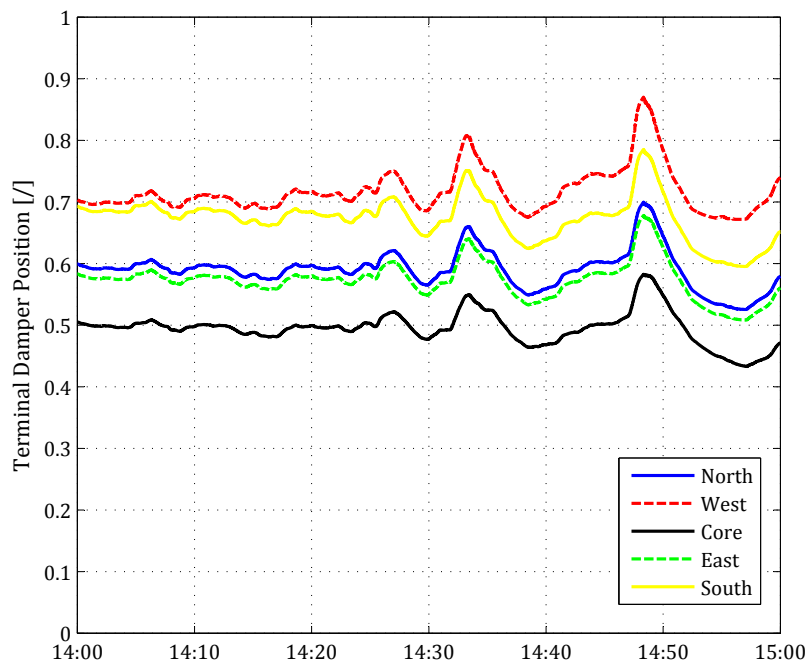


Figure 5.7: Terminal damper positions of  $P_{\text{static}}$  setpoint injection

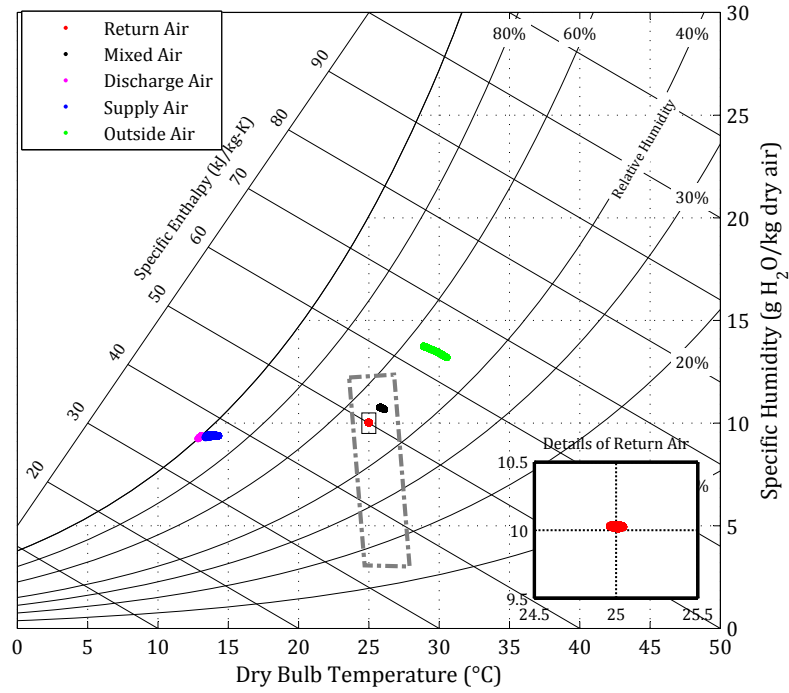


Figure 5.8: Air properties along the duct system of  $P_{\text{static}}$  setpoint injection

Table 5.2: Summary of  $T_{\text{zone}}$  setpoint injection

| Hour           | $PL - T_{\text{zone}}$ |           | Performance Score |        |           | TReg<br>[kW] | Revenue<br>[\$] |
|----------------|------------------------|-----------|-------------------|--------|-----------|--------------|-----------------|
|                | [K]                    | Composite | Correlation       | Delay  | Precision |              |                 |
| 9              | 0.4                    | 0.9134    | 0.9652            | 0.9991 | 0.7759    | 548          | 31.38           |
| 10             | 0.5                    | 0.8646    | 0.9642            | 0.9928 | 0.6367    | 573          | 36.36           |
| 11             | 1                      | 0.8768    | 0.9491            | 0.9992 | 0.6821    | 1265         | 78.31           |
| 12             | 0.8                    | 0.8252    | 0.9650            | 0.9981 | 0.5126    | 676          | 44.46           |
| 13             | 1                      | 0.7757    | 0.9154            | 0.9909 | 0.4208    | 778          | 38.26           |
| 14             | 0.3                    | 0.8932    | 0.9611            | 0.9999 | 0.7185    | 409          | 37.96           |
| 15             | 0.8                    | 0.8205    | 0.9101            | 0.9933 | 0.5582    | 677          | 22.39           |
| 16             | 0.7                    | 0.7896    | 0.9403            | 0.9753 | 0.4533    | 528          | 27.06           |
| Total Revenue: |                        |           |                   |        |           |              | \$316.18        |

Signal closely as revealed by high correlation, delay and precision scores (Figure. 5.9). However, the Response tends to overshoot in the positive direction and undershoot in the negative direction. Here, positive direction implies  $T_{\text{zone}}$  setpoint depression downward in response to regulation up and vice versa. The overshoot is because setting a lower  $T_{\text{zone}}$  setpoint causes the HVAC system to work harder and requires extra time to turn back when the Signal changes directions. The undershoot is observed mostly from the supply and return fan components in Figure. 5.10. As the RegD signal dips abruptly during time periods of 14:31 to 14:35 and 14:45 to 14:50, the  $T_{\text{zone}}$  setpoint quickly resets to  $25.3^{\circ}\text{C}$  (i.e., a 0.3 K participation level is selected for this hour). However, the zone temperature is not able to follow the setpoint in such a short time period. This causes the error term  $T_{\text{error}}$  (i.e., input to the zone temperature controller on the outer-loop of the cascade controllers) to accumulate very quickly and trigger the volume flow rate controller on the inner loop to push dampers to close. Referring to Figure. 5.11, when  $T_{\text{error}}$  rises fast but the zone temperature rises slow (e.g., the core zone), the control signal output of the zone temperature controller can become negative. Since this output signal sets the floating setpoint of air volume flow rate of the inner loop, its value must be positive. Thus, the negative values are saturated with a minimum value of zero. Under such conditions, the saturated volume flow rate is requested to the supply fan and thus the terminal dampers cannot be motorized (as well as the fan power) to respond the Signal. Referring to Figure. 5.12, the zone air is deviated in the range of around  $-0.25\text{ K}$  to  $0.2\text{ K}$  — a wider range of zone air disturbance due to higher volume flow rate of air into the zones. However, the zone air is still observed inside the comfort zone.

### 5.1.3 $T_{\text{DA}}$ Setpoint Injection

Table 5.3 summarizes the simulation results of  $T_{\text{DA}}$  setpoint injection. The results show smaller FR capacity and lower performance scores compare to the previous two methods. Thus, less revenue (i.e., approximately \$50) results from the same 8 hours of FR participation. The participation levels determined by supervisory control is found occasionally limited by the chiller sequencing protocol.

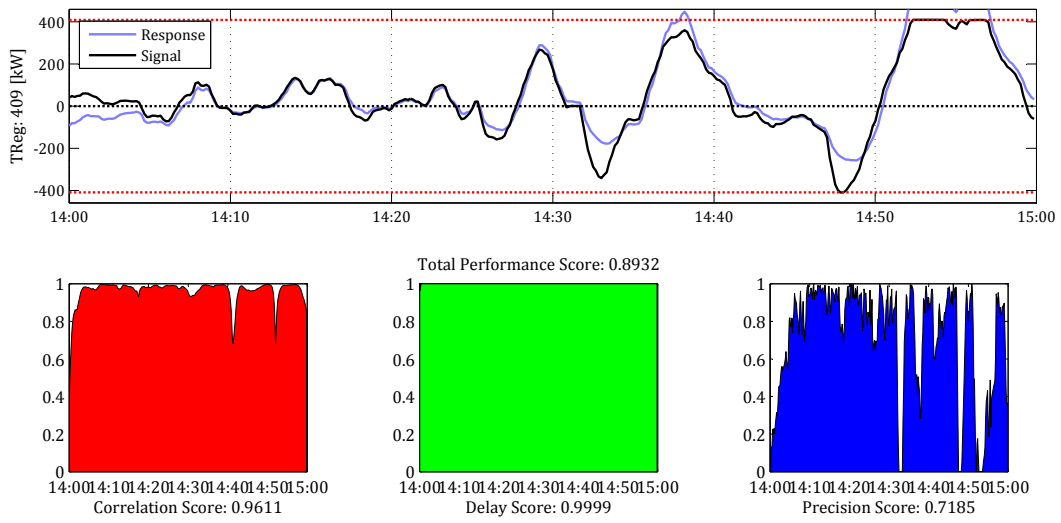


Figure 5.9: Performance score of  $T_{zone}$  setpoint injection of a selected hour

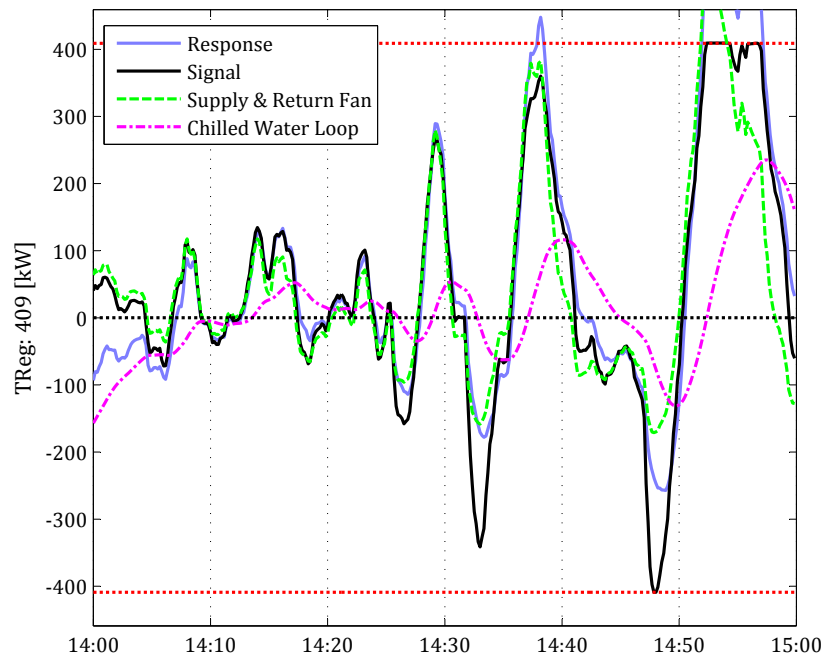


Figure 5.10: System dynamics of HVAC components of  $T_{zone}$  setpoint injection of a selected hour

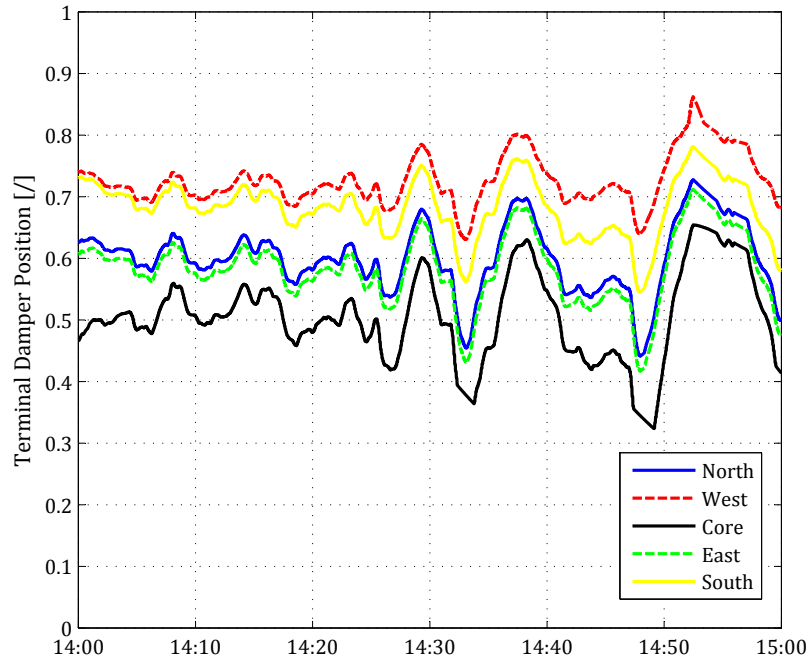


Figure 5.11: Performance score of  $T_{zone}$  setpoint injection of a selected hour

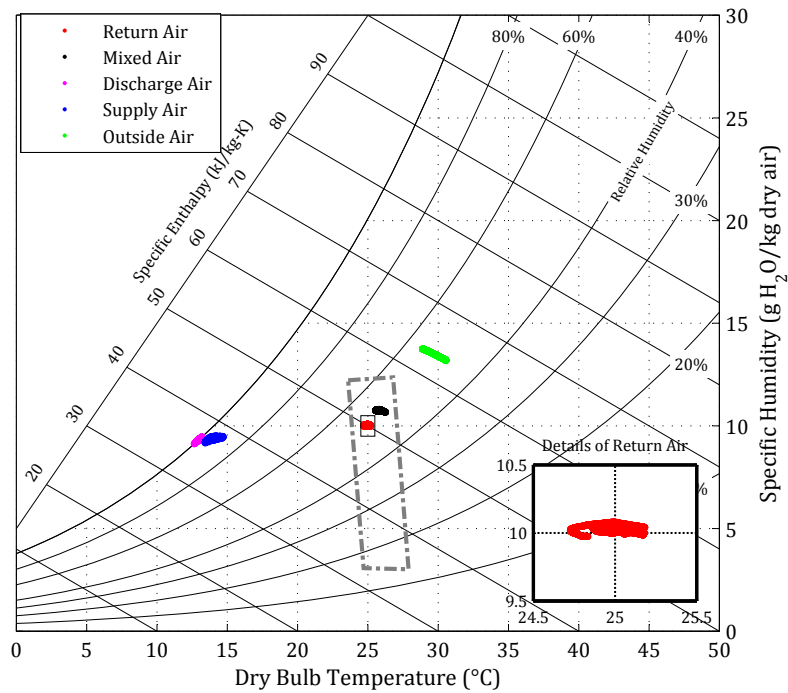


Figure 5.12: Terminal damper positions of  $T_{zone}$  setpoint injection of a selected hour

Table 5.3: Summary of  $T_{DA}$  setpoint injection

| Hour           | $PL - T_{DA}$ |           | Performance Score |        |           | TReg<br>[kW] | Revenue<br>[\$] |
|----------------|---------------|-----------|-------------------|--------|-----------|--------------|-----------------|
|                | [K]           | Composite | Correlation       | Delay  | Precision |              |                 |
| 9              | 6             | 0.6917    | 0.8045            | 0.9139 | 0.3566    | 168          | 7.29            |
| 10             | 7             | 0.6716    | 0.7839            | 0.9260 | 0.3050    | 136          | 6.70            |
| 11             | 7             | 0.6918    | 0.7537            | 0.9376 | 0.3840    | 213          | 10.40           |
| 12             | 7             | 0.6552    | 0.8049            | 0.9344 | 0.2262    | 121          | 6.32            |
| 13             | 7             | 0.6671    | 0.7758            | 0.9018 | 0.3238    | 125          | 5.29            |
| 14             | 5             | 0.7088    | 0.8391            | 0.9140 | 0.3734    | 112          | 8.25            |
| 15             | 5             | 0.6679    | 0.7408            | 0.9039 | 0.3591    | 112          | 3.01            |
| 16             | 7             | 0.5981    | 0.6876            | 0.8750 | 0.2316    | 87           | 3.38            |
| Total Revenue: |               |           |                   |        |           |              | \$50.64         |

Referring to Figure. 5.14, the counteractions between the airside system and the waterside system dominate the HVAC system dynamics. By adjusting  $T_{DA}$  setpoint, the chilled water mass flow rate into the cooling coil is varied. Thus, the air volume flow rate (as well as fan power) must be counteracted in order to meet the zone cooling loads. Thus, significant portion of the power movement of the airside and the waterside systems are canceled out by each other — a significant waste of energy. Therefore, this method is not suggested to be employed individually. However, if the counteraction of the supply and return fan could be limited but maintaining the zone air inside occupants' comfort zone, the chilled water loop alone seems to provide acceptable tracking of the Signal. Thus, the  $T_{DA}$  setpoint injection method combined with other methods is still worth to evaluate. Referring to Figure. 5.15, The zone air is observed to be deviated vertically on the psychrometric chart because of the  $T_{DA}$  setpoint variation brings in chilled water mass flow variations into the cooling coil. Thus, the humidity ratio of the discharge air, supply air and zone air are varied, which are detailed on Figure. 5.15.

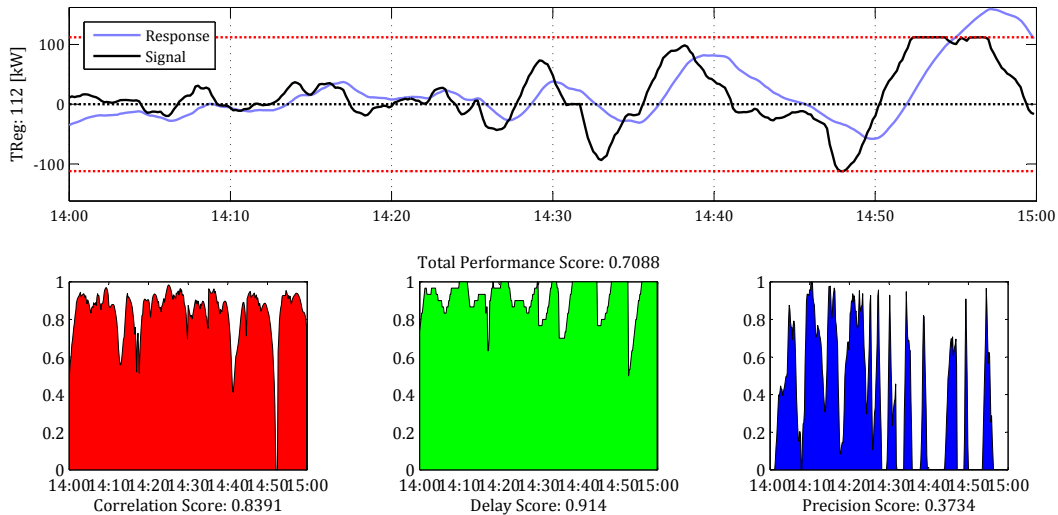


Figure 5.13: Performance score of  $T_{DA}$  setpoint injection of a selected hour

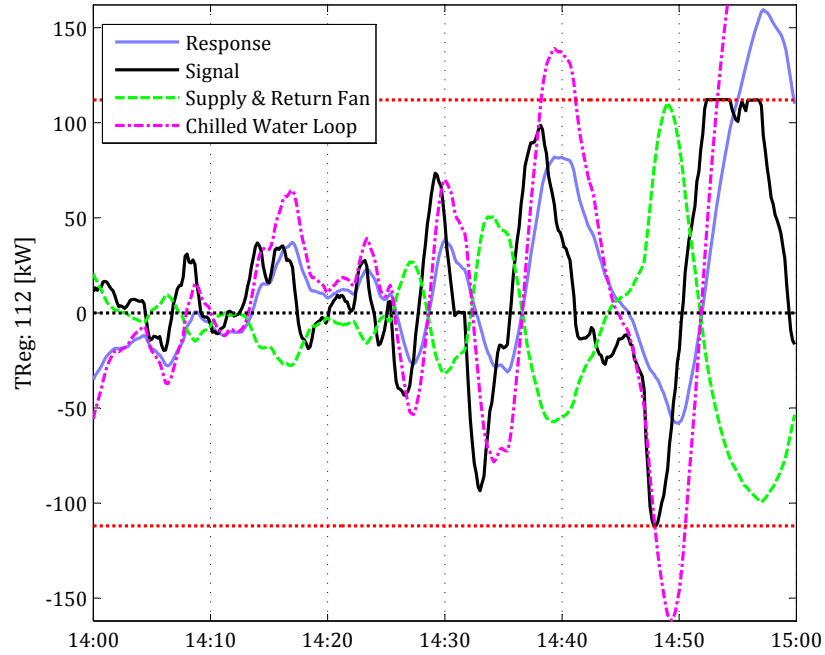


Figure 5.14: System dynamics of HVAC components of  $T_{DA}$  setpoint injection

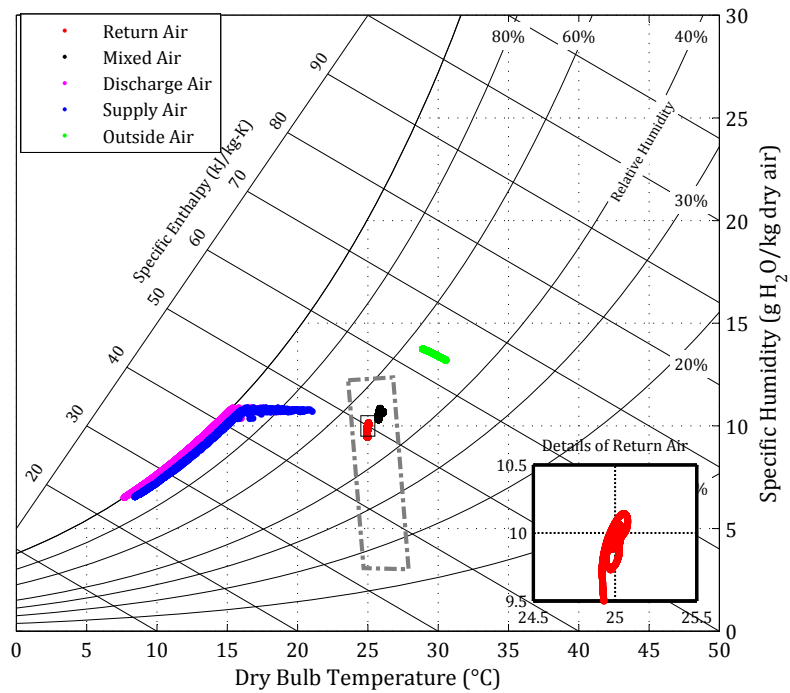


Figure 5.15: Air properties along the duct system of  $T_{DA}$  setpoint injection

Table 5.4: Summary of OAF superposition

| Hour           | PL — OAF | Performance Score |             |        |           | TReg<br>[kW] | Revenue<br>[\$] |
|----------------|----------|-------------------|-------------|--------|-----------|--------------|-----------------|
|                | [%]      | Composite         | Correlation | Delay  | Precision |              |                 |
| 9              | 20       | 0.6240            | 0.7631      | 0.8267 | 0.2822    | 92           | 3.60            |
| 10             | 20       | 0.5957            | 0.7167      | 0.8501 | 0.2202    | 76           | 3.32            |
| 11             | 20       | 0.5999            | 0.6661      | 0.8567 | 0.2768    | 97           | 4.11            |
| 12             | 20       | 0.6073            | 0.7709      | 0.8283 | 0.2226    | 42           | 2.03            |
| 13             | 20       | 0.5912            | 0.7195      | 0.8247 | 0.2295    | 66           | 2.47            |
| 14             | 20       | 0.6517            | 0.7969      | 0.8285 | 0.3297    | 70           | 4.74            |
| 15             | 20       | 0.6470            | 0.7612      | 0.8467 | 0.3332    | 76           | 1.98            |
| 16             | 20       | 0.5918            | 0.6669      | 0.8208 | 0.2878    | 53           | 2.04            |
| Total Revenue: |          |                   |             |        |           |              | \$24.29         |

### 5.1.4 OAF Superposition

Table 5.4 summarizes the simulation results of the OAF superposition method. It is worth noting that this method is not injected to a setpoint; rather, the dynamic RegD signal is superimposed on top of the OAF, which is determined by the MA temperature controller. The results show that the Response can only loosely track the Signal as revealed by low performance scores because OAF is determined by an open-loop  $T_{MA}$  controller with a proportional band of 18 K (described in section 3.2.3). However, a closed-loop control for OAF is not possible because both  $T_{OA}$  and  $T_{RA}$  are not in direct control of the  $T_{MA}$  controller. In addition, the FR capacity of all the 8-hour participation are less than 100 kW; thus, this method is not suggested to be employed individually.

Referring to Figure. 5.17, only the power of the chilled water loop contribute to the Response through regulating the cooling coil load. The supply and return fan power is not stimulated by this method. Thus, adding  $P_{static}$  setpoint injection along with the OAF superposition would be a reasonable solution to improve the Response. Referring to Figure. 5.18, the zone air is not disturbed by this method since the air volume flow rate into the zones are not affected.

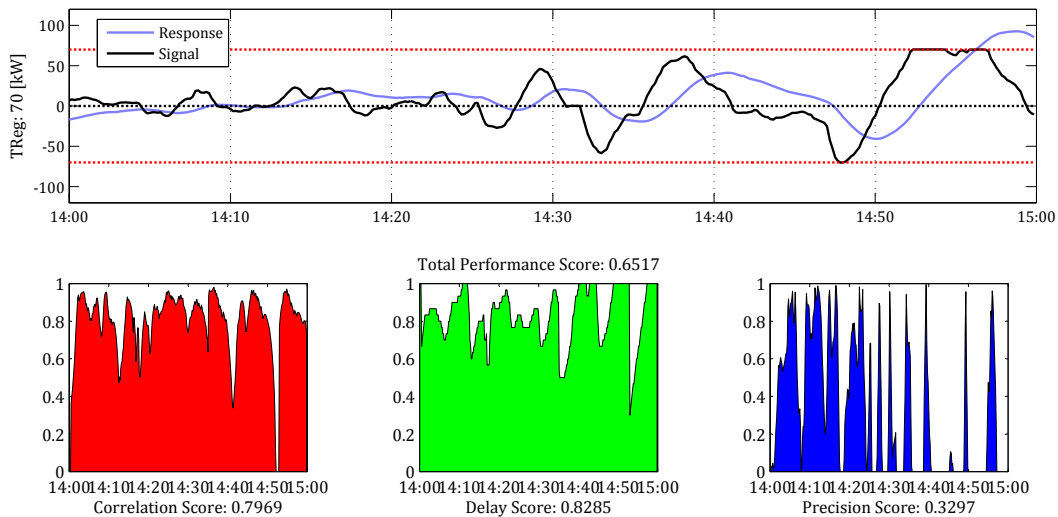


Figure 5.16: Performance score of OAF superposition of a selected hour

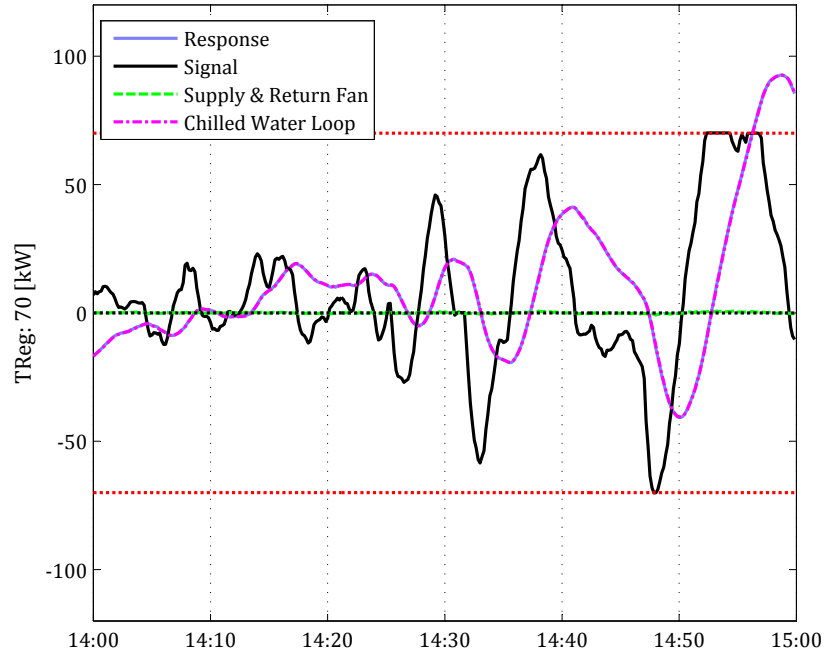


Figure 5.17: System dynamics of HVAC components of OAF superposition

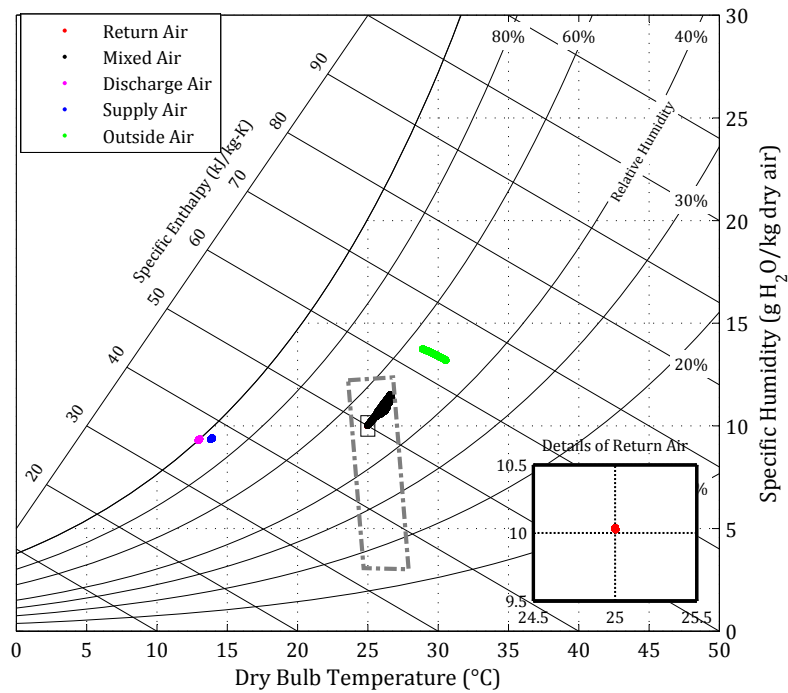


Figure 5.18: Air properties along the duct system of OAF superposition

## 5.2 Summary of Single Injections

The single injection case studies investigated the four proposed FR injection methods individually. Although each method has its own strengths and weaknesses, the  $P_{\text{static}}$  setpoint injection and the  $T_{\text{zone}}$  setpoint injection methods are found more effective to stimulate building HVAC systems for FR as revealed by larger FR capacity and higher revenue on the selected day. The  $T_{\text{DA}}$  setpoint injection and the OAF superposition methods are found more suitable for being combined with other methods but for different reasons. Here, the  $T_{\text{DA}}$  setpoint injection method needs to be combined with other methods to depress the counteractions between the airside system and the waterside system; whereas; the OAF superposition method needs to be combined with other methods to increase the FR capacity and performance score.

The four proposed methods for FR injection are found eventually reduced to only two effective points: 1) supply and return fan speed and 2) chilled water mass flow rate into the cooling coil. Thus, any single injection method more directly stimulate these two effective points for FR can reduce the impact of counteractions between subsystems and reach higher performance scores. However, these two effective points should not be adjusted directly; otherwise, the building operation would violate chiller, AHU and control protocols or occupants' comfort. Thus, counteractions observed in the results are actually important to maintain the building HVAC operation in a reasonable range. Therefore, supervisory control of multiple injections is important to investigate that takes the advantage of interactions between HVAC subsystems for a global optimum solution. The counteractions between airside and waterside systems are expected to be depressed by injecting the FR signal into the airside system and waterside system simultaneously in order to override both sides for the movement in response to the Signal.

## 5.3 Case Study 2: Multiple Injection Results

The single injection results indicate that larger participation levels push the HVAC system to its boundaries and takes longer time to follow the FR signal when signal changes directions. On the

other hand, smaller participation levels allow better responses to abrupt changes of FR signal but sacrifice FR capacity and revenue. Since performance score and FR capacity are both important to the revenue calculation, a comprehensive package of participation levels from multiple FR signal injections takes advantage of interactions between HVAC subsystems and is expected to achieve the global optimum solution. Although the participation levels for each method in this package may not be as large as the value that it should have reached in its single injection solution, the FR capacity and revenue from the combined resources reach their maximum.

Six multiple injection packages are evaluated. Combinations of two methods are evaluated first; then followed by evaluations of three methods and all four methods. The single injection results show that the  $P_{\text{static}}$  setpoint injection result in high performance scores with symmetrical Response and therefore a promising method to improve the results of all the other three methods. Thus, the evaluations of multiple injection methods are carried out with the  $P_{\text{static}}$  setpoint injection plus the other three methods individually or simultaneously. Referring to Figure. 5.19, multiple injections can improve the performance score than single injections. The six multiple injection packages can stimulate the building systems to achieve composite scores in the range of [0.8, 0.9] on average. The FR capacity and revenue from a multiple injection package is also improved than any of the single injections of that combined package.

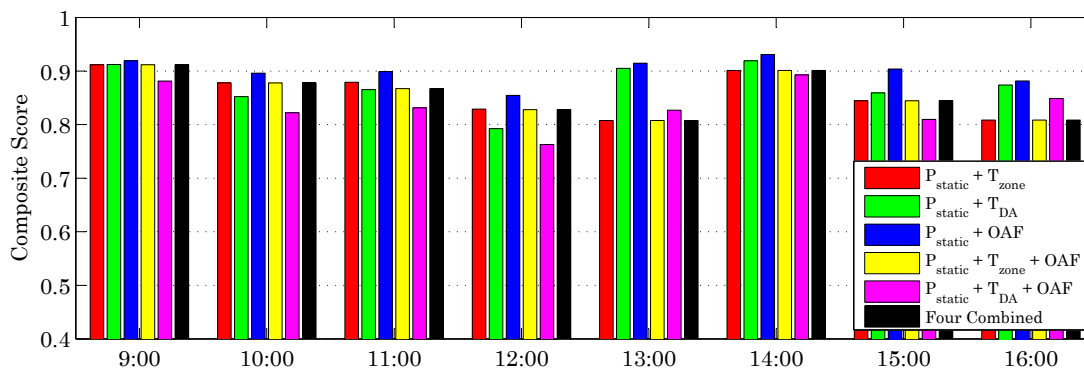


Figure 5.19: Hourly composite performance scores of the multiple injection methods

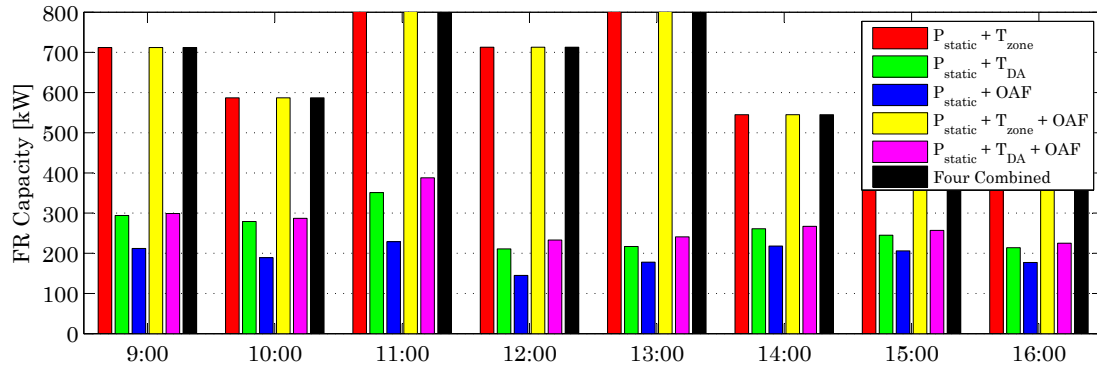


Figure 5.20: Hourly frequency regulation capacities of the multiple injection methods

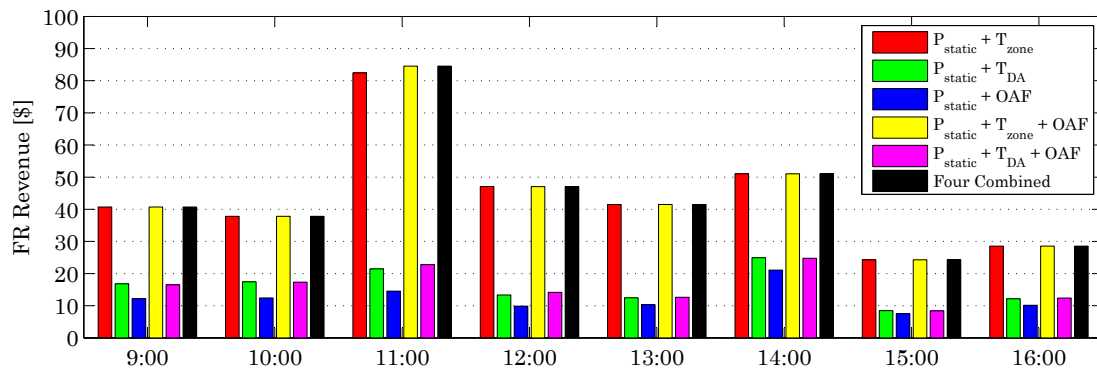


Figure 5.21: Hourly composite performance scores of the multiple injection methods

Table 5.5: Summary of two methods combined:  $P_{\text{static}}$  setpoint and  $T_{\text{zone}}$  setpoint

| Hour                  | Participation Level      |                       | Performance Score |             |        |           | TReg [kW]       | Revenue [\$] |  |
|-----------------------|--------------------------|-----------------------|-------------------|-------------|--------|-----------|-----------------|--------------|--|
|                       | $P_{\text{static}}$ [Pa] | $T_{\text{zone}}$ [K] | Composite         | Correlation | Delay  | Precision |                 |              |  |
| 9                     | 175                      | 0.4                   | 0.9118            | 0.9759      | 1      | 0.7594    | 712             | 40.70        |  |
| 10                    | 175                      | 0.4                   | 0.8778            | 0.9745      | 0.9985 | 0.6605    | 587             | 37.82        |  |
| 11                    | 175                      | 1                     | 0.8791            | 0.9568      | 1      | 0.6804    | 1328            | 82.42        |  |
| 12                    | 175                      | 0.8                   | 0.8289            | 0.9673      | 0.999  | 0.5204    | 713             | 47.10        |  |
| 13                    | 175                      | 0.9                   | 0.8076            | 0.9391      | 0.9968 | 0.4870    | 810             | 41.48        |  |
| 14                    | 175                      | 0.3                   | 0.9011            | 0.9684      | 1      | 0.7349    | 545             | 51.03        |  |
| 15                    | 175                      | 0.7                   | 0.8445            | 0.9295      | 0.9974 | 0.6067    | 713             | 24.27        |  |
| 16                    | 175                      | 0.6                   | 0.8085            | 0.9604      | 0.9794 | 0.4857    | 544             | 28.54        |  |
| <b>Total Revenue:</b> |                          |                       |                   |             |        |           | <b>\$353.36</b> |              |  |

### 5.3.1 Two Methods Combined: $P_{\text{static}}$ Setpoint and $T_{\text{zone}}$ Setpoint

Table 5.5 summarizes the results of combined response through  $P_{\text{static}}$  setpoint and  $T_{\text{zone}}$  setpoint injection. Compared to Table 5.2 of the single  $T_{\text{zone}}$  setpoint injection summary, adding the  $P_{\text{static}}$  setpoint injection on top of the  $T_{\text{zone}}$  setpoint injection improves the performance score, FR capacity and revenue of every single hour of the 8-hour FR participation. In addition, smaller participation levels of the  $T_{\text{zone}}$  setpoint injection is observed for 4 out of the 8 hours due to capacity limits of many forms. Thus, two methods are combined interactively but are not simple additive. The revenue is observed to increase by about 12% compare to that of the  $T_{\text{zone}}$  setpoint injection alone.

The similar asymmetrical Response is observed in Figure. 5.22. Although adding the  $P_{\text{static}}$  setpoint injection slightly corrects the asymmetrical situation as revealed by the improved correlation and delay scores in Table 5.5, the fact that causes the overshoot and undershoot remains unchanged. Referring to Figure. 5.23, the overshoot is observed when the Signal is increased abruptly, which pushes the HVAC system to its boundaries and takes longer time when the Signal changes directions. Referring to Figure. 5.24, the terminal damper of the core zone is still observed to be saturated because the  $T_{\text{zone}}$  setpoint still rises fast compared to the zone temperature. Thus, the combination of two methods bring in each individual's strengths (e.g., the fast-ramping of the

$P_{\text{static}}$  injection and the large FR capacity of the  $T_{\text{zone}}$  injection) and weaknesses (e.g., counteractions of both methods) into the combined Response. In addition, the Response of the  $T_{\text{zone}}$  setpoint injection is observed to dominate the combined Response because of its capability of stimulating a larger FR capacity.

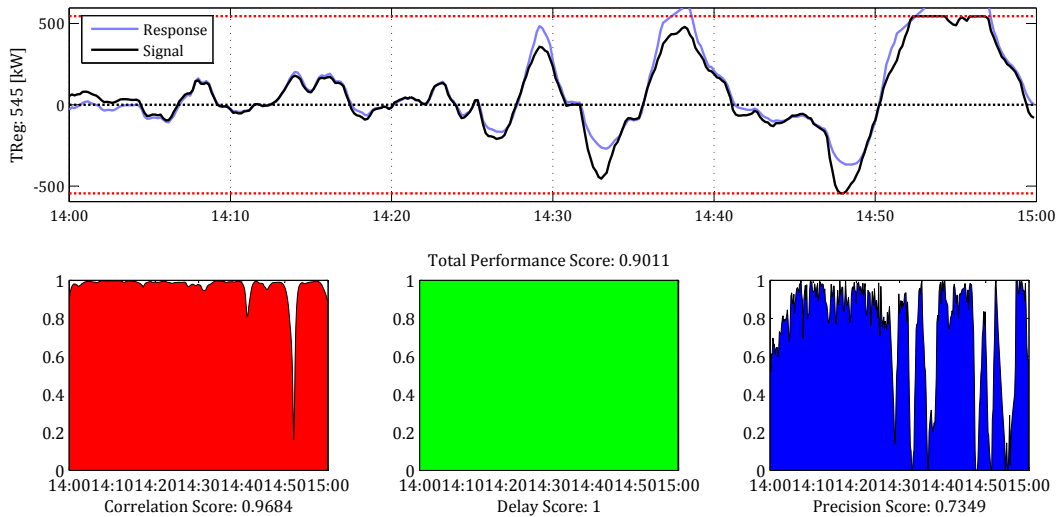


Figure 5.22: Performance score of  $P_{\text{static}}$  setpoint and  $T_{\text{zone}}$  injection

### 5.3.2 Two Methods Combined: $P_{\text{static}}$ Setpoint and $T_{\text{DA}}$ Setpoint

Table 5.6 summarizes the results of combined response through  $P_{\text{static}}$  setpoint and  $T_{\text{DA}}$  setpoint injection. Compare to Table 5.3 of the single  $T_{\text{DA}}$  setpoint injection summary, significant improvements are observed on the performance score, FR capacity and revenue. Thus, the counteractions between the airside system and the waterside system must be effectively depressed by adding the  $P_{\text{static}}$  setpoint injection method. Additionally, in comparing the results of single injections into the  $P_{\text{static}}$  setpoint tabulated in Table 5.1, improved performance scores observed in five out of the eight hours of participation (mostly from improved precision score) and much improved FR capacity and revenue of all hours. The revenue of the two methods combined is nearly the sum of the revenue from two single injection methods. Thus, this combination improves both methods with much improved results.

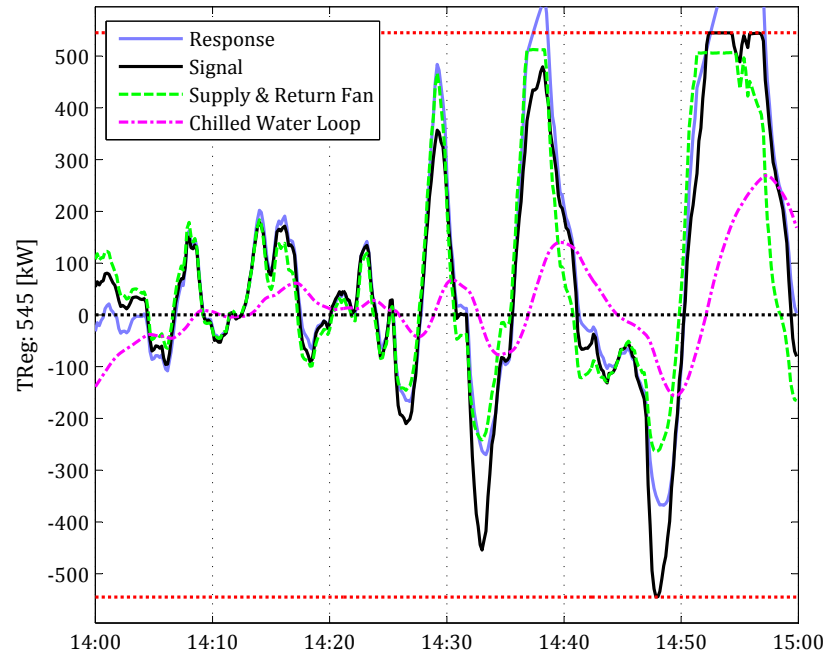


Figure 5.23: System dynamics of  $P_{\text{static}}$  setpoint and  $T_{\text{zone}}$  injection

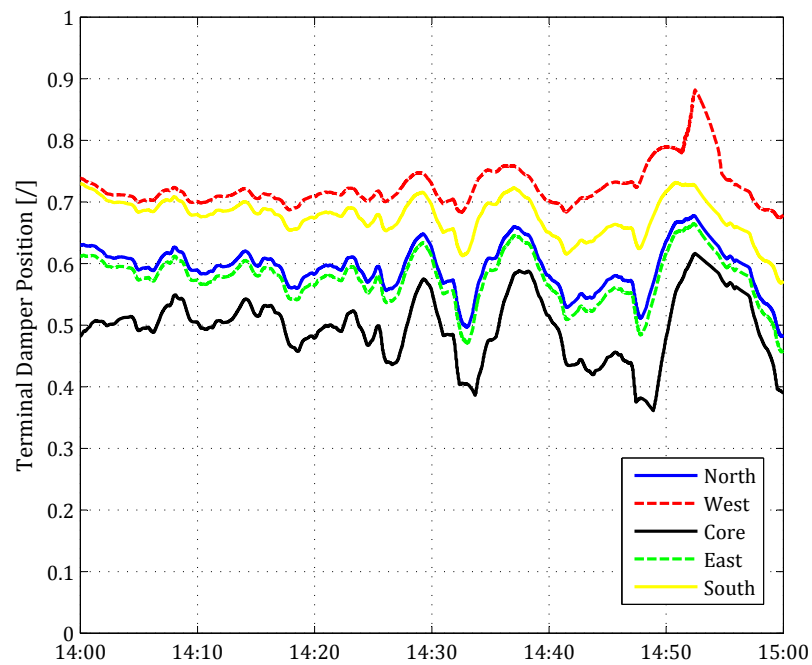


Figure 5.24: Terminal damper positions of  $P_{\text{static}}$  setpoint and  $T_{\text{zone}}$  injection

Table 5.6: Summary of two methods combined:  $P_{\text{static}}$  setpoint and  $T_{\text{DA}}$  setpoint

| Hour                  | Participation Level      |                     | Performance Score |             |        |           | TReg [kW] | Revenue [\$]    |
|-----------------------|--------------------------|---------------------|-------------------|-------------|--------|-----------|-----------|-----------------|
|                       | $P_{\text{static}}$ [Pa] | $T_{\text{DA}}$ [K] | Composite         | Correlation | Delay  | Precision |           |                 |
| 9                     | 175                      | 6                   | 0.9121            | 0.9794      | 1      | 0.7568    | 294       | 16.81           |
| 10                    | 175                      | 7                   | 0.8522            | 0.9529      | 0.9983 | 0.6054    | 279       | 17.45           |
| 11                    | 175                      | 7                   | 0.8654            | 0.9589      | 0.9996 | 0.6378    | 351       | 21.45           |
| 12                    | 175                      | 7                   | 0.7926            | 0.9713      | 1      | 0.4064    | 211       | 13.33           |
| 13                    | 175                      | 5                   | 0.9051            | 0.9758      | 1      | 0.7394    | 217       | 12.45           |
| 14                    | 175                      | 4                   | 0.9191            | 0.9811      | 0.9999 | 0.7763    | 261       | 24.92           |
| 15                    | 175                      | 5                   | 0.8592            | 0.9487      | 0.9998 | 0.629     | 245       | 8.48            |
| 16                    | 175                      | 4                   | 0.8740            | 0.9834      | 1      | 0.6386    | 214       | 12.14           |
| <u>Total Revenue:</u> |                          |                     |                   |             |        |           |           | <u>\$127.04</u> |

Referring to Figure. 5.25, the Response is observed to closely track the Signal — significant improvement compared to the results of single injections. Referring to Figure. 5.26, the counteraction between the airside system and the waterside system is much depressed compared to employing  $T_{DA}$  setpoint injection alone. The counteraction between the airside and waterside systems is not eliminated but is transferred to the terminal dampers' movement. Referring to Figure. 5.27, terminal dampers are observed to move in wider ranges compare to that of the  $P_{static}$  single injection method shown in Figure. 5.7. Thus, the impact of the zone air disturbance is expanded on the horizontal direction on the psychrometric chart as shown in Figure. 5.28. This is the result of more active terminal damper regulations of air volume flow rate in a wider range. Yet, these small changes of zone air should not be noticeable to occupants and is still inside the comfort zone. Thus, this combination of injection methods effectively depresses the counteractions by taking the advantage of interactions between subsystems for an improved Response.

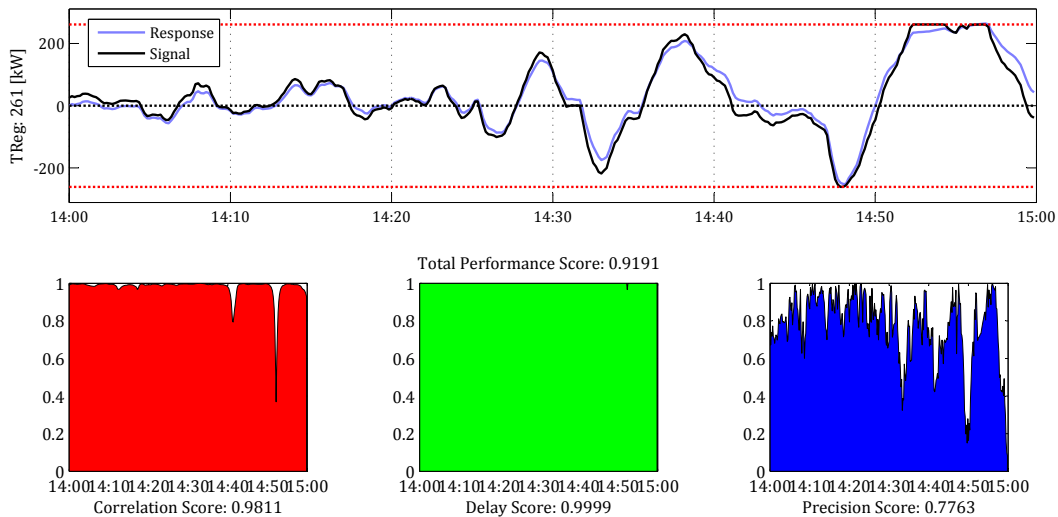


Figure 5.25: Performance score of  $P_{static}$  setpoint and  $T_{DA}$  injection

### 5.3.3 Two Methods Combined: $P_{static}$ Setpoint and OAF

Table 5.7 summarizes the results of the combined response through  $P_{static}$  setpoint injection and OAF superposition. The average performance score of the 8 hours is 0.9, which is the maximum

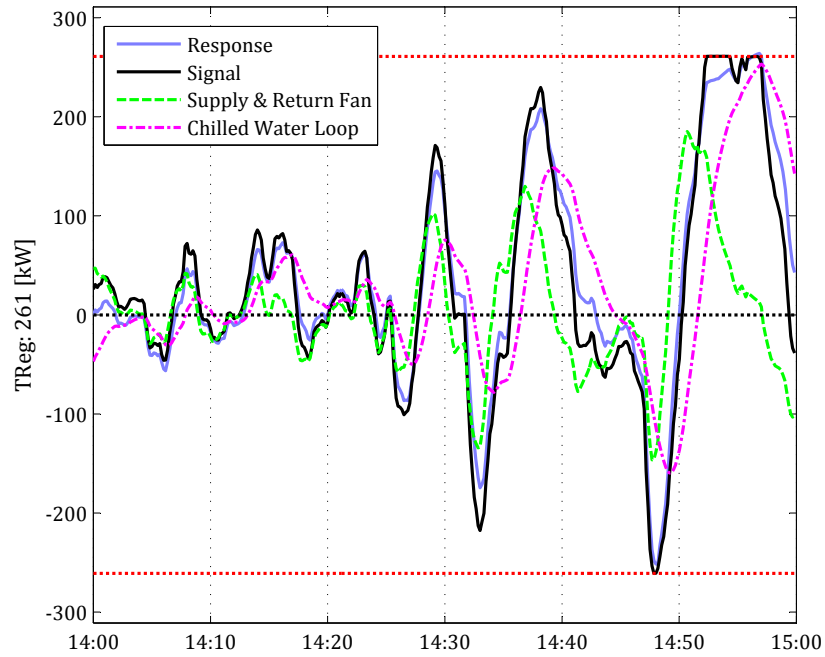


Figure 5.26: System dynamics of  $P_{\text{static}}$  setpoint and  $T_{\text{DA}}$  injection

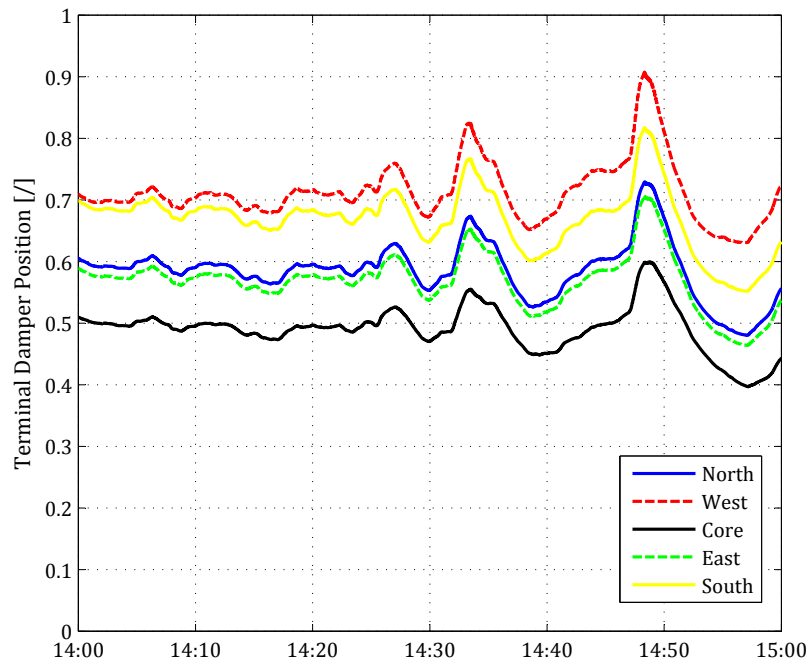
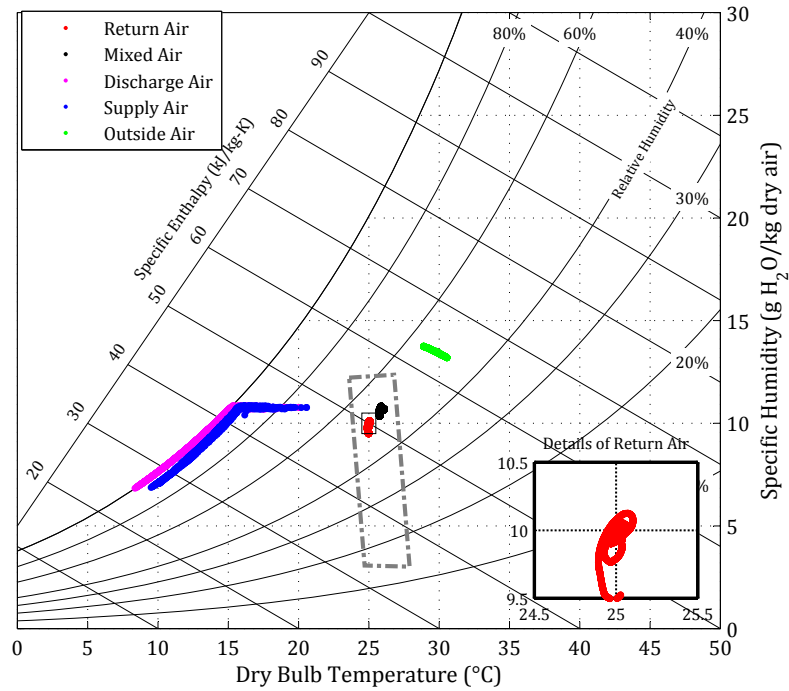


Figure 5.27: Terminal damper positions of  $P_{\text{static}}$  setpoint and  $T_{\text{DA}}$  injection

Figure 5.28: Air properties of  $P_{\text{static}}$  setpoint and  $T_{\text{DA}}$  injectionTable 5.7: Summary of two methods combined:  $P_{\text{static}}$  setpoint and OAF

| Hour                  | Participation Level      |         | Performance Score |             |       |           | TReg [kW] | Revenue [\$]   |
|-----------------------|--------------------------|---------|-------------------|-------------|-------|-----------|-----------|----------------|
|                       | $P_{\text{static}}$ [Pa] | OAF [%] | Composite         | Correlation | Delay | Precision |           |                |
| 9                     | 175                      | 20      | 0.9192            | 0.9920      | 1     | 0.7656    | 212       | 12.22          |
| 10                    | 175                      | 20      | 0.8960            | 0.9934      | 1     | 0.6946    | 189       | 12.43          |
| 11                    | 175                      | 20      | 0.8989            | 0.9941      | 1     | 0.7027    | 229       | 14.53          |
| 12                    | 175                      | 20      | 0.8545            | 0.9956      | 1     | 0.5680    | 145       | 9.88           |
| 13                    | 175                      | 20      | 0.9147            | 0.9951      | 1     | 0.7489    | 178       | 10.32          |
| 14                    | 175                      | 20      | 0.9307            | 0.9953      | 1     | 0.7968    | 218       | 21.08          |
| 15                    | 175                      | 20      | 0.9037            | 0.9709      | 1     | 0.7401    | 206       | 7.50           |
| 16                    | 175                      | 16      | 0.8815            | 0.9814      | 1     | 0.6632    | 177       | 10.13          |
| <b>Total Revenue:</b> |                          |         |                   |             |       |           |           | <b>\$98.09</b> |

of all the simulated cases. Referring to the summary of the two individual injection methods in Table 5.1 and Table 5.4, adding the OAF superposition on top of the  $P_{\text{static}}$  setpoint injection improves the FR capacity for six out of the eight hours of FR participation and improves revenue for seven out of the eight hours of FR participation. Referring to Figure. 5.29, the combined Response through these two methods shows a very accurate tracking of the Signal. The terminal dampers' counteraction effect is effectively reduced in the combined Response.

Referring to Figure. 5.30, when the terminal dampers' counteraction effect becomes significant (e.g., the static pressure setpoint is maintained in a single direction for 14:52 to 14:58), the power consumption of the chilled water loop gradually rises to contribute more in tracking the Signal. Thus, the performance score is observed to be greatly improved than either of the single injection results. However, adding OAF superposition on top of the  $P_{\text{static}}$  setpoint injection introduces the counteraction between the airside system and waterside system, which is observed to become significant when the Signal changes directions. During such time periods, the Response is found even less accurately tracking the Signal than the  $P_{\text{static}}$  injection only. Because the power variation of the chilled water loop is mostly triggered by the  $T_{\text{MA}}$  controller, which can only regulate slowly. This could result in smaller FR capacity and less revenue (e.g., hour 16:00 to 17:00). Referring to Figure. 5.31, the zone air is found less disturbed and maintained around the 25 °C setpoint.

The combined response through  $P_{\text{static}}$  setpoint injection and OAF superposition results in high performance scores with symmetrical Response. In addition, the counteraction effect between subsystems is less significant compared to that of other multiple injection cases. Therefore, the evaluation of three injection methods simultaneously is carried out with the  $P_{\text{static}}$  setpoint injection and OAF superposition plus the  $T_{\text{zone}}$  setpoint injection or  $T_{\text{DA}}$  setpoint injection.

#### 5.3.4 Three Methods Combined: $P_{\text{static}}$ Setpoint, $T_{\text{zone}}$ Setpoint and OAF

Table 5.8 summarizes the results of combined response of these three FR injection methods. The participation level of OAF is found to be mostly zero. Referring to Table 5.5, the FR capacity of combining  $P_{\text{static}}$  setpoint and  $T_{\text{zone}}$  setpoint injection is already limited by chiller sequencing

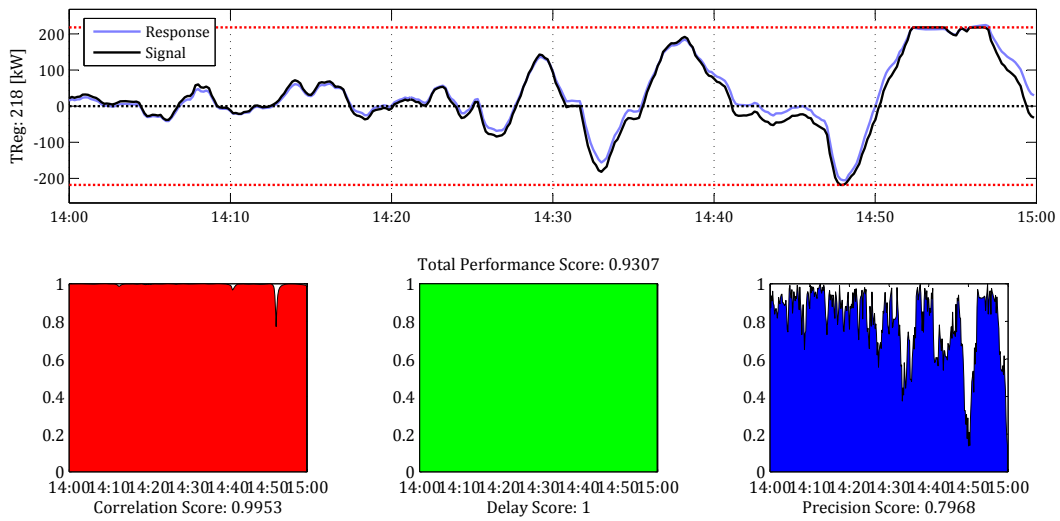


Figure 5.29: Performance score of  $P_{\text{static}}$  setpoint injection and OAF superposition

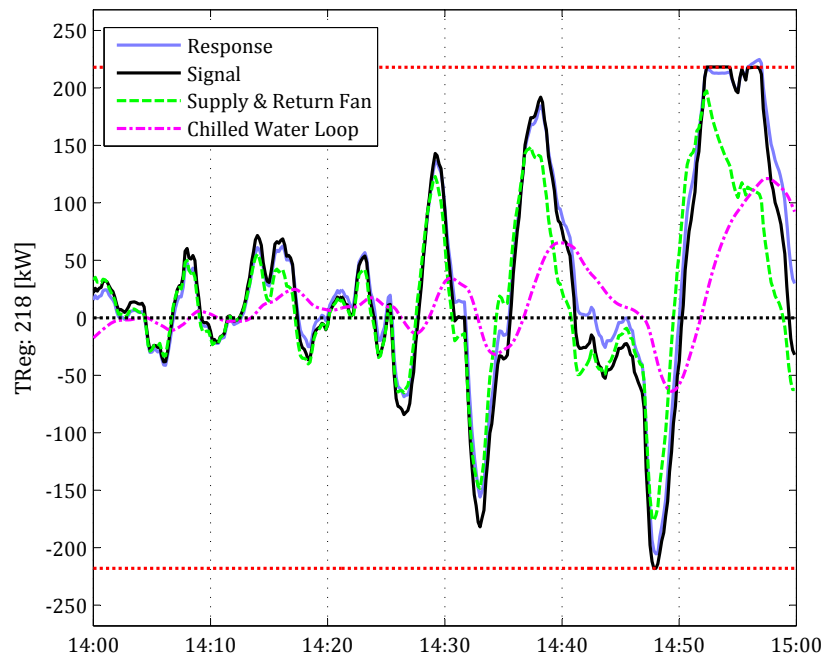
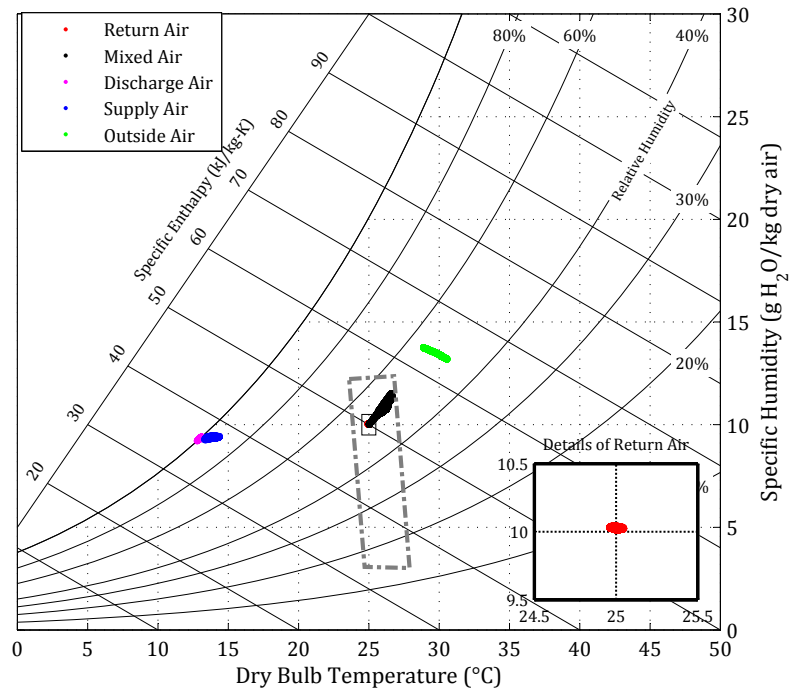


Figure 5.30: System dynamics of  $P_{\text{static}}$  setpoint injection and OAF superposition

Figure 5.31: Air properties of  $P_{\text{static}}$  setpoint injection and OAF superpositionTable 5.8: Summary of three methods combined:  $P_{\text{static}}$  setpoint,  $T_{\text{zone}}$  setpoint and OAF

| Hour                  | Participation Level      |                       |         | Performance Score |             |        |           | TReg [kW]       | Revenue [\$] |
|-----------------------|--------------------------|-----------------------|---------|-------------------|-------------|--------|-----------|-----------------|--------------|
|                       | $P_{\text{static}}$ [Pa] | $T_{\text{zone}}$ [K] | OAF [%] | Composite         | Correlation | Delay  | Precision |                 |              |
| 9                     | 175                      | 0.4                   | 0       | 0.9118            | 0.9759      | 1      | 0.7594    | 712             | 40.70        |
| 10                    | 175                      | 0.4                   | 0       | 0.8778            | 0.9745      | 0.9985 | 0.6605    | 587             | 37.82        |
| 11                    | 175                      | 1                     | 20      | 0.8671            | 0.9521      | 0.9997 | 0.6494    | 1381            | 84.54        |
| 12                    | 175                      | 0.8                   | 0       | 0.8280            | 0.9674      | 0.9989 | 0.5177    | 713             | 47.05        |
| 13                    | 175                      | 0.9                   | 0       | 0.8076            | 0.9391      | 0.9968 | 0.4870    | 810             | 41.48        |
| 14                    | 175                      | 0.3                   | 0       | 0.9011            | 0.9684      | 1      | 0.7349    | 545             | 51.03        |
| 15                    | 175                      | 0.7                   | 0       | 0.8445            | 0.9295      | 0.9974 | 0.6067    | 713             | 24.27        |
| 16                    | 175                      | 0.6                   | 0       | 0.8085            | 0.9604      | 0.9794 | 0.4857    | 544             | 28.54        |
| <b>Total Revenue:</b> |                          |                       |         |                   |             |        |           | <b>\$355.43</b> |              |

Table 5.9: Summary of three methods combined:  $P_{\text{static}}$  setpoint,  $T_{\text{DA}}$  Setpoint and OAF

| Hour | Participation Level      |                     |         | Performance Score |             |        |           | TReg [kW]                      | Revenue [\$] |
|------|--------------------------|---------------------|---------|-------------------|-------------|--------|-----------|--------------------------------|--------------|
|      | $P_{\text{static}}$ [Pa] | $T_{\text{DA}}$ [K] | OAF [%] | Composite         | Correlation | Delay  | Precision |                                |              |
| 9    | 175                      | 3                   | 20      | 0.8813            | 0.9676      | 0.9992 | 0.677     | 299                            | 16.52        |
| 10   | 175                      | 5                   | 20      | 0.8221            | 0.929       | 0.9965 | 0.5407    | 287                            | 17.32        |
| 11   | 175                      | 7                   | 20      | 0.8314            | 0.9289      | 0.9984 | 0.567     | 388                            | 22.78        |
| 12   | 175                      | 7                   | 20      | 0.7628            | 0.9545      | 0.9989 | 0.3349    | 233                            | 14.16        |
| 13   | 175                      | 7                   | 20      | 0.8268            | 0.9248      | 0.9956 | 0.5599    | 241                            | 12.63        |
| 14   | 175                      | 2                   | 20      | 0.8928            | 0.971       | 0.9986 | 0.7089    | 267                            | 24.77        |
| 15   | 175                      | 5                   | 18      | 0.8097            | 0.9303      | 0.9995 | 0.4993    | 257                            | 8.39         |
| 16   | 175                      | 4                   | 20      | 0.8487            | 0.9656      | 1      | 0.5806    | 225                            | 12.39        |
|      |                          |                     |         |                   |             |        |           | <b>Total Revenue: \$128.96</b> |              |

protocols and occupants' comfort. Thus, the employment of OAF superposition only happens if it brings in more accurate tracking of the Signal (i.e., higher quality of Response) to replace or reduce the participation levels of the original FR injection methods. However, the OAF superposition is found to result in low performance scores and slow tracking of Signal when employed individually. Thus, the supervisory control determined to exclude OAF superposition for most of the FR participation hours. The HVAC system dynamics of the hour 14:00 to 15:00 are found to be the same as that shown in Figure. 5.22 and Figure. 5.23. Thus, the analysis of results is not repeated here.

### 5.3.5 Three Methods Combined: $P_{\text{static}}$ Setpoint, $T_{\text{DA}}$ Setpoint and OAF

Table 5.9 summarizes the results of the combined response of these three FR injection methods. The maximum participation level of the OAF superposition is employed for most of the hours. Additionally, the participation level of the  $T_{\text{DA}}$  setpoint injection is observed to be reduced for five out of the eight hours of FR participation. Although  $T_{\text{DA}}$  setpoint injection and OAF superposition both bring in counteractions between the airside and the waterside systems, the supervisory control determined that the counteraction of the OAF superposition is less significant than that of the  $T_{\text{DA}}$  setpoint injection. Referring to Table 5.6, the FR capacity of the three methods combined is greater than that of the  $P_{\text{static}}$  setpoint and  $T_{\text{DA}}$  setpoint methods combined; however, perfor-

mance scores are reduced due to the introduction of OAF superposition. Thus, the three methods combined do not generate much higher revenue (i.e., about \$2 increase for the 8 FR hours). The HVAC system dynamics are found to be similar to that shown in Figure. 5.25 and Figure. 5.26. Thus, similar analysis of results is not repeated here. Referring to Figure. 5.32, the footprint of the zone air disturbance is found limited to a smaller range than that of Figure. 5.28 because of the smaller participation level of  $T_{DA}$  setpoint injection. Thus, these three methods combined can achieve a steadier zone air and ensure the revenue stimulated by the combination of  $P_{static}$  setpoint and  $T_{DA}$  setpoint injection. Adding OAF superposition method on top of the injection of the other two methods provides the HVAC system higher degree of freedom to respond to the RegD signal injection. Compare to Table 5.8, the participation level of the OAF superposition is nonzero for the 8 FR hours. Although adding OAF superposition introduces less accurate traction of the RegD signal for the combination of  $P_{static}$  setpoint and  $T_{zone}$  setpoint, it helps for the combination of  $P_{static}$  setpoint and  $T_{DA}$  setpoint. The strong counteraction between the airside system and waterside system introduced by the  $T_{DA}$  setpoint injection can be transferred to the less significant counteraction between the airside system and the zone air. Thus, the steadier zone air (Figure. 5.32) is achieved compare to the two methods combined as shown in Figure. 5.28.

### 5.3.6 All Four Methods Combined

The adoption of all four methods results in the same comprehensive package of participation levels as the three injection methods of  $P_{static}$  setpoint,  $T_{zone}$  setpoint and OAF combined. The supervisory control determined the participation levels of  $T_{DA}$  to be zero for all FR participation hours because this method introduces strong counteractions between the airside system and the waterside system that degrades the combined Response. Thus, the  $T_{zone}$  setpoint injection and  $T_{DA}$  setpoint injection methods should not be employed simultaneously.

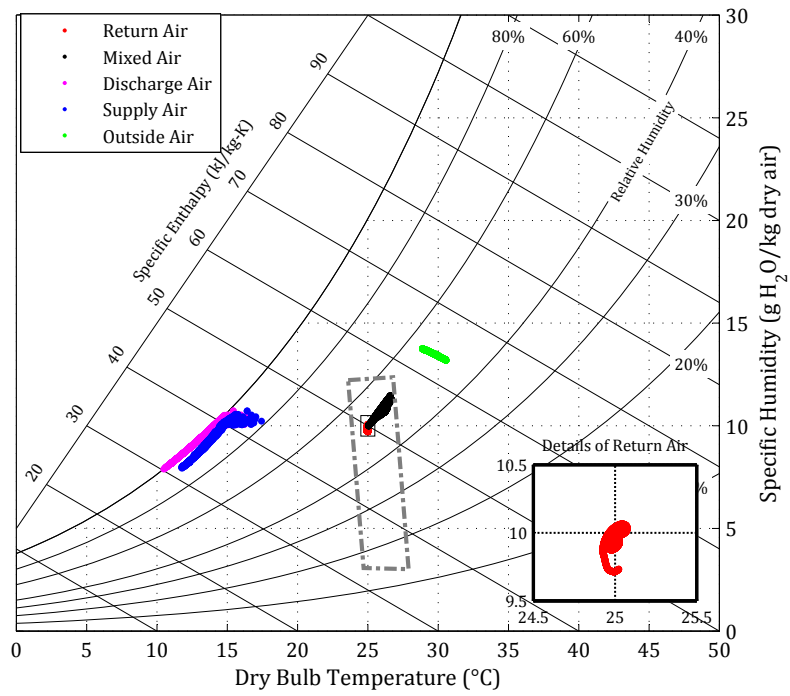


Figure 5.32: Air properties of  $P_{\text{static}}$  setpoint injection and OAF superposition

## 5.4 Summary of Multiple Injections

The multiple injection cases show significant improvements in the Response in tracking the Signal in comparison with the responses of the single injection cases. By combining multiple FR signal injection methods simultaneously, major counteractions between HVAC subsystems are found either 1) depressed or 2) transferred to and/or replaced by other less significant counteractions. Thus, combinations of multiple FR injection methods typically involve improvements in performance score, FR capacity and revenue simultaneously.

The results of multiple FR signal injections show significant improvements on both FR capacity and revenue. Because multiple injections can more effectively stimulate the building systems for a building-wide participation. The major counteractions are found either depressed or replaced by less significant counteractions. Because multiple FR injections introduce higher degree of freedom for the HVAC system to work out a solution that can strength interactions and depress counteractions. Referring to Figure. 5.33, a FR injection method is more likely to adopt smaller participation levels in a multiple injection package than its individual injections. These participation levels are determined through hundreds of simulations and select the one package of multiple injections can reach the highest revenue. Compare to single injections, the increased cost of multiple injections would be more data transmission to the setpoints. A recent field test has successfully implemented sending RegD data at near real time though internet [61]. This approach makes multiple injections a practical approach to implement for improved FR capacity and revenue.

For the objective of the supervisory control in pursuing the highest revenue, the combination of  $P_{\text{static}}$  setpoint,  $T_{\text{zone}}$  setpoint and OAF should be employed for FR signal injection because the 8-hour offline simulation suggests \$355 revenue, which is the highest among all simulated cases. The objective of the supervisory control can be adjusted for different reasons under various conditions or building types. For example, a hospital building to participate in FR may want to prioritize the steady zone air temperature over the pursuit of the highest revenue. Thus, the zone air variation should be limited in a smaller range in that case and ensuring the revenue is

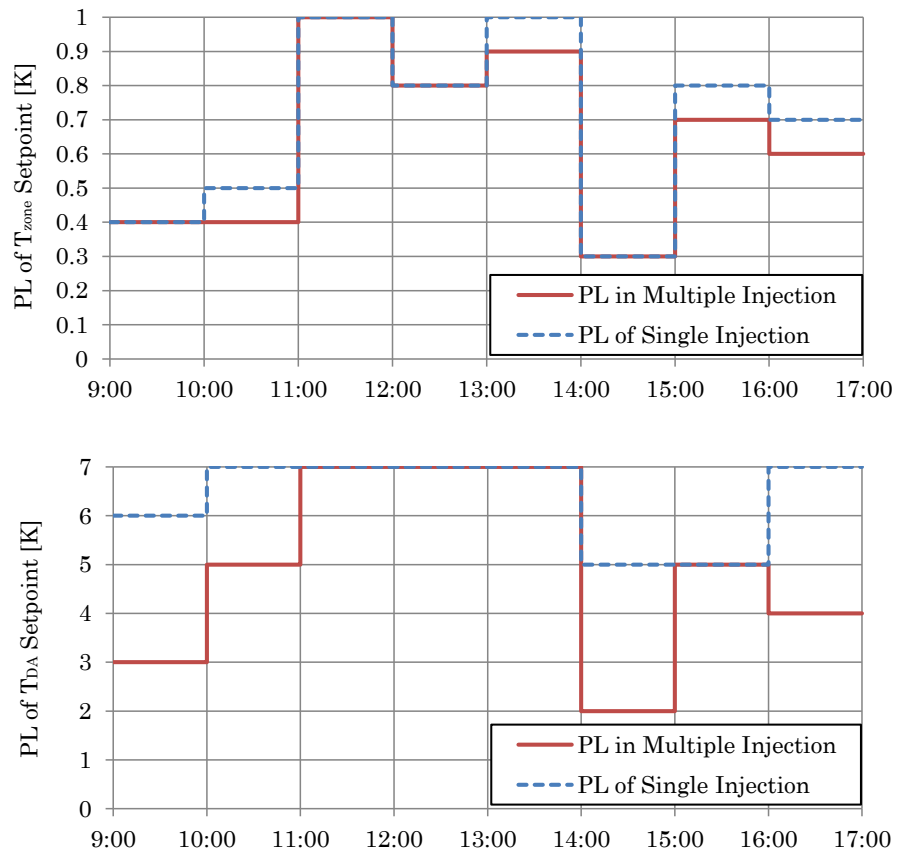


Figure 5.33: The participation levels of two selected methods of their single injections and in their multiple injection packages

maintained high. Additionally, if a big building complex is employed as a major demand side FR resource, it may want to pursue the highest performance score to provide more accurate tracking of the FR signal. Thus, different combinations of FR injection methods would be employed with the specific participation levels determined by the supervisory control.

Although the  $T_{\text{zone}}$  setpoint injection method stimulates the building HVAC system for high FR revenue, it needs to be tested in field for applicability. FR data injection requires data transmission on a 2-4 seconds basis to a large number of zone thermostats in a high-rise commercial building. The delay of data transmission may significantly degrade the performance score and thus impact the revenue. In comparison, sending setpoint profiles to the  $P_{\text{static}}$  setpoint, the  $T_{\text{DA}}$  setpoint and superposing on the OAF are considered easier to accomplish through the building automation system.

## Chapter 6

### Conclusions and Future Work

This work investigates the technical potential and possible methods for utilizing commercial buildings through combined HVAC system response for frequency regulation. A commercial building HVAC systems and low-level controls are developed that allow evaluation of HVAC system dynamics on a second-to-second basis. Then, a high-level supervisory control is developed to operate on top of the building model that provides a comprehensive package of FR methods and their respective participation levels. Case studies of single and multiple FR signal injections are carried out. The simulation results suggest that accurately tracking of the FR signal (as revealed by high performance scores) and large FR capacity can be provided from buildings as demand side FR resources. In return, buildings benefit from the payment for FR participation. The amount of payment can be on the order of a few hundred dollars per day depending on the size of the building and the number of hours for FR participation. The simulation case studies indicate that the payment for FR participation during the steady-state HVAC operation hours (e.g., 8 hours) can compensate as high as more than one hour of energy expenses.

This work is the first to consider managing the interdependent HVAC systems through a supervisory control method for demand side FR participation. The supervisory control method provides a comprehensive package of FR signal injection methods to stimulate certain setpoints for a combined building HVAC response in response to the FR signal. Thus, it dynamically integrates building operations into the ancillary service market and is expected to change the landscape of electric grid operation. Traditionally, commercial buildings participate in demand response

programs are notified by utilities to shed loads during critical periods mostly a day ahead. Dynamic integration changes the time frame of providing demand side solutions for balancing supply and demand from hours to seconds. The result would be significant if many large commercial buildings, facilities and demand side resources have fast-ramping capabilities all participate in FR. As the current 490 MW of RegD-following resources have already reduced the FR requirement from 1% to 0.7% of total generation (i.e., a reduction of 240 MW to 420 MW of FR capacity in the PJM territory) [22], dynamic response from all major loads on the grid potentially provide a solution to reduce the need for peaking generators, non-spinning reserves and demand response programs

## 6.1 Summary of Results and Contributions

A number of research questions introduced in Chapter 1 have directed to this research. Each of the questions is provided with a summary to highlight the important contributions of this work.

### (1) **Can commercial building HVAC systems be used as demand side frequency regulation resources?**

Simulation results suggest that high-rise commercial buildings can provide significant capacity for FR with high performance scores. In 2013, the 19 RegD-following resources (e.g., batteries and flywheels) in PJM's FR market with a total of about 490 MW had achieved performance score distribution of: 70% in 0.9 to 0.99, 16% in 0.8 to 0.89 and 11% in 0.7 to 0.79 in the first year's operation of the performance-based regulation rule [22]. The simulation results of high performance scores with large FR capacities suggest that commercial building HVAC systems can provide FR with fast-ramping capability which is similar to the prevailing grid-scale batteries and flywheels. In addition, the simulation results found that the FR capacity from the HVAC system of a 1 million sq. ft building is typically greatly larger than the minimum requirement of the PJM territory (i.e., 100 kW). Thus, commercial buildings of less than 1 million sq. ft. should be potentially considered as qualified candidates to participate. Thus, the potential of the total FR capacity from

commercial buildings is significant. A research estimated that at least 4 GW of dynamic regulation capability is available in the U.S. based on the total floor area of commercial buildings equipped with variable frequency drives [54]. Similar to the idea of virtual power plant (VPP) to the energy market, the idea of building portfolio to the FR market is proposed in this dissertation. A building portfolio is a bundle of buildings with different but complementary HVAC components and performance characteristics which can respond to FR signal with a near constant FR capacity. The building portfolio is expected to provide improved FR performance and capacity by taking advantage of the temporal diversity of capacity limits and part load ratios.

- (2) **If yes, what are the possible methods that can be adopted to vary the HVAC system power consumption with the FR signal? Which methods are more effective in stimulating building HVAC systems for FR participation? What are the interaction and counteraction effects when several FR methods are adopted simultaneously?**

Four methods are proposed that intend to inject the FR signal into certain setpoints to offer significant power responses from a whole-building participation. The four FR injection methods are: 1) static pressure ( $P_{\text{static}}$ ) setpoint, 2) zone temperature ( $T_{\text{zone}}$ ) setpoint, 3) discharge air temperature ( $T_{\text{DA}}$ ) setpoint and 4) outside air fraction (OAF) for FR signal superposition. These four methods and their respective sensors are labeled in Figure. 3.1 for illustration purpose. In simulation evaluations, these four methods are first evaluated individually and then evaluated simultaneously.

Although each method has its own strengths and weaknesses, the  $P_{\text{static}}$  setpoint injection and the  $T_{\text{zone}}$  setpoint injection methods are found more effective in stimulating building HVAC systems for FR as revealed by larger FR capacity and higher revenue on the selected day. The  $T_{\text{DA}}$  setpoint injection and the OAF superposition methods are found more suitable for being combined with other methods. Additionally, the four proposed methods

for FR injection are found eventually reduced to only two effective points: 1) supply and return fan speed and 2) chilled water mass flow rate into the cooling coil. Thus, any injection methods more directly stimulate these two effective points for FR can reduce the impact of counteractions between subsystems and reach higher performance scores. For example, the simulation results show that the  $P_{\text{static}}$  setpoint injection method and OAF superposition method can more directly stimulate the airside system and the waterside system, respectively. Thus, the combination of these two methods reach the maximum average performance score of all the simulated cases.

Injecting FR signal into a particular setpoint stimulates a series of response, which involve reinforcing or damping actions of the interdependent HVAC subsystems and components in the simulation case studies. Major interaction and counteraction effects are found 1) between the airside system and the waterside system through the regulation of the chilled water mass flow rate into the cooling coil and 2) between the airside system and the zone air through the regulation of the terminal damper positions. In addition, building operations must honor the capacity limits of many forms. This include chiller sequencing protocols, control signal limit of low-level controllers, occupants' comfort and the designed capacities of many interconnected subsystems. Thus, although interaction effects are helpful for improving the performance and FR capacity when one particular HVAC subsystem is stimulated for FR, counteraction effects are also important to maintain the building HVAC operation in a reasonable range. Multiple injection case studies show significant improvements on the Response in tracking the Signal in comparing with the responses of the single injection cases. By combining multiple FR signal injection methods simultaneously, major counteractions between HVAC subsystems are found either 1) depressed or 2) transferred to and/or replaced by other less significant counteractions. Thus, combinations of multiple FR injection methods typically involve improvements on performance score, FR capacity and revenue simultaneously.

(3) **How to model a commercial building HVAC system and its controls that allow evaluations of HVAC system interactions and counteractions on a second-by-second time basis?**

The simulation model developed in this dissertation is a scalable commercial building HVAC system with well-tuned low-level controls, which is built in a technical computing environment for dynamic systems and system controls (i.e., Matlab/Simulink). The resolution of RegD signal is four seconds; thus, the commercial building model is simulated with 1 second timestep in order to capture the system responses effected by the RegD signal injection. Most prevailing simulation environment for building energy analysis typically do not simulate on second-to-second basis since the analysis of heat transfer rate on minute-to-minute basis is more practical and useful. For example, EnergyPlus only allow the simulation timestep as short as one minute. In the beginning of this research, simulations with EnergyPlus models were carried out with an artificial RegD signal profile, whose resolution is one minute instead of four seconds; because setting the data resolution shorter than the timestep would not be accepted in simulations. Poor correlations between the Response and Signal were observed. Because the artificial RegD profile can only stimulate the HVAC system once in the beginning of a minute (instead of fifteen continuous and correlated stimulations in a minute if following the actual RegD signal). The one stimulation creates “ripple effect” on the power consumption of HVAC systems in the rest of that minute because of interacting and counteracting responses between HVAC subsystems. As a matter of fact, the effect on the power consumption to the next minute is captured by EnergyPlus. However, the artificial RegD profile maintains constant for the minute and makes a significant step change at the beginning of the next minute. This example shows that using a simplified RegD profile, which eliminates fourteen values of a minute and only keeps the value at the beginning, is not a valid approach to explore the FR potential of commercial building HVAC systems. Thus, modeling in a simulation environment that allows

evaluations of system dynamics on second-to-second basis is important to this research. In addition, modeling the controls of HVAC system (with PI controllers and variable frequency drives) and tuning the controllers are also important to understand the system dynamics in following the RegD signal. Thus, Matlab/Simulink is selected for this research task.

The model is built up with four sections and is described in details in Chapter 3: 1) A five-zone model with exterior walls, interior walls and floors modeled 3R2C reduced-order model, which represents the heat transfer through opaque multilayer construction element. For each zone, both sensible and latent energy balance are calculated for dry-bulb temperature and humidity ratio. 2) A pressure-independent airside system with a dry-bulb economizer system (i.e., an outside air damper positioning system); 3) A waterside system with two chillers operating based on the designed sequencing rules and the chilled water loop storage effect modeled as a first-order state-space model and 4) The fan power consumption is calculated based on a manufacturer's fan power map, which is calculated based on the static pressure increase and the total volume flow rate — both are determined through the airside control system. The chilled water loop power is based on a data model fitted based on the formula of an empirical model [29]. The control of this building model is implemented through local PI controllers but a building automation system is assumed that can supervise these controllers. The simulated results are sampled on ten second basis for performance score and payment calculations according to PJM's rules. Thus, simulations on second-to-second basis allow the results calculations exactly based on PJM's requirements.

**(4) How to design a high-level supervisory control that directs the building power consumption to deviate from the baseline for FR participation?**

The supervisory control directs the building HVAC system's operation from high-level. It directs the HVAC system power consumption in response to the RegD signal. This research found four setpoints can effectively stimulate a building-wide participation from either single or combined injections. A new concept, participation level (PL), is introduced

here to define the range of setpoint deviations around the baseline setpoint. PL is a setpoint-specific value and is determined through supervisory control ahead of time and is limited by the system physical characteristics, capacity limits and occupants comfort. The design of supervisory control is described in section 4.2 and is illustrated in Figure. 4.1. It uses a building energy simulation model that accurately simulates hourly operations ahead of time in order to 1) determine building FR capacity and the baseline power consumption; 2) capture capacity limits of HVAC subsystems and the interactions and counteractions between these subsystems; and 3) determine the appropriate PL's of employed FR methods in order to direct the actual building HVAC system in the actual hour.

(5) **How to evaluate/quantify the FR service provided by commercial buildings?**

The “performance-based regulation” rule that PJM launched in 2012 is adopted for evaluations. Here, the performance score is calculated by comparing the simulated results of the HVAC system with the injected FR signal. Any FR resources currently in PJM's FR market, either RegA-following or RegD-following, is evaluated based on the same evaluation rules and receives an hourly score in the scale of 0 to 1 in rewarding its hourly FR service. The performance score calculation rules and equations are described in PJM's manual[38, 39]. The equations are programmed into a Matlab function as one of the functions that the supervisory control calls for computation. The performance score quantifies how closely the FR resource follows the FR signal. The higher the score, the higher payment for the same mileage travels.

## 6.2 Limitations of Current Methods

This section provides the limitations of the methods developed in this dissertation. The limitations are based on the objective of this research, which is to explore the opportunities and methods of dynamic building-to-grid integration for FR. With this research moving forward to implementation, methods presented in this dissertation must be improved for field tests with online

supervisory control. The major limitations of the current method are listed in the following:

- (1) RegD signal is assumed known ahead of time. The supervisory control method designed in this dissertation intends to use a calibrated simulation model to predict the applicable participation levels for a controlled commercial building. This requires the RegD signal of two hour ahead is known at the time of running simulations. Because the deviation range of the RegD signal in that hour (in the range of  $[-1,1]$ ) is important to determine the appropriate participation levels. For example, if the deviation range of RegD signal is predicted from -1 to 1 for that FR hour, the participation level of a particular setpoint is determined at  $PL_1$  and the FR capacity is committed at  $TReg_1$ . Assume the deviation range of RegD signal turns out to be from -0.5 to 0.5 in reality. If  $PL_1$  is still applied for the actual FR hour, the FR capacity stimulated would be  $TReg_2$ , which must be less than the committed value  $TReg_1$ . In such cases, the performance scores would be degraded and result in economic penalties.

Thus, the possible improvements should include either 1) a method to accurately predict the deviation range of the RegD signal, or 2) a method to adjust intra-hour participation levels during the actual FR hour. In reality, RegD signal is the high-pass filtered product of area control error (ACE). Thus, if RegD signal is assumed predictable, that means ACE is assumed predictable. Although previous research has provided some methods to predict ACE with simplified interconnected power system models. The accuracy of the methods for online supervisory control remains unknown. In addition, incorporating RegD signal predictions into the supervisory control would be cumbersome and time-consuming to deal with. Thus, a method that can adjust intra-hour participation levels to accommodate the committed FR capacity seems a more practical approach.

- (2) The power consumption of the waterside system is calculated based on an empirical data model, which is fitted with the annual simulation results of an EnergyPlus model surrogate on 10 minute basis. However, this empirical data model is used to predict the dynamic

power consumption of the waterside system on second-to-second basis. Since the Energy-Plus surrogate for validation was simulated on 10 minute timestep, the accuracy of this empirical data model in capturing second-to-second dynamics of the waterside system is still uncertain. To achieve accurate simulation results of system dynamics, the best approach would be employing explicit physical models, such as the way of modeling the airside system, motors and VFDs in this dissertation. However, incorporating explicit models of the waterside system would further slow down simulations of each participation level and thus makes the online supervisory control more difficult to implement in field tests. Therefore, the future work need to find a solution that improves the model's accuracy in capturing system dynamics and also improves simulation speed.

- (3) The simulation speed determines the success of online supervisory control. The benefit of a Matlab/Simulink model is for detailed analysis of system dynamics and controls; however, the analysis is more important to the purpose of research and development (R & D). With this research moving forward to implementation in buildings, the concern would be how to quickly and accurately simulate thousands of combinations of participation levels and send the required information to PJM before the FR market closes for the intended FR hour. Thus, the most important question need to answer before moving to the phase of demonstration would be “how important is the Matlab/Simulink model to online supervisory control?” or the question can be paraphrased as “is simplified model acceptable for online supervisory control for the sake of simulation speed?” Thus, using forward prediction models (e.g., neural networks) may be a possible solution for online supervisory control. A preliminary approach of training the forward prediction model is proposed in section 6.3.

### **6.3 Future Work**

The objective of this section is two-fold — 1) to develop some possible strategies that may be used in this particular research moving down the road for demonstration purposes and 2) to

determine the potential research areas that explore the impact of significant number of buildings participating in FR with respect to the electric power systems.

### **6.3.1 Future Work Pertains to this Particular Research**

- (1) Explore more setpoints for FR signal injection and evaluate their impact. This research found that the four FR injection setpoints are reduced to only two effective points. Due to the capacity limits of HVAC subsystems and their counteracting responses, combinations of several methods simultaneously do not provide additive FR capacity. Thus, exploring other effective points is important to expand the FR capacity. Lighting systems consume 40% of total power in commercial office buildings; thus, potentially a good candidate for FR if traditional light dimming devices are modified for two-way regulation [13]. However, appropriate participation levels need to be determined through field tests based on occupants' acceptance on illuminance variations [1]. Incorporating lighting system should not be viewed independently from HVAC systems for FR. The thermal load variation caused by lighting power deviation must be compensated for by HVAC systems. Thus, a comprehensive package of participation levels including lighting power should be provided by a similar but improved comprehensive control method. The major benefit of including lighting system into the comprehensive package is a year-round opportunity for FR participation when HVAC systems are not used at full load. In addition, the chilled water setpoint and the condenser water setpoint are also good setpoint candidates that can potentially stimulate building-wide participations. The zone CO<sub>2</sub> concentration should be set as another limit for the supervisory control. For example, when the zone CO<sub>2</sub> concentration reaches 1200 ppm, the outside air damper must be forced to open regardless of the FR signal superposition.
- (2) To improve the two inter-related limitations of model accuracy and simulation speed raised in section 6.2, the future work may incorporate methods, such as artificial neural networks. Using forward prediction models would potentially accelerate the simulation speed signif-

icantly; in addition, accuracy of the model can also potentially improved if the building’s actual operation data is used to train the forward prediction model. For Matlab implementation of the neural network model, I suggest to use the function of “time series prediction” in the neural network toolbox. In particular, the problem should be modeled as “nonlinear autoregressive with external (exogenous) input” [59]. For the hour-to-hour supervisory control, two types of data should be fed into the neural network model: 1) historical data of building power consumption (of a defined moving timeframe, such as one hour); and 2) external input data of weather, RegD signal, occupants and light/plug loads. Then, the HVAC power consumption of the upcoming hour is predicted from the neural network model.

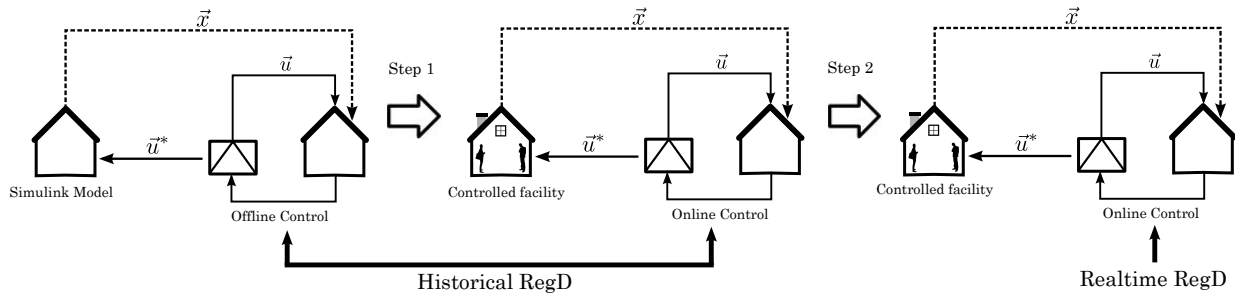


Figure 6.1: Two-step approach of training forward prediction model

I suggest a two-step approach to train the forward prediction model. Referring to Figure 6.1, the first step of training the forward prediction model uses historical RegD data so that the one hour time constraint is not a concern. The training is started with offline supervisory control of the calibrated Matlab/Simulink model. After the neural network model is established, the controlled building is used to replace the Matlab/Simulink model to improve the forward prediction model. The reason to start the training from the Matlab/Simulink model is because simulations can provide enough data samples of various conditions in relatively shorter time; thus, potentially reduces the time required to train

the model to achieve a high level of accuracy. Once the forward prediction model is properly trained, the field tests can move forward to the second step, which integrates the controlled building into PJM's FR market and receives real time RegD signal. Under such condition, simulation speed becomes the most important to ensure the smooth operation of the online supervisory control.

- (3) The current objective of the supervisory control explores the maximum possible FR capacity and pursues the highest revenue from hour to hour. Thus, significant wear and tear would be added to HVAC equipments if a commercial building is controlled to pursue such an objective. Thus, it is necessary to rethink if the current objective of the supervisory control is practical to implement. The impact of implementation should be considered not only to the building side but also to the ISO/RTO side. For a building participate in PJM's performance-based FR market, the limitation of the current method is that the building would not know how much FR capacity it would commit to PJM until the last minute before the information needs to be submitted to PJM. For PJM, incorporating a building into the FR market would introduce uncertainty of FR capacity from hour to hour. This impact to the FR market may be not significant if only one or two buildings are incorporated; but what about a large number of buildings? Ultimately, buildings need to compete with flywheels and batteries for a share of the dynamic FR market. The biggest advantage of buildings for FR is the availability of their HVAC systems and no initial investment on equipment. However, if the FR service from buildings is labeled as unreliable or unpredictable (because of the objective of supervisory control), this "disadvantage" would make buildings uncompetitive in the FR market. Last but not least, the objective of pursuing the highest revenue from hour to hour is based on the assumption that RegD signal is known or perfectly predictable. As discussed in the first limitation of section 6.2, inaccurate predictions of RegD signal would result in economic penalties. Since PJM does not offer a method to predict RegD, prediction of RegD from the demand side would be more difficult.

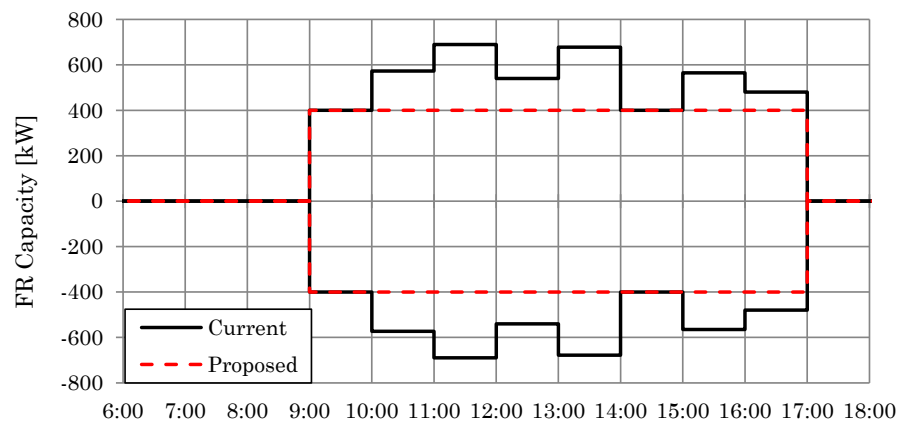


Figure 6.2: Possible FR capacity calculated by the current method and the proposed method

Based on these concerns, a more practical way for implementation would be a commitment of constant FR capacity throughout the scheduled FR hours. Referring to Figure. 6.2, the supervisory control is set to achieve the target FR capacity collaboratively by allocating the available FR resources of the building, such as fans, pumps, chillers and lighting systems. The objective of the supervisory control is to select the participation levels that can stimulate the building's HVAC system for the target FR capacity. Potentially, several combinations of participation levels may reach that capacity target; and the one reaches the highest performance score is selected.

This proposed method may potentially resolve the concerns of implementation. First, the target FR capacity is set at a level that can provide effective FR participation (e.g., 200 kW to 400 kW capacity for a 1 million sq. ft. building) but also not adding lots of wear and tear that can significantly shorten the life span of HVAC equipments. Because a significant number of buildings are expected to participate in the FR market in the future; so each building should contribute with high quality FR service (as quantified by performance scores) instead of its maximum capacity. Second, a commitment of constant FR capacity would provide the building a very competitive position compare to flywheels and batteries. Because the FR service that the building can offer would be: constant FR capacity, very competitive performance scores and no initial equipment investment. Third, pursuing a constant but conservative FR capacity provides more flexibility to the building. The supervisory control can allocate other available FR resources of the building to meet the target of FR capacity in cases that some unexpected situations happen (e.g., malfunction of HVAC components, high CO<sub>2</sub> concentration level that overrides the OA fraction or inaccurate RegD predictions). Thus, the supervisory control can make intra-hour adjustments of participation levels to accommodate the consistent FR capacity as committed to PJM. The intra-hour adjustments can be made based on the five-minute FR data through PJM's eMKT system for participating FR resources.

- (4) Evaluation the durability of HVAC systems for FR participation as a function of the committed FR capacity. Constantly ramping up/down the HVAC components would definitely require special treatment to prevent malfunction, failure and any chances that can cause greater loss to the entire HVAC system. If the HVAC system was controlled for an aggressive FR capacity, higher revenue should be rewarded to FR service provided; however, more wear and tear is also added to those HVAC components. Thus, an economic calculation is needed in order to set a realistic FR capacity target. This may be determined by the type and age of the HVAC components and the controls.

### **6.3.2 Exploration of the Broader Impact to the Electric Power System**

This research only explored the system dynamics inside the building. Imagine a bundle of a large number of buildings are controlled for FR participation, the impact to the electric power system would be significant. The distribution system of the U.S. is aging and large metropolitan cities expect peak-shavings to defer the investment into the expansions of the grid system [63]. If a large number of high-rise commercial buildings are controlled for FR, that means about 50% of the time these buildings actually consume more electric power than their baseline. What would be the possible impact to the distribution system? Simulation work of both buildings and the electric grid system can be helpful to answer this question.

This research explored some methods to stimulate a building-wide participation for FR. One of the objectives is to commit at least 100 kW of FR capacity in order to bid into PJM's market for payment. With the modernization of the electric grid system as enabled by smart grid technologies, "DR-ready" appliances and plug loads may potentially installed in large scale [34]. These loads can receive signals from the grid in real time and take actions to execute the command. They may participate in demand response programs and may also in the ancillary services as well (e.g., FR). Based on the FR capacity that these resources can provide, they may or may not get paid for their ramping in response to the FR signal but may still required to do so as part of the smart grid. However, counting all these FR resources would significantly change the landscape of the FR market

and also the operation of electric power system. What would be the percentage of generators in the FR market at that time? Would payment to FR resources still remain high? Would non-spinning reserves are still needed? These questions may be partly answered through simulations and more clearer answers are expected with implementations start with the large commercial buildings.

## Bibliography

- [1] Y. Akashi. Is it okay to dim your lights for load shedding? Rensselaer Polytechnic Institute Lighting Research Center, 2004.
- [2] M. H. Albadi and E. F. El-Saadany. A summary of demand response in electricity markets. Elsevier Electric Power Systems Research, 78 (11):1989–1996, May, 2008.
- [3] California Energy Storage Alliance. Energy storage a cheaper, faster and cleaner alternative to conventional frequency regulation, 2013.
- [4] ASHRAE. ASHRAE 55-2004 Thermal Environmental Conditions for Human Occupancy. ASHRAE, 2004.
- [5] ASHRAE. ASHRAE Handbook of Fundamentals. ASHRAE, 2004.
- [6] ASHRAE. Chapter 18 Fans. ASHRAE Handbook of Fundamentals, 2009.
- [7] ASHRAE. Chapter 21 Duct Design. ASHRAE Handbook of Fundamentals, 2009.
- [8] I. Beil, I.A. Hiskens, and S. Backhaus. Round trip efficiency of fast demand response in a large commercial air conditioner, May 2014.
- [9] H. Bevrani, A. Ghosh, and G. Ledwich. Renewable energy sources and frequency regulation: Survey and new perspectives. IEEE Renewable Power Generation, 4 (5):438–457, September 2010.
- [10] P.C. Bomrad and B. Cushing. Turning your buildings into a battery to reduce energy costs. Automated Buildings, November 2011.
- [11] B. K. Bose. Modern Power Electronics and AC Drives 1st edition. Prentice Hall, 2002.
- [12] J.E. Braun. Load control using building thermal mass. Transactions of ASME, 125, August 2003.
- [13] Lighting Research Center. Lighting research program project 3.2 energy efficient load-shedding lighting technology. California Energy Commission Public Interest Energy Research Program, October 2005.
- [14] M. Chhabra, T. Harnesswalla, M. Lim, and F. Barnes. Frequency regulation and economic dispatch using integrated storage in a hybrid renewable grid. In International Conference on Energy, Automation, and Controls, pages 1–6, December 2011.

- [15] Federal Energy Regulatory Commission. FERC order 755, 2011.
- [16] Federal Energy Regulatory Commission. FERC order 784, 2013.
- [17] C. D. Corbin, G. P. Henze, and P. May-Ostendorp. A model predictive control optimization environment for real-time commercial building application. Journal of Building Performance Simulation, 6 (3):159–174, 2014.
- [18] North America Electric Reliability Corporation. Balancing and frequency control, 2011.
- [19] S. Eichorn. Performance based regulation (pbr) phase i. <http://www.pjm.com/committees-and-groups/closed-groups/rpstf.aspx>, 2012.
- [20] S. Eichorn. Performance based regulation (pbr) phase ii. <http://www.pjm.com/committees-and-groups/closed-groups/rpstf.aspx>, 2012.
- [21] Beckwith Electric. Generator protection using multifunction digital relays (ECNE 10/92), 2014.
- [22] Regulation Performance Senior Task Force. Performance Based Regulation: Year One Analysis. PJM Interconnection, October 2013.
- [23] GreenHeck. Centrifugal utility fans-model sfd, sfb and swb, 2014.
- [24] H. Hao, A. Kowli, Y. Lin, P. Barooah, and S. Meyn. Ancillary service for the grid via control of commercial building hvac systems. In 2013 American Control Conference, pages 467–472, June 2013.
- [25] H. Hao, B. M. Sanandaji, K. Poolla, and T. L. Vincent. Frequency regulation from flexible loads: Potential, economics, and implementation. Embala Power Networks, September, 2013.
- [26] G. P. Henze. Construction element modeling using the lumped parameter analysis. In-class material of HVAC Controls, 2014.
- [27] G. P. Henze. Energy system simulation: Room modeling. In-class material of HVAC Controls, 2014.
- [28] G. P. Henze and A. G. Floss. Evaluation of temperature degradation in hydraulic flow networks. Energy and Buildings Journal, 43 (8):1820–1828, 2011.
- [29] G.P. Henze, M. J. Brandemuehl, C. Felsmann, A. Florita, and H. Cheng. Final project report for ashrae research project 1313-rp: Evaluation of building thermal mass savings. American Society of Heating, Refrigerating, and Air-Conditioning Engineers, 2007.
- [30] G.P. Henze, C. Felsmann, and G. Knabe. Evaluation of optimal control for active and passive building thermal storage. International Journal of Thermal Sciences, 43:173–183, June 2003.
- [31] C. Hinman and J. Riessen. Pay for performance regulation. California ISO, February, 2013.
- [32] H. F. Illian. Frequency control performance measurement and requirement. Ernest Orlando Lawrence Berkeley National Laboratory, page December 2010, 2010.
- [33] Inoutic. The german profile engineers for windows and doors, 2014.
- [34] Electric Power Research Institute. Demand response devices, 2014.

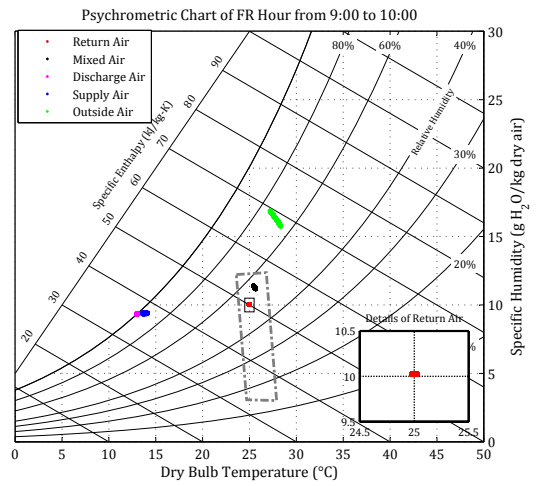
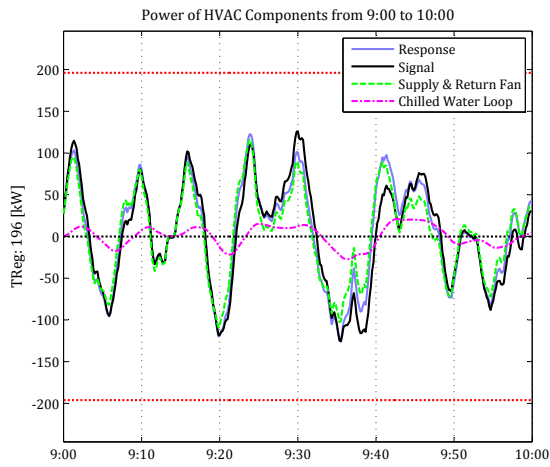
- [35] PJM Interconnection. Daily real-time lmp files, daily rmecp prices and rmpcp prices. Daily LMP files, 2014.
- [36] PJM Interconnection. Fast response regulation signal. RegA and RegD signal from 12/18/2012 to 1/18/2013, 2014.
- [37] PJM Interconnection. Performance based regulation: Year one analysis. PJM Interconnection, 2014.
- [38] PJM Interconnection. Performance score calculation equations. Performance-score-template.xlsm, 2014.
- [39] PJM Interconnection. PJM manual 11: Energy and ancillary services market operations, 2014.
- [40] PJM Interconnection. PJM manual 12: Balancing operations, 2014.
- [41] PJM Interconnection. PJM manual 28: Operating agreement accounting, 2014.
- [42] PJM Interconnection. Regulation self-test signals. Test Signals of RegA and RegD Signal, 2014.
- [43] PJM Interconnection. Performance based regulation glossary, June, 2012.
- [44] PJM Interconnection. PJM interconnection order no. 755 compliance filing, March, 2012.
- [45] New York ISO. Ancillary services manual, December, 2013.
- [46] N. Jaleeli and L.S. Vanslyck. NERC's new control performance standards. IEEE Transactions of Power Systems, 14 (3):1092–1099, 1999.
- [47] D. Kathan. Policy and technical issues associated with iso demand response programs. The National Association of Regulatory Utility Commissioners, July, 2002.
- [48] KEMA. Kermit study report to determine the effectiveness of the agc in controlling fast and conventional resources in the pjm frequency regulation market. Regulation Performance Senior Task Force of PJM Interconnection, December, 2011.
- [49] B. Kirby. Ancillary services: Technical and commercial insights. Wartsila North America Inc., 2007.
- [50] B. J. Kirby, J. Dyer, C. Martinez, R. A. Shoureshi, R. Guttromson, and J. Dagle. Frequency control concerns in the north american electric power system. Transmission Reliability Program, 2002.
- [51] M.L. Lazarewicz and T.M. Ryan. Integration of flywheel-based energy storage for frequency regulation in deregulated markets. In Power and Energy Society General Meeting, pages 1–6. IEEE, July 2010.
- [52] D. Letto, S. Snowling, R. George, C. Morrissey, H. Andres, and C. Fox. Creating new revenue with existing process: Evaluating grid balance with demand-side loads at wastewater treatment plants using dynamic modeling. Embala Power Networks, 2012.
- [53] C. Lyons. A smart grid approach to regulation and ramping. California Energy Storage Alliance, August 2009.

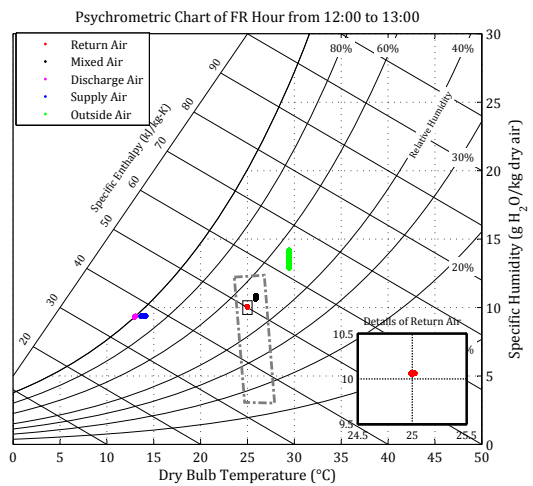
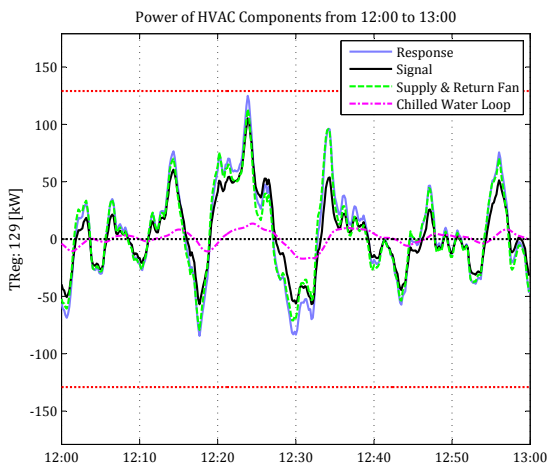
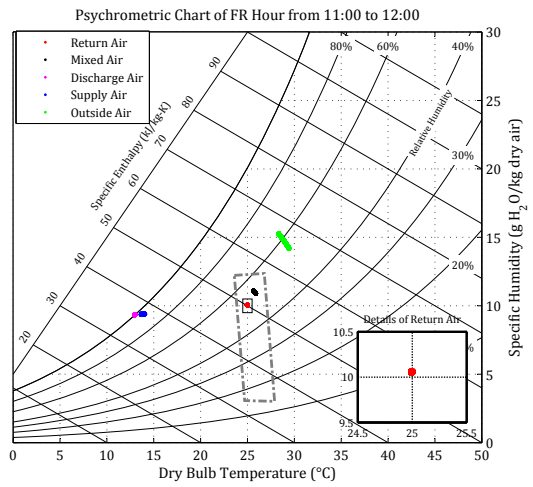
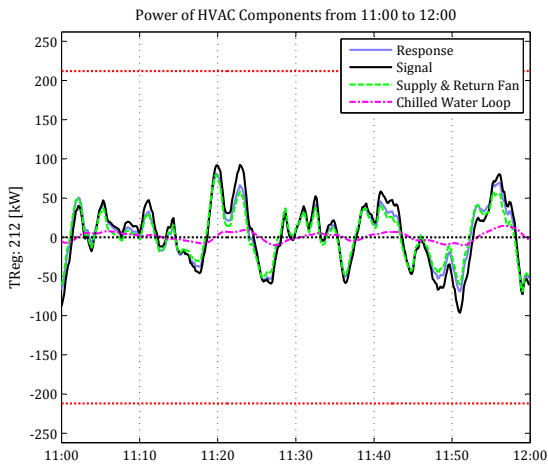
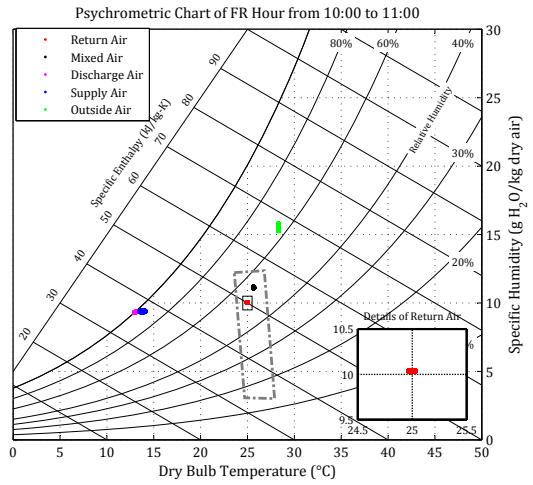
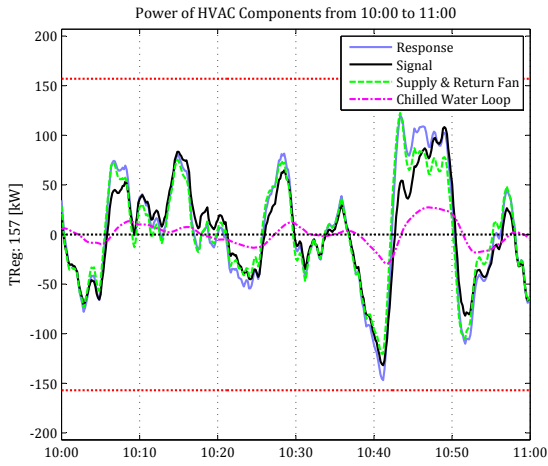
- [54] M. Maasoumy, Jorge Ortiz, D. Culler, and A. Sangiovanni-Vincentelli. Flexibility of commercial building hvac fan as ancillary service for smart grid. In Proceedings of Green Energy and Systems Conference 2013, pages 1–6, November 25.
- [55] Y. V. Makarov, C. Loutan, J. Ma, and P. D. Mello. Operational impacts of wind generation on california power systems. Pacific Northwest National Laboratory, 24 (2), May 2009.
- [56] Y. V. Makarov, J. Ma, S. Lu, and T.B. Nguyen. Assessing the value of regulation resources based on their time response characteristics. Pacific Northwest National Laboratory, June 2008.
- [57] J. L. Mathieu. Demand response today. CDC Workshop: Ancillary Services from Flexible Loads to Help the Electric Grid of the Future, December, 2013.
- [58] J. L. Mathieu, P. N. Price, Kiliccote S, and M. A. Piette. Quantifying changes in building electricity use, with application to demand response. IEEE Transactions on Smart Grid, 2 (3):507–518, September 2011.
- [59] Mathworks. Neural network time series prediction and modeling. Neural Network Toolbox, 2014.
- [60] F. C. McQuinston, J. D. Parker, and J. D. Spitler. Heating, Ventilating and Air Conditioning Analysis and Design 6th edition. Wiley, 2004.
- [61] Greentech Media. Wal-mart, schneider electric test the grid-to-building energy connection, May 2014.
- [62] F.B. Morris, J.E. Braun, and S.J. Treado. Experimental and simulated performance of optimal control of building thermal storage. ASHRAE Transactions, 100 (1), January 1994.
- [63] Office of Electric Transmission and Distribution of the U.S. Department of Energy. Grid 2030: A National Vision for Electricity’s Second 100 Years. U.S. Department of Energy, 2003.
- [64] Department of Energy. Office of electricity delivery and energy reliability. National Electric Transmission Congestion Study, 2012.
- [65] U.S. Department of Energy. Improving fan system performance: A sourcebook for industry, April, 2003.
- [66] B. Ozpineci and L. M. Tolbert. Simulink implementation of induction machine model a modular approach. In Electric Machine Drives Conference (IEMDC 2003), pages 728–734, 2004.
- [67] G. S. Pavlak, G. P. Henze, and V. J. Cushing. Optimizing commercial building participation in energy and ancillary service markets. Elsevier Energy and Buildings (In transaction), 2014.
- [68] K. Porter, S. Fink, J. Rogers, C. Mudd, M. Buckley, and C. Clark. Review of industry practice and experiences in the integration of wind and solar generation. PJM Renewable Integration Study, November 2012.
- [69] QCoefficient. Case studies, 2014.
- [70] QCoefficient. Grid-scale energy storage, 2014.

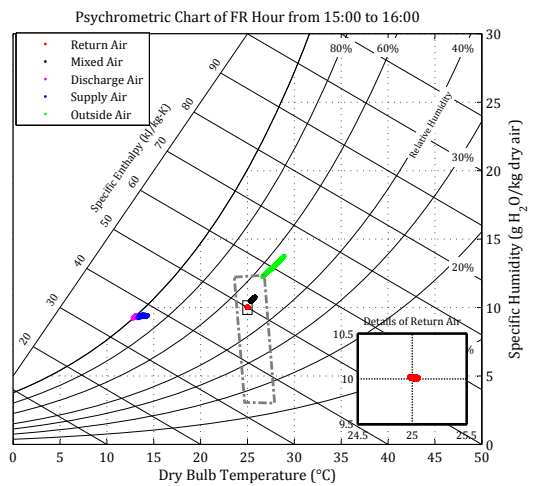
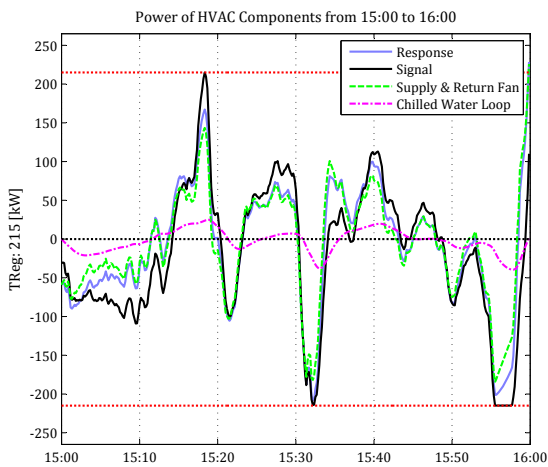
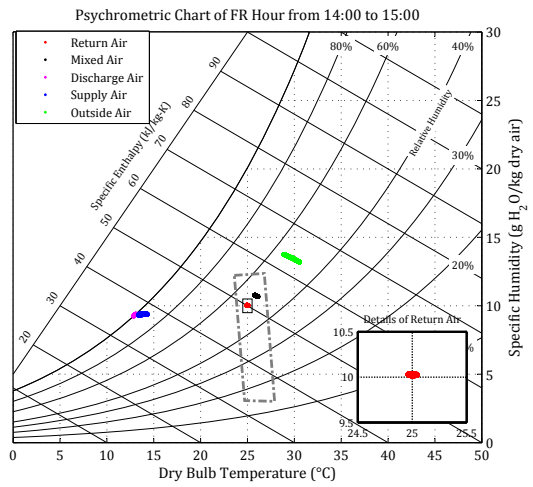
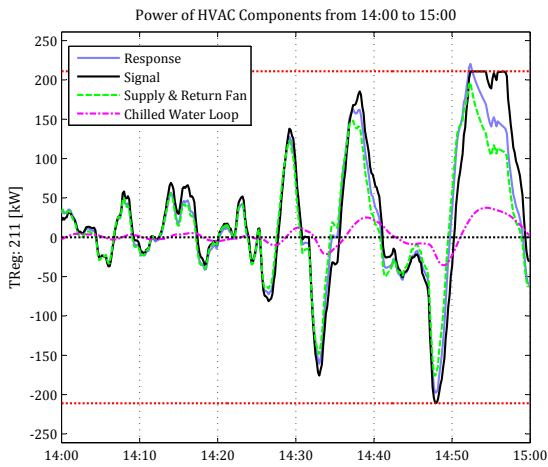
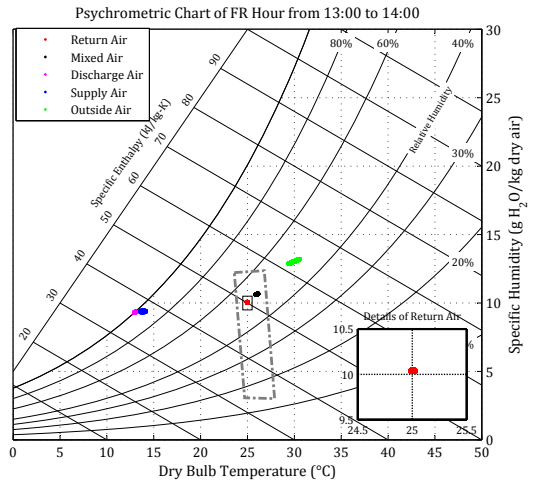
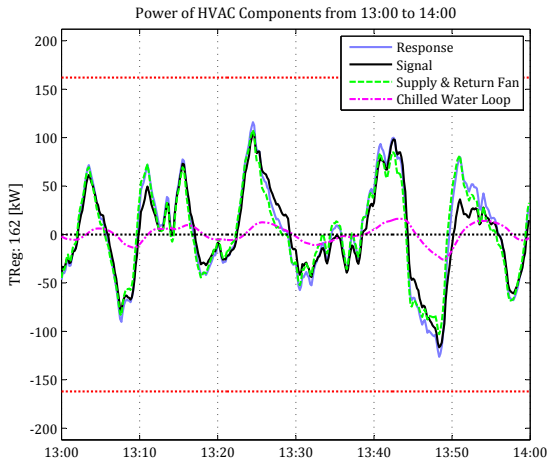
- [71] Forest Reider. Wet cooling coil model. In developing model, 2013.
- [72] T. Rindlisbaker. Air handler supply air temperature set point (ah sat stpt) control based on vav box cooling demand. <http://www.totalbuildingcommissioning.com/2010/06/air-handler-supply-air-temperature-set-point-ah-sat-stpt-control-based-on-vav-box-cooling-demand/>, June 2010.
- [73] B.P. Roberts and C. Sandberg. The role of energy storage in development of smart grids. In Proceedings of the IEEE, 99 (6), pages 1139–1144. IEEE, June 2011.
- [74] H.E. Shaalan. Handbook of Electric Power Calculation, 3rd edition. McGraw-Hill, 2003.
- [75] P. Steffes. Grid-interactive renewable water heating. Steffes Corporation, 2014.
- [76] R. Stull. Wet-bulb temperature from relative humidity and air temperature. Journal of Applied Meteorology and Climatology, 43 (8):1820–1828, November 2011.
- [77] Arcom Control Systems. PJM DNP specification (release: 1.6), 2006.
- [78] P. Zhao, G.P. Henze, S. Plamp, and V.J. Cushing. Evaluation of commercial building hvac systems as frequency regulation providers. Elsevier Energy and Buildings Journal, 67:225–235, December 2013.

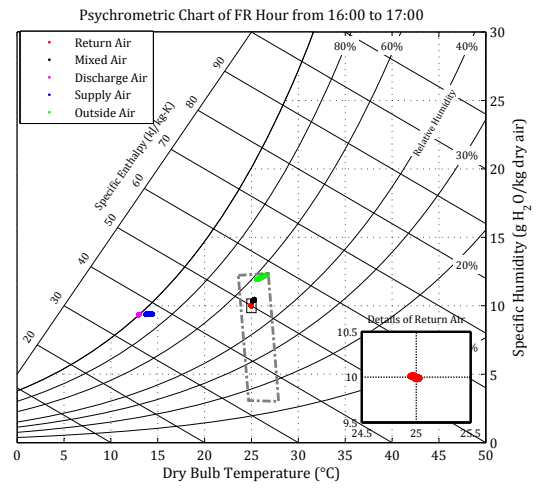
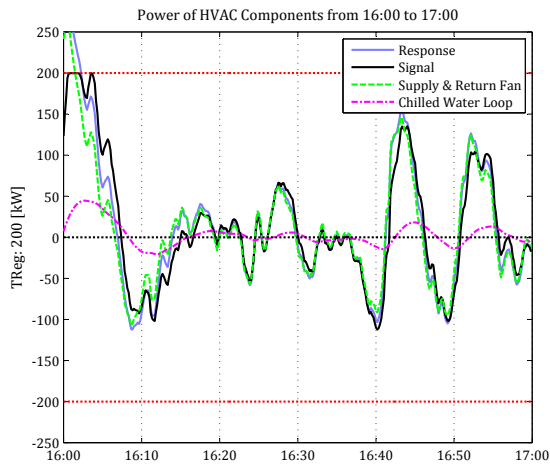
# Appendix A

## Results of $P_{static}$ Setpoint Injection



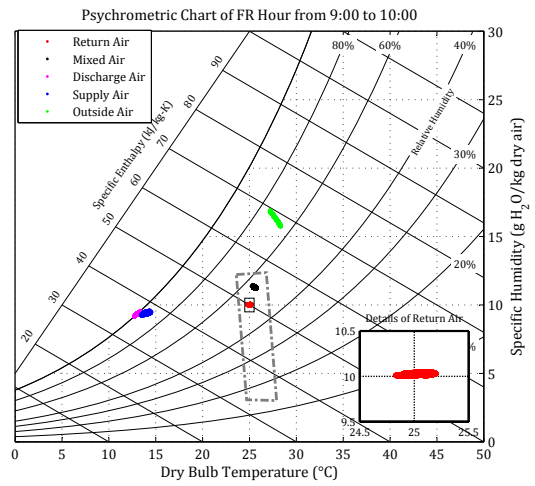
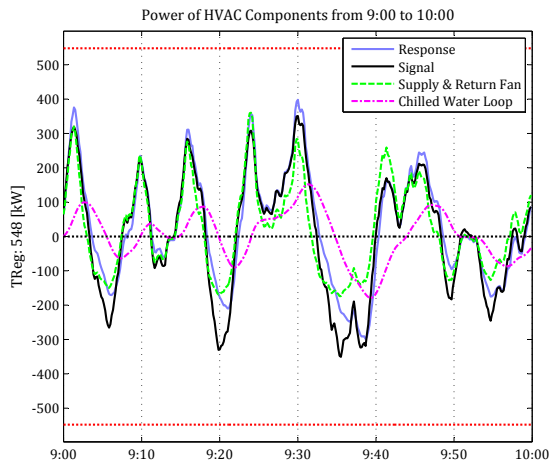


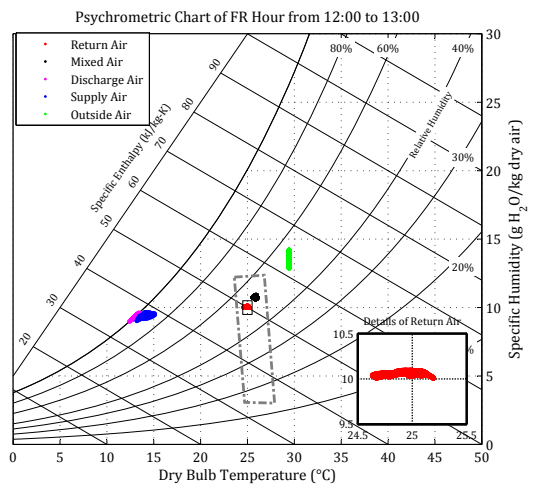
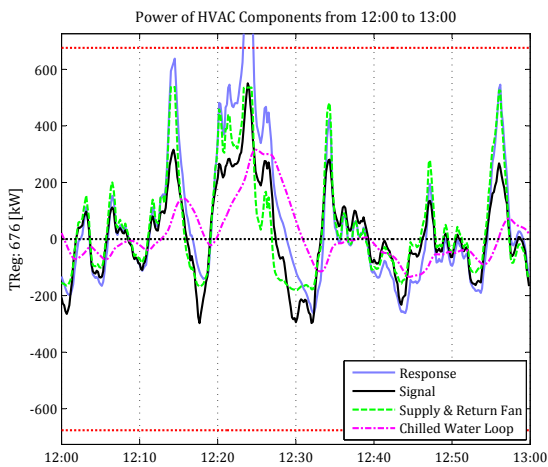
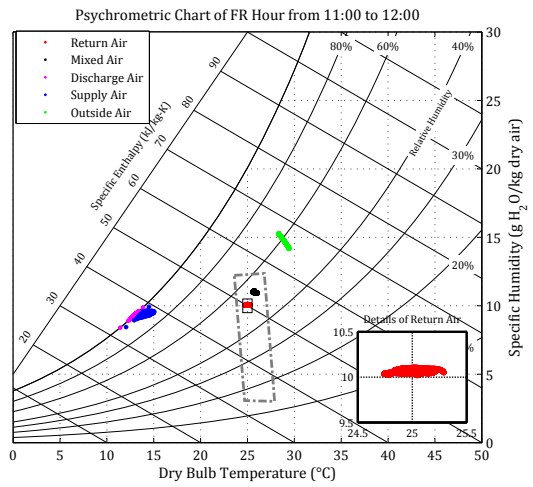
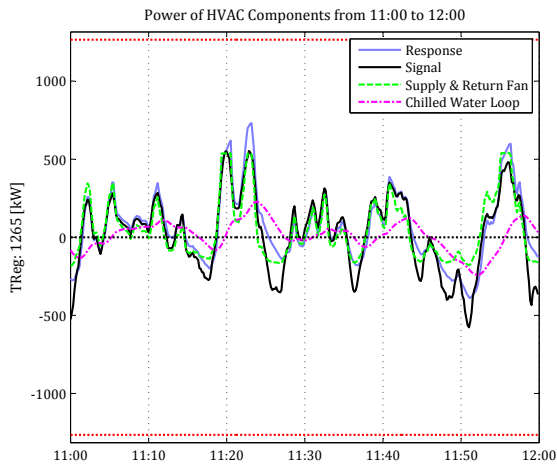
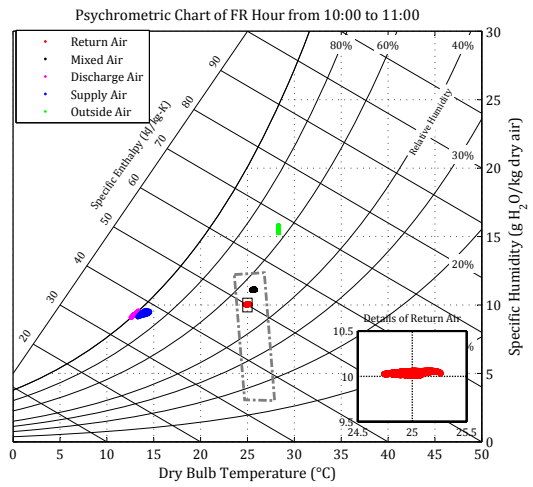
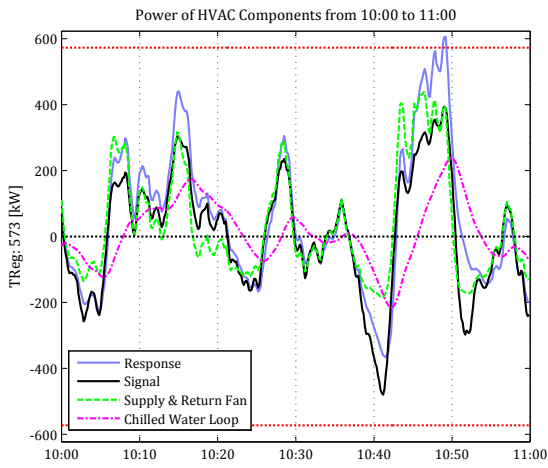


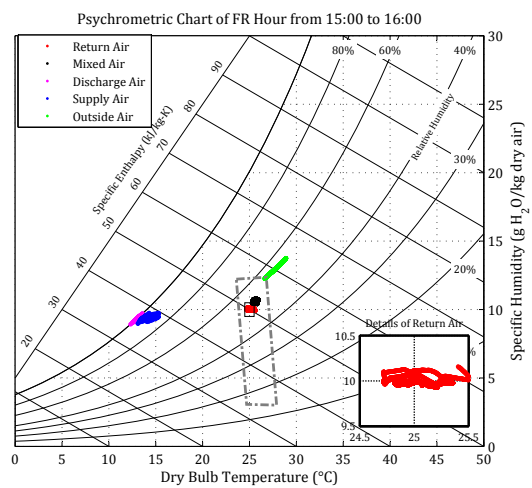
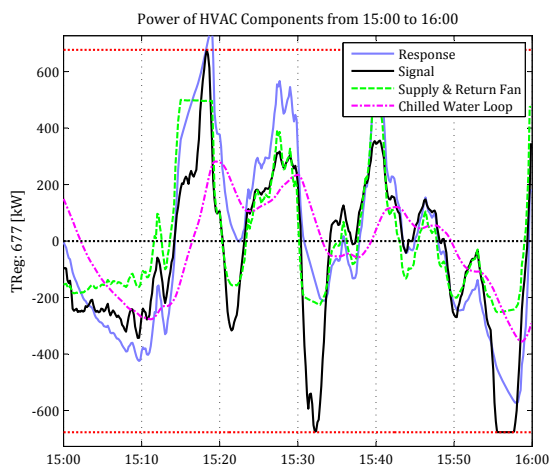
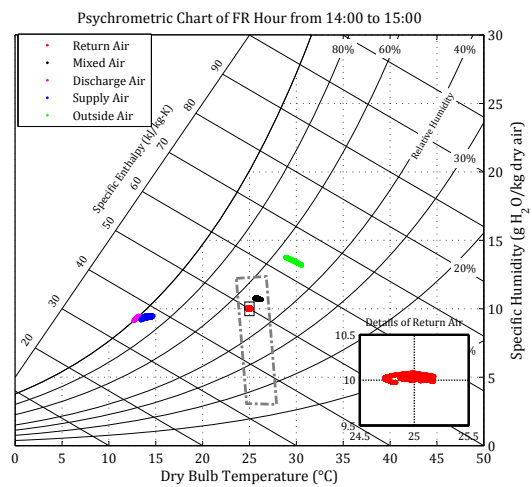
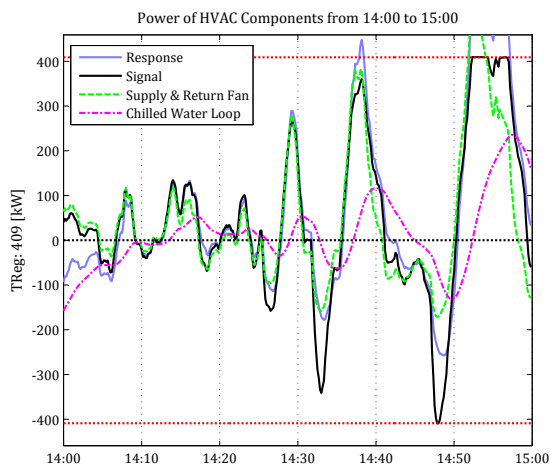
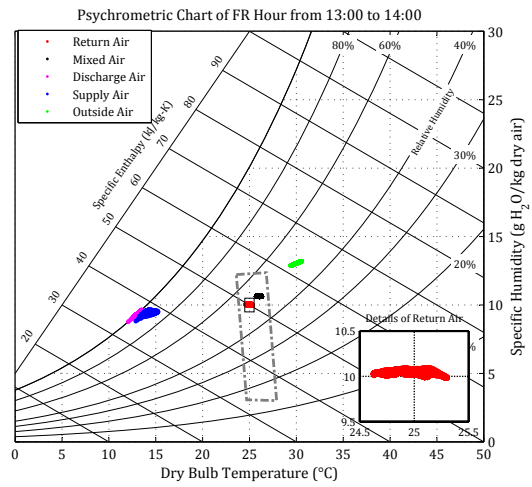
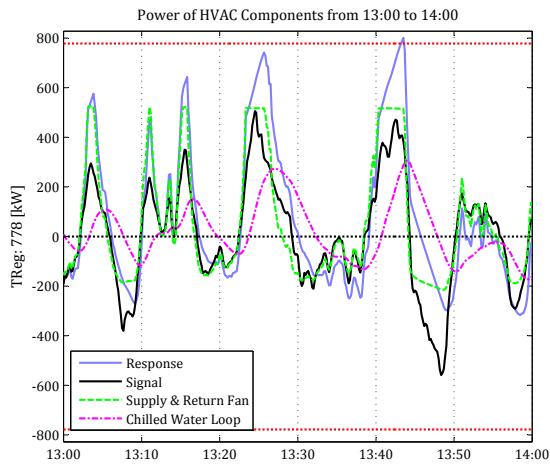


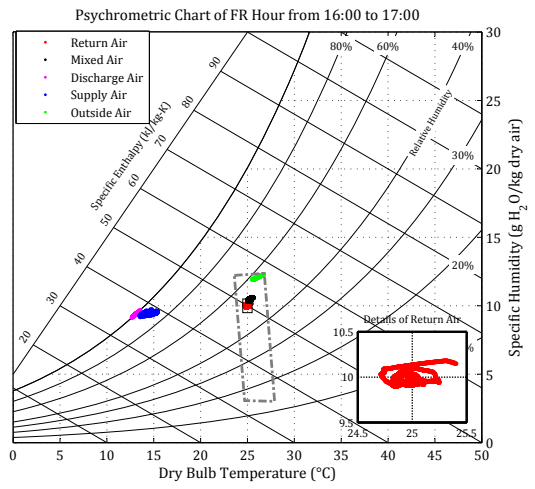
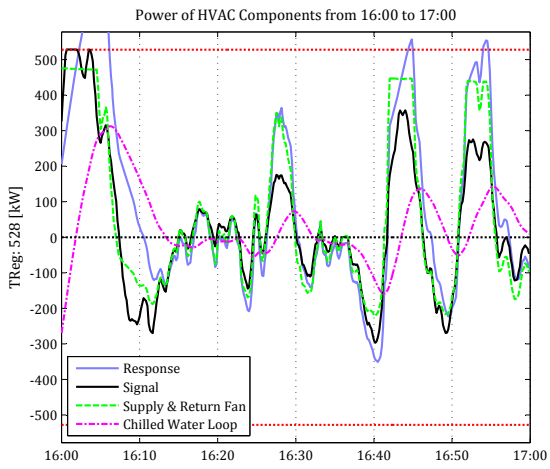
## Appendix B

### Results of $T_{zone}$ Setpoint Injection



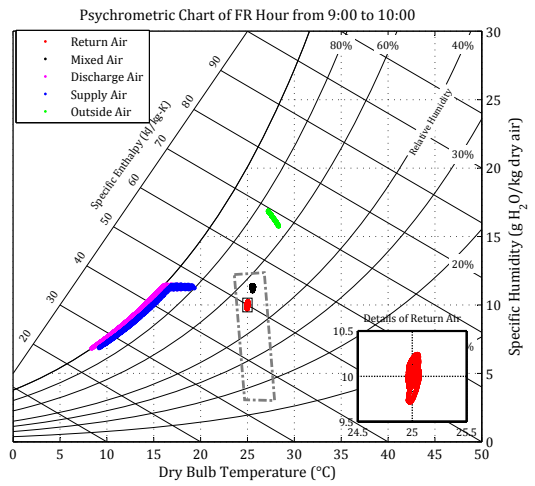
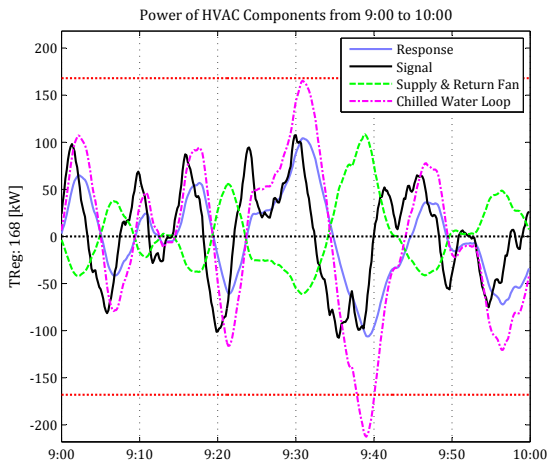


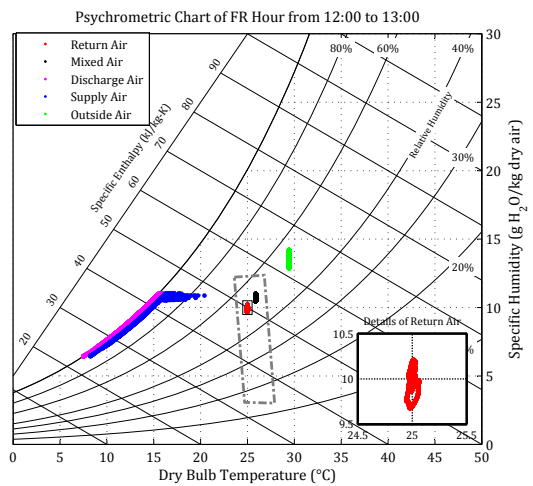
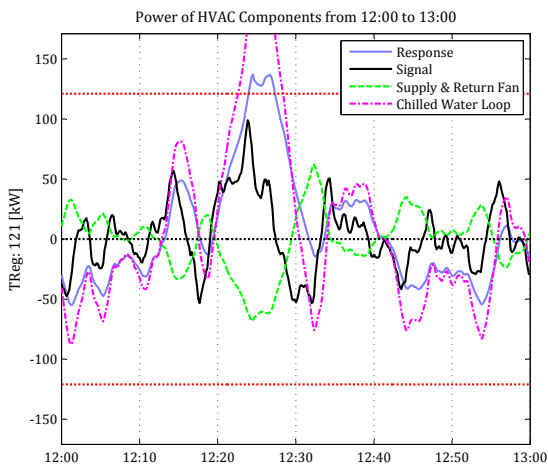
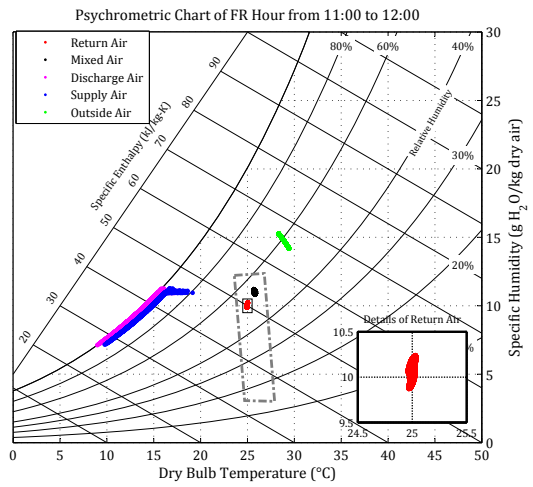
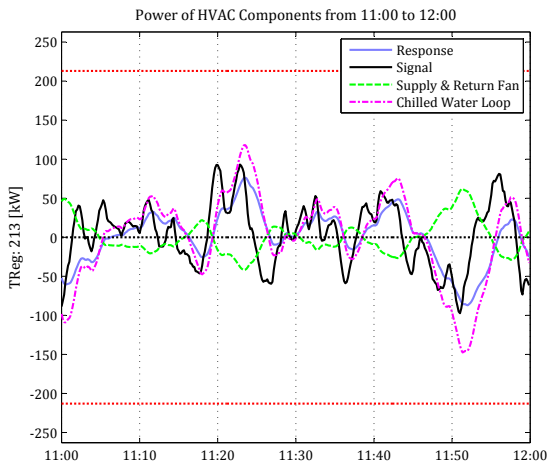
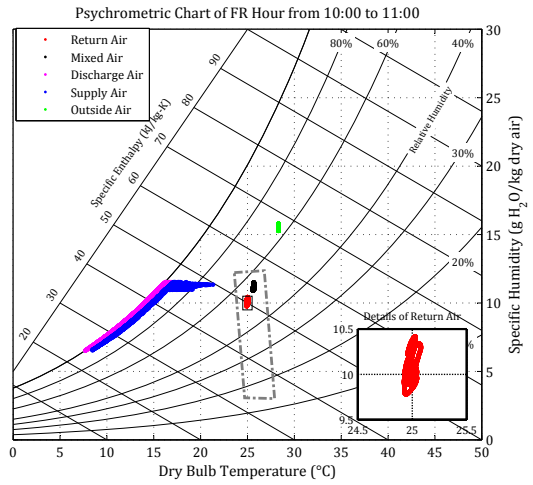
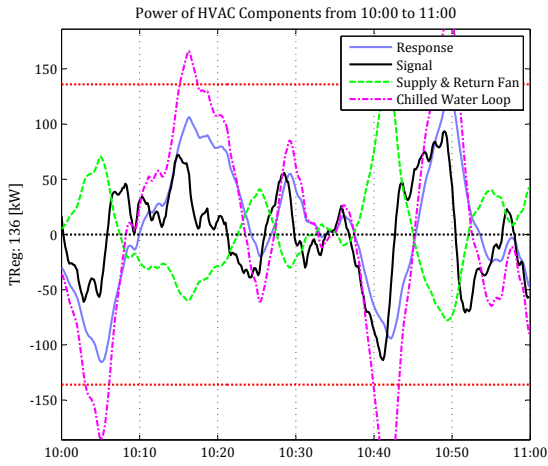


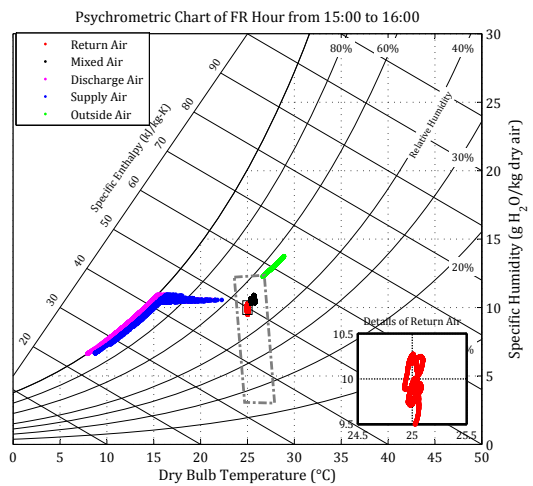
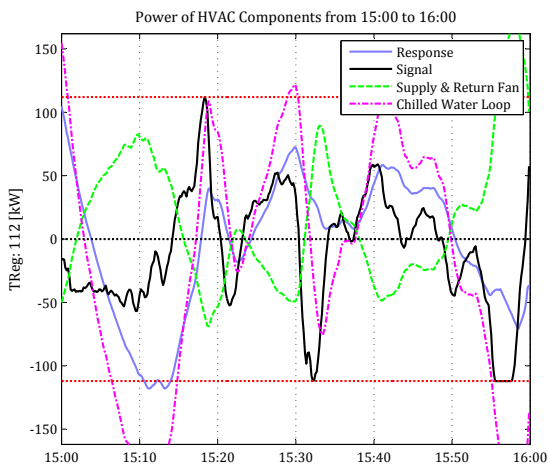
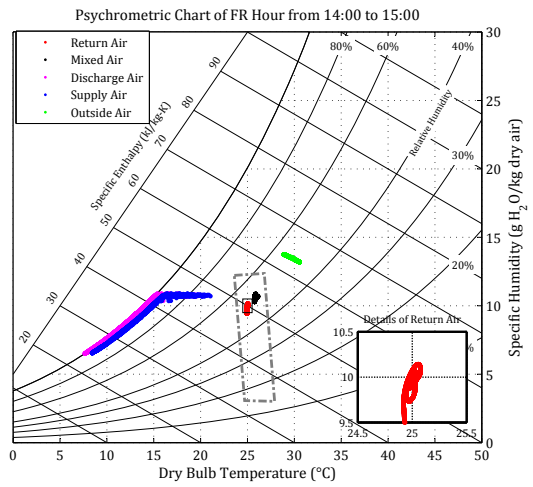
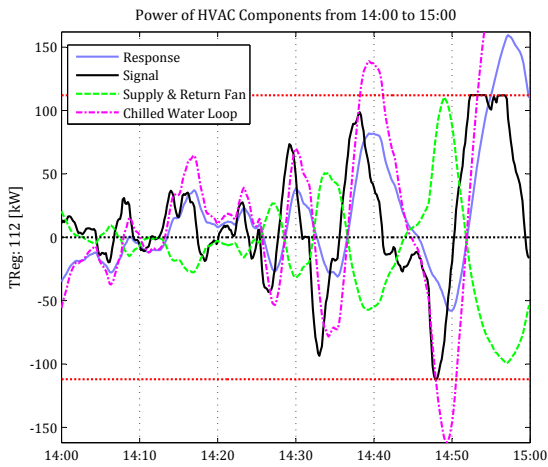
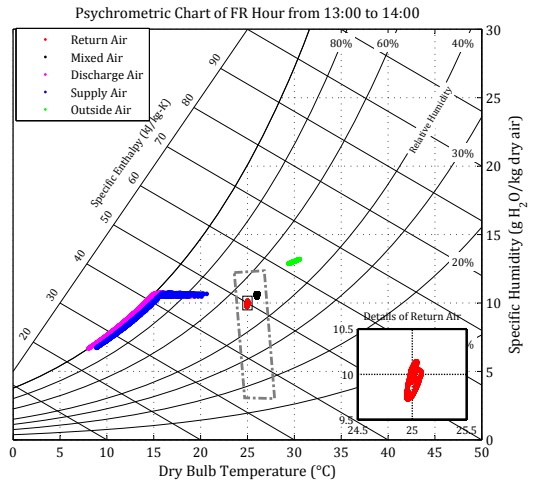
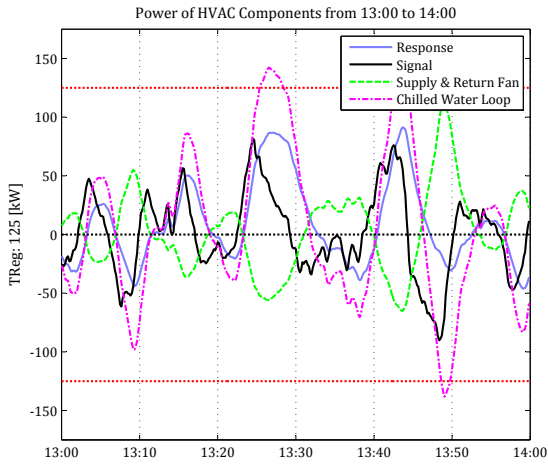


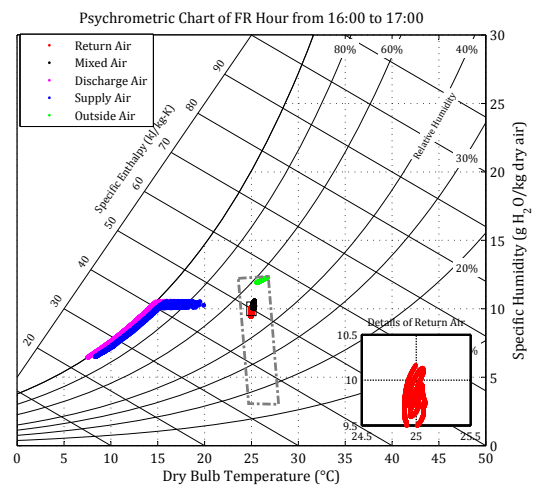
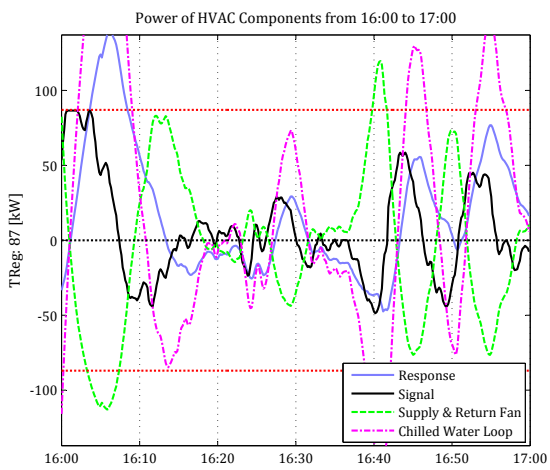
# Appendix C

## Results of $T_{DA}$ Setpoint Injection



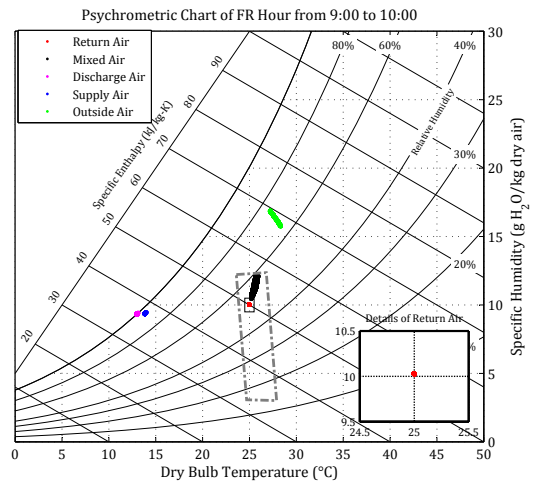
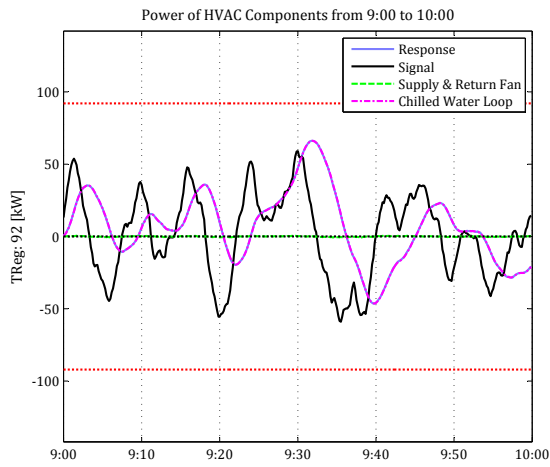


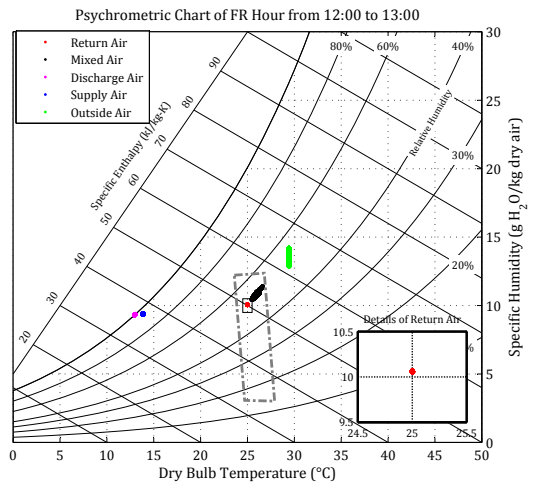
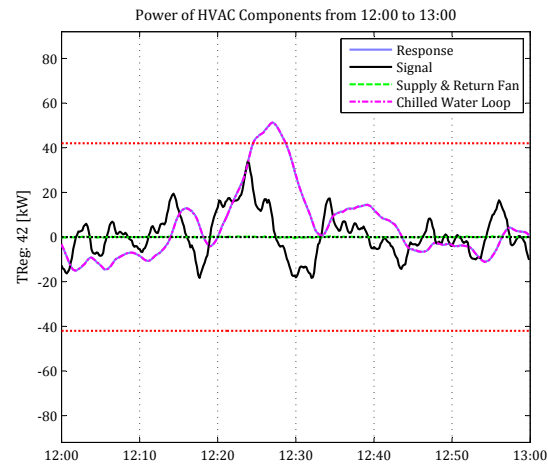
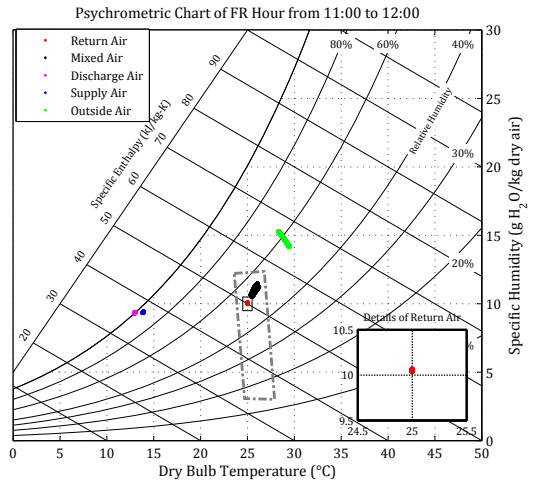
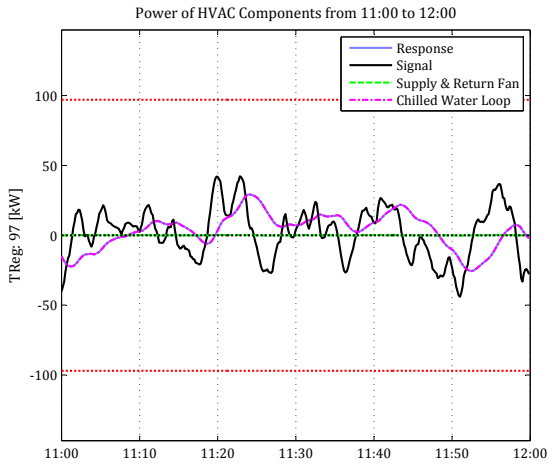
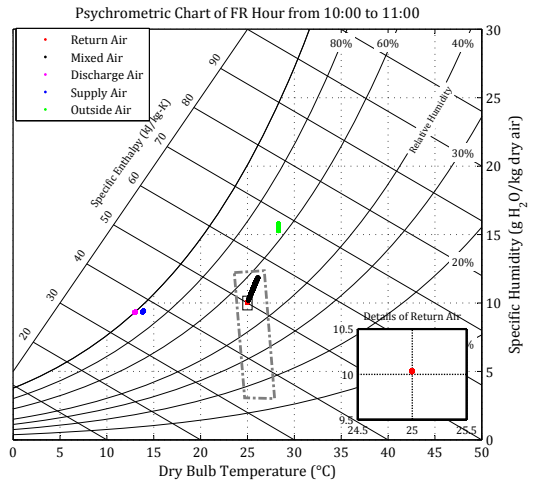
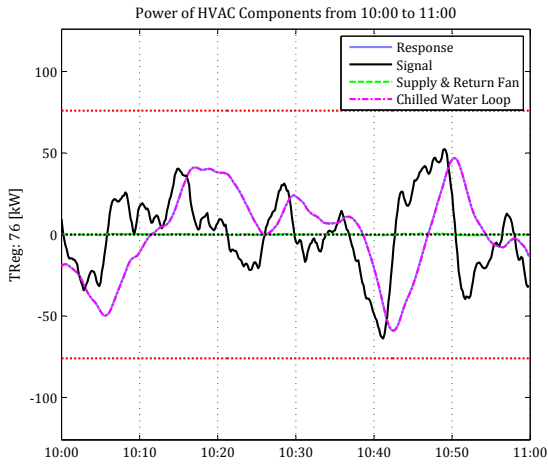


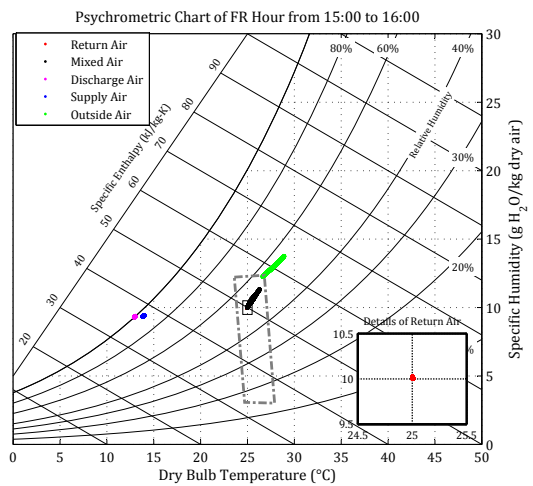
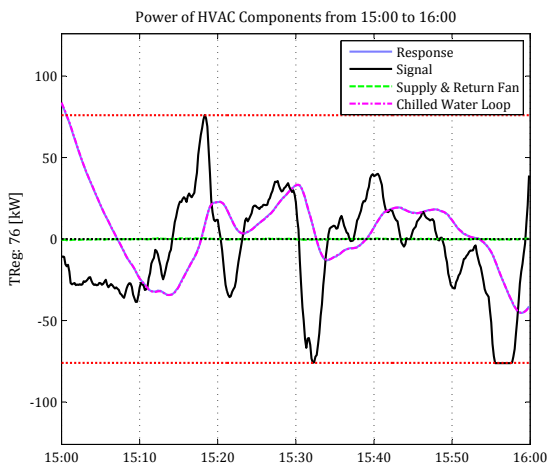
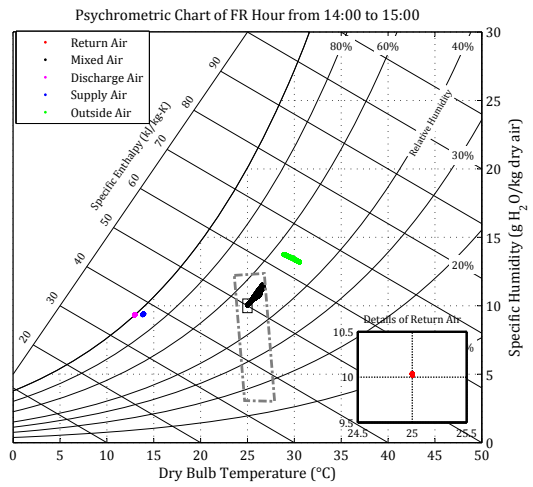
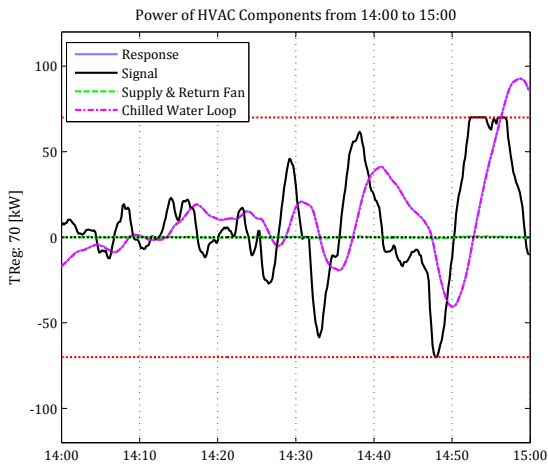
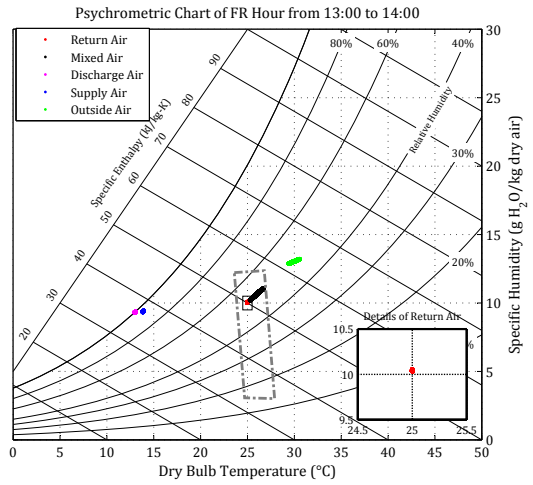
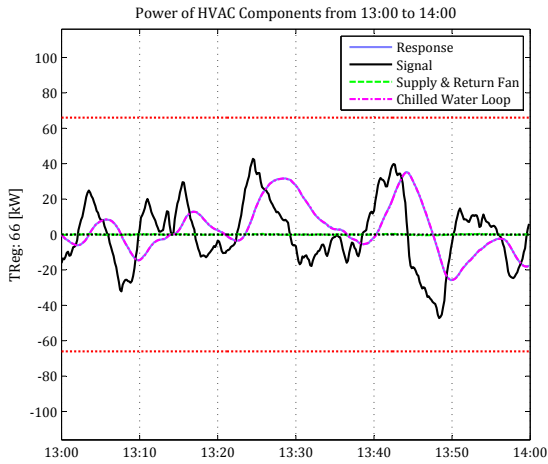


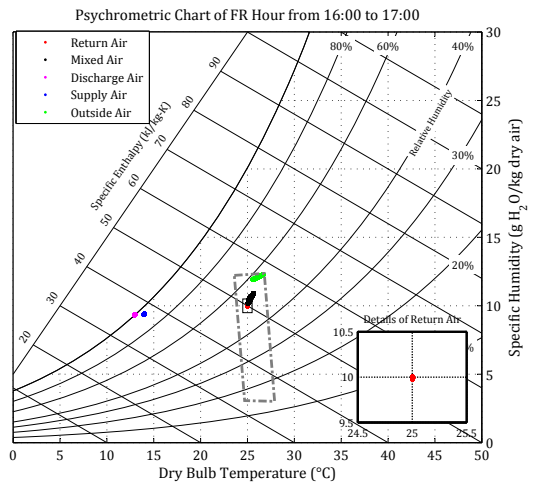
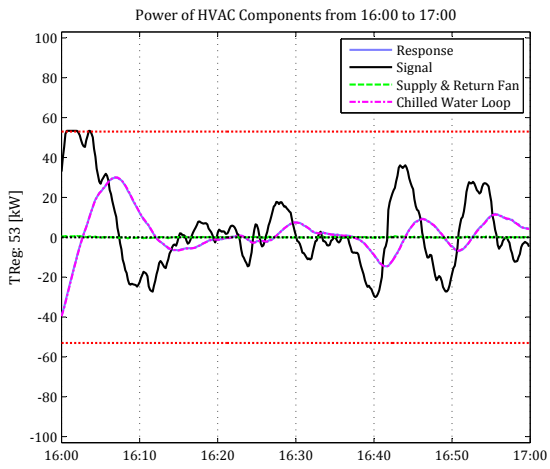
## Appendix D

### Results of OAF Setpoint Superposition



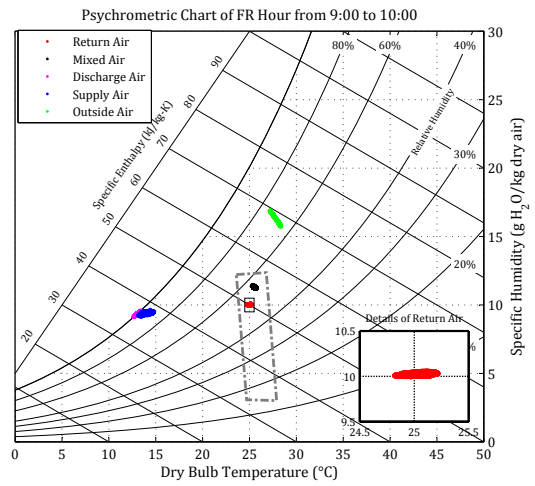
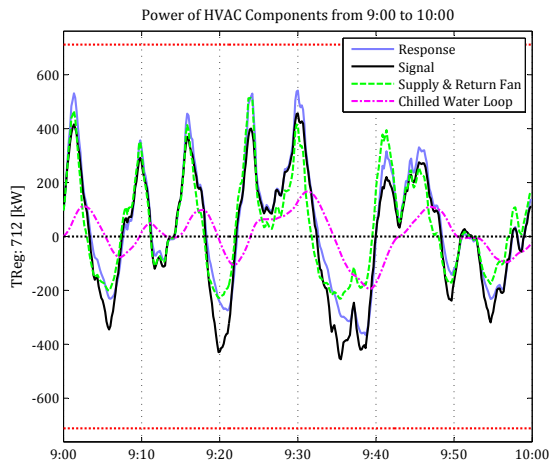


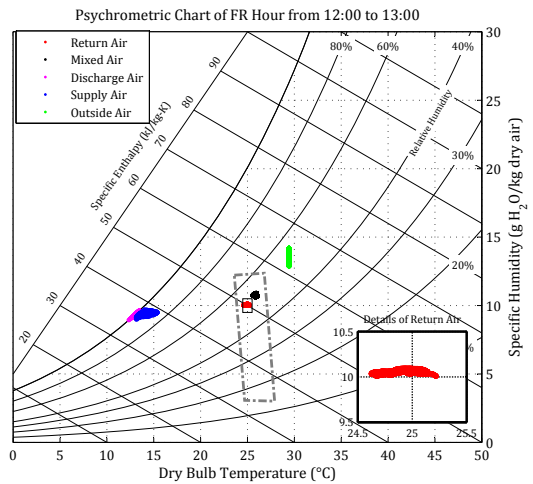
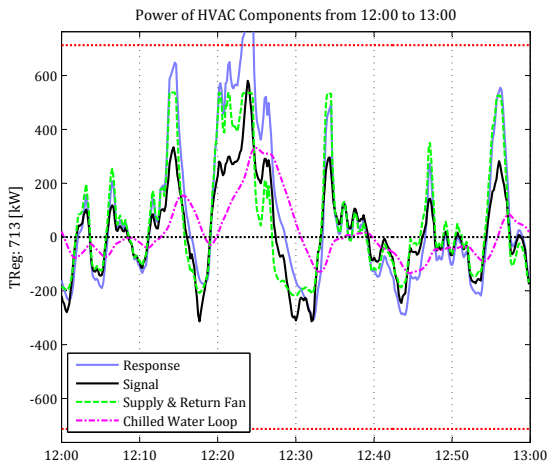
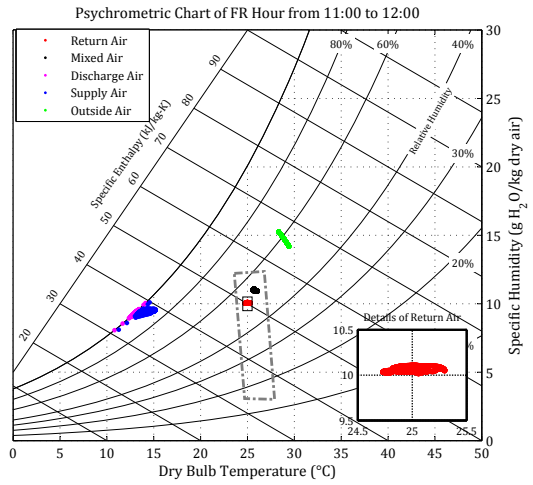
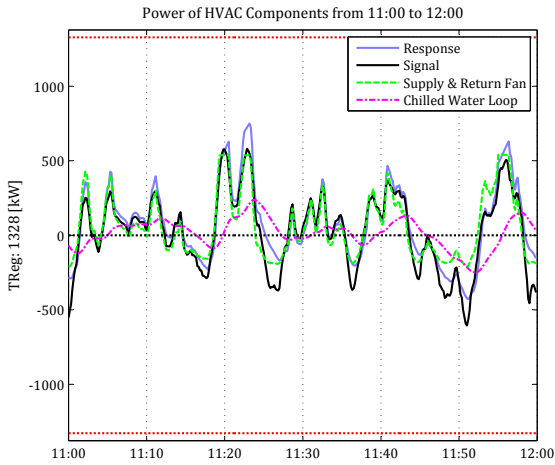
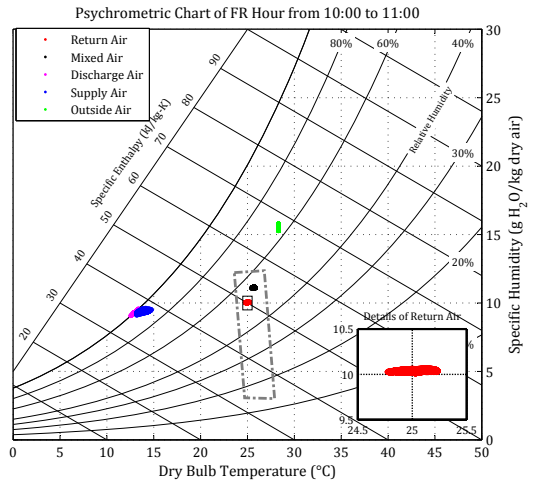
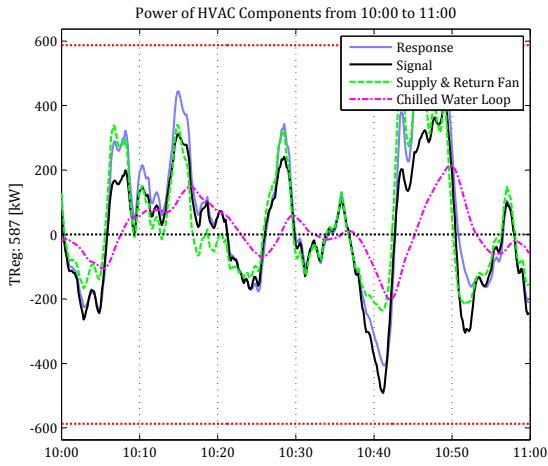


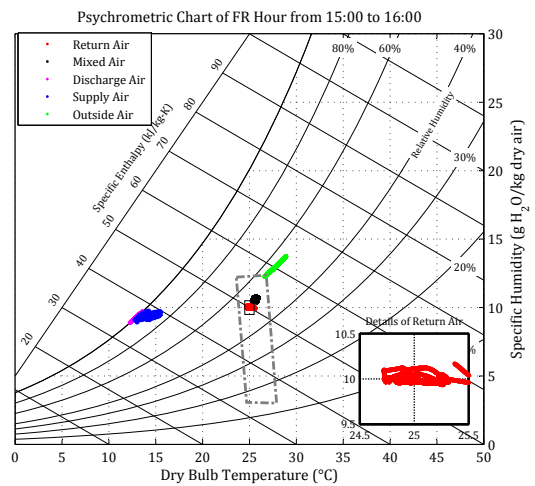
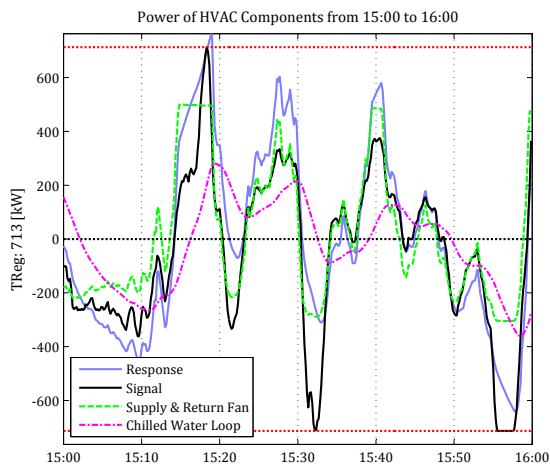
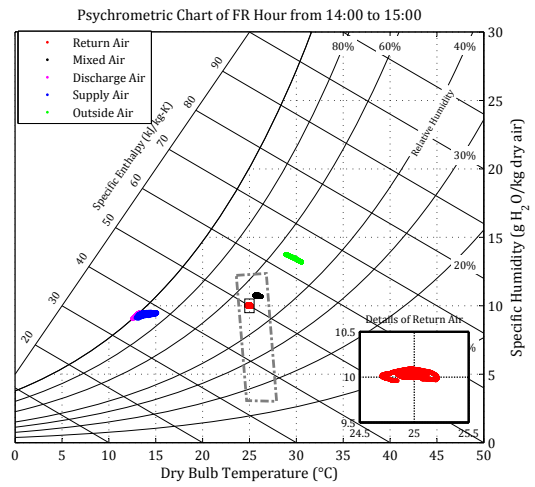
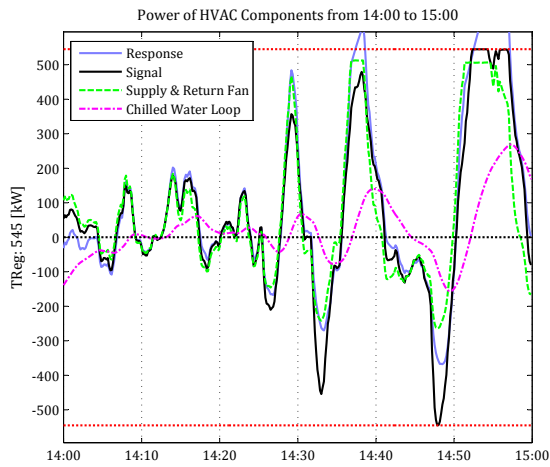
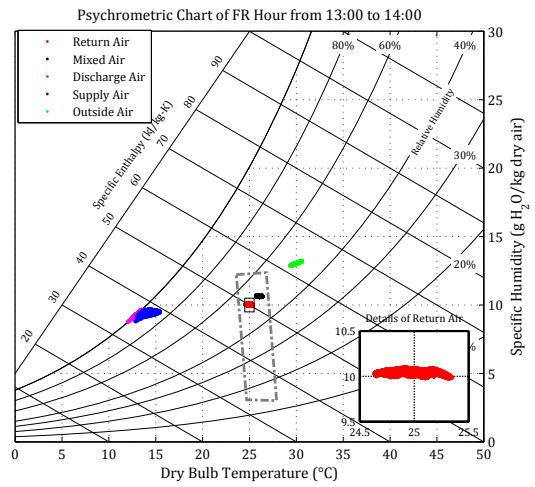
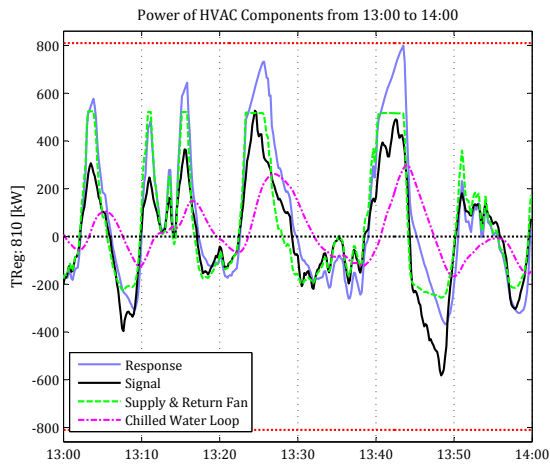


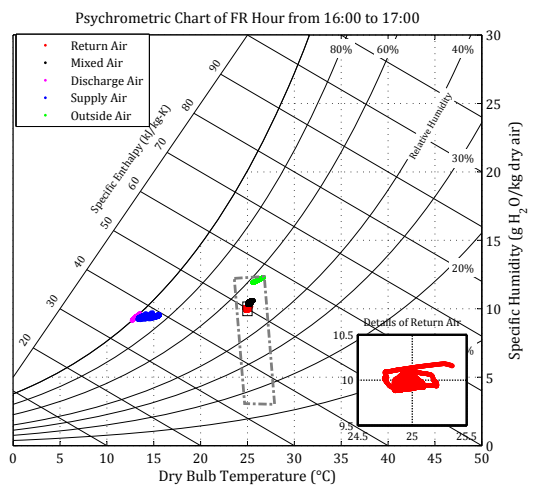
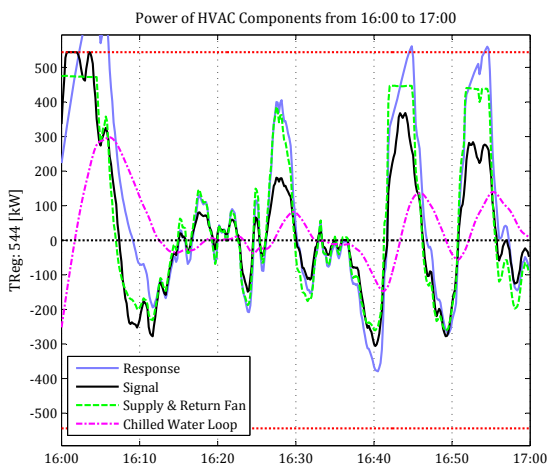
## Appendix E

### Results of Combined Injection: $P_{\text{static}}$ Setpoint and $T_{\text{zone}}$ Setpoint



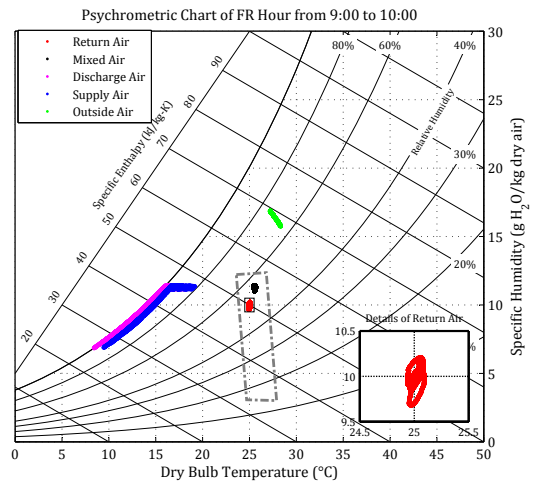
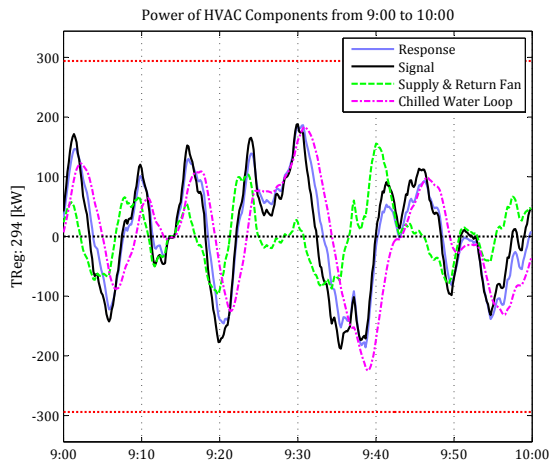


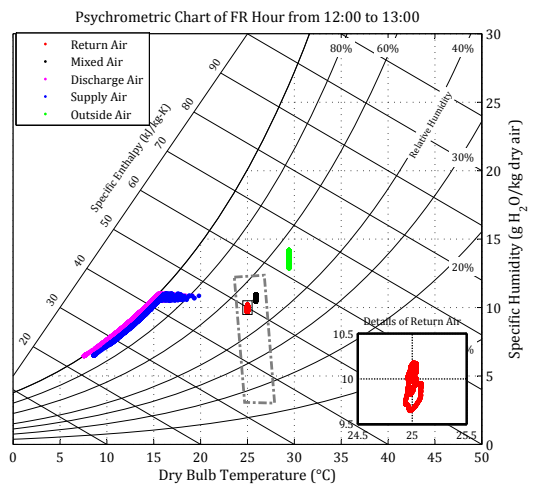
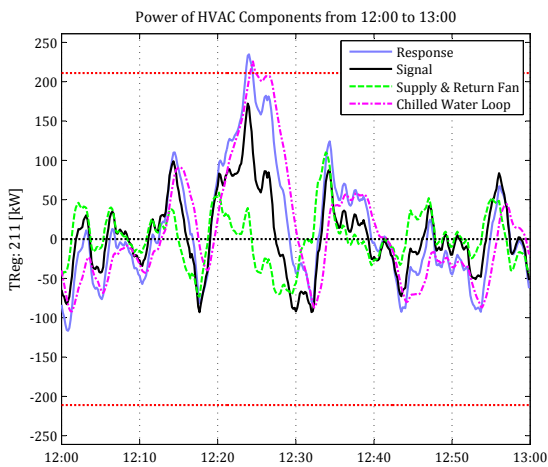
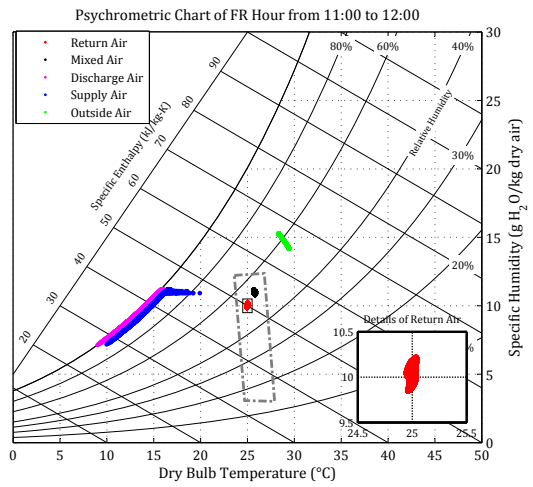
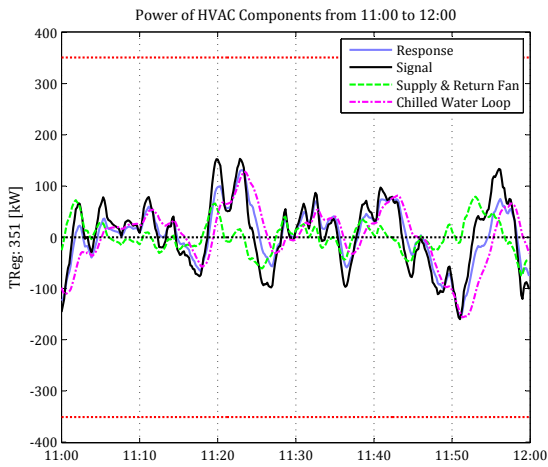
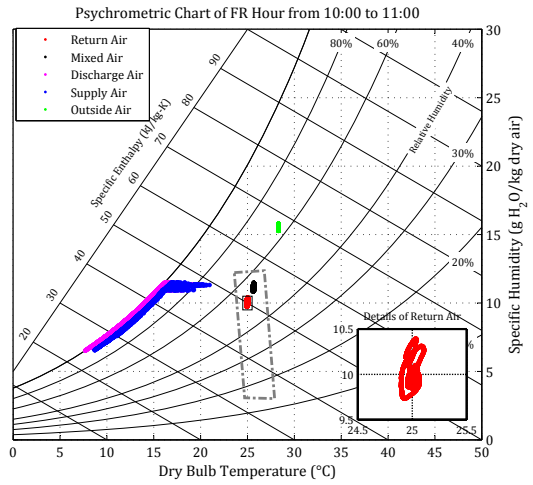
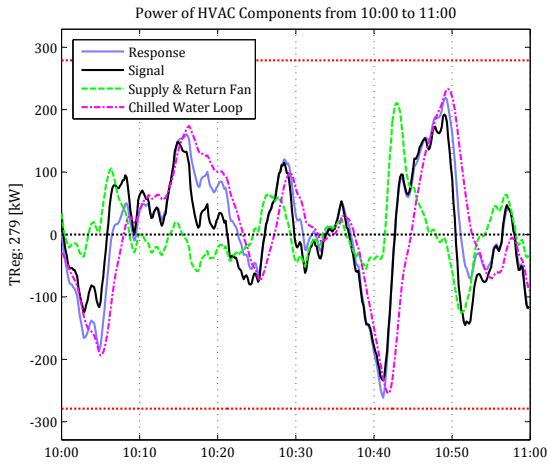


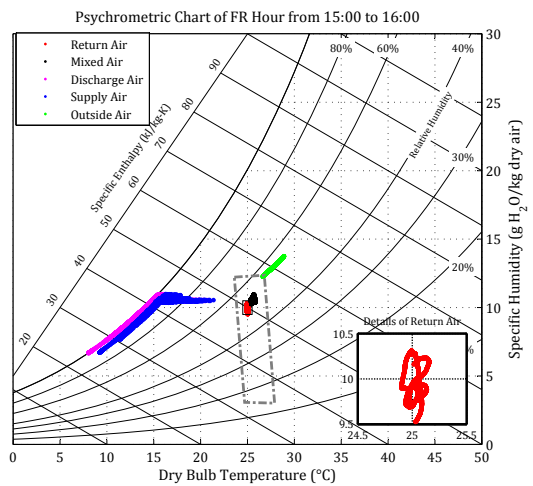
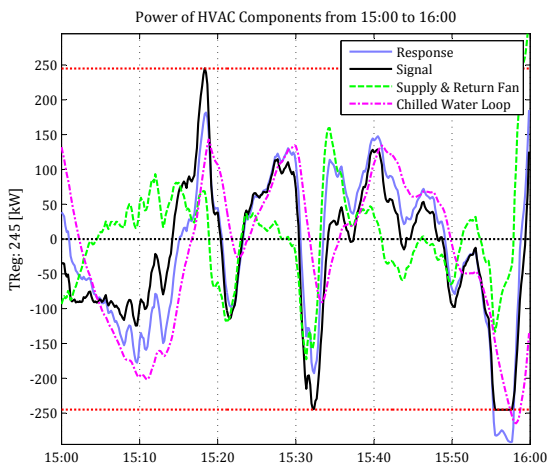
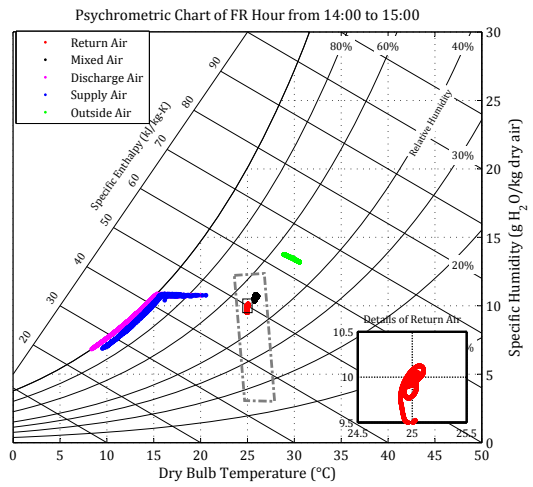
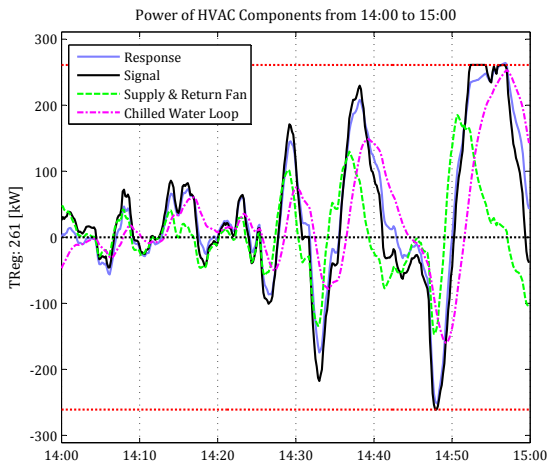
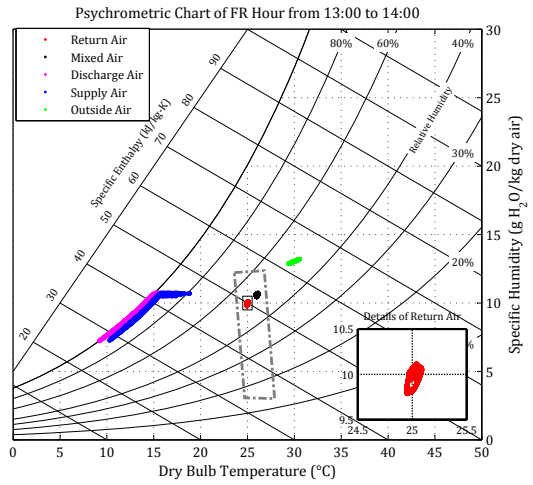
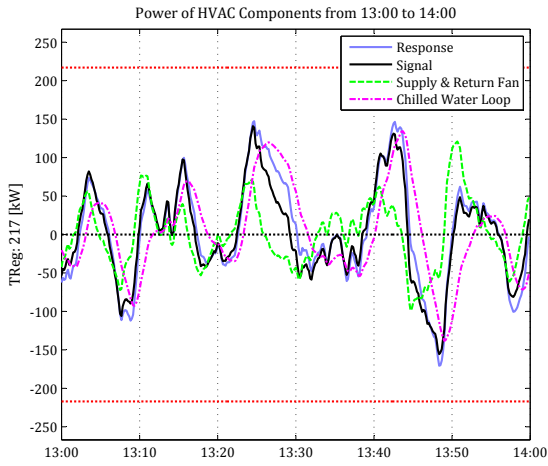


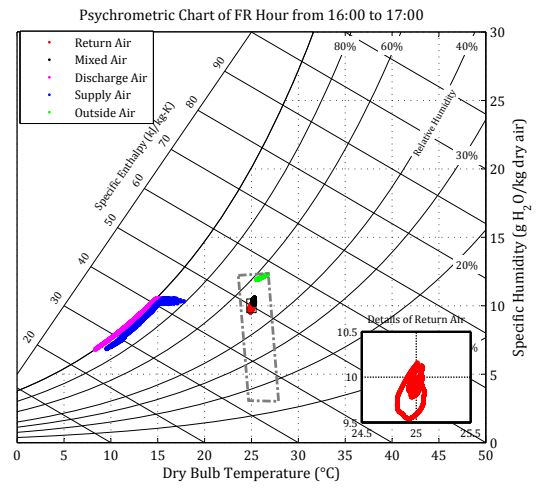
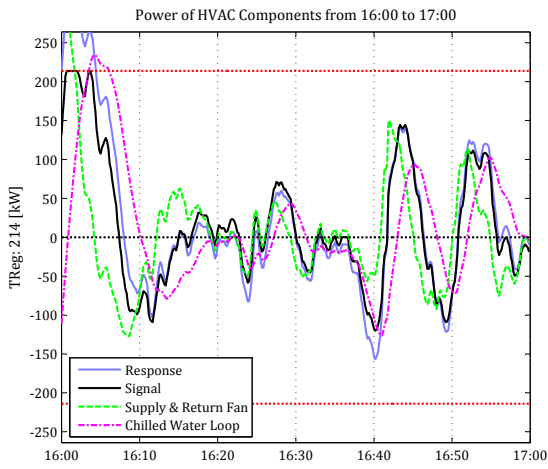
## Appendix F

### Results of Combined Injection: $P_{\text{static}}$ Setpoint and $T_{\text{DA}}$ Setpoint



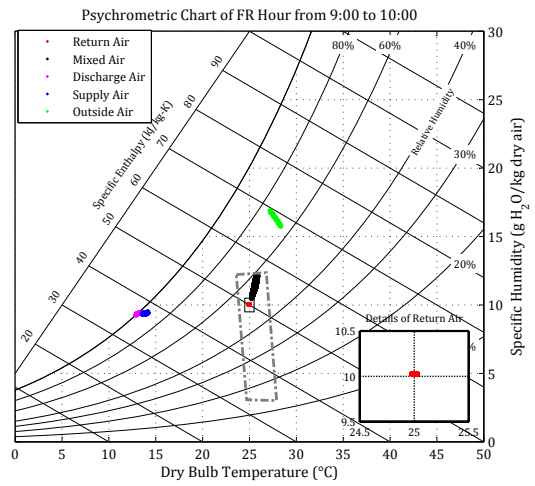
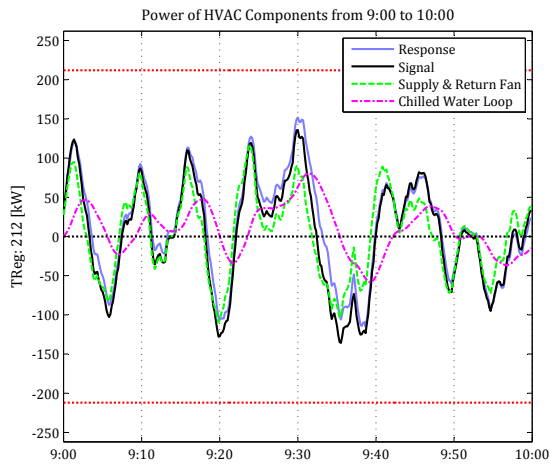


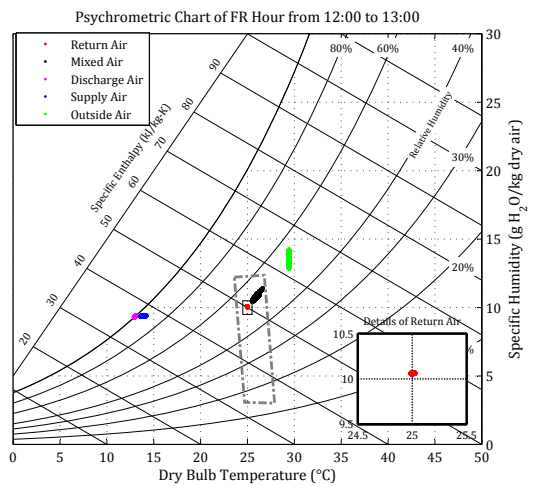
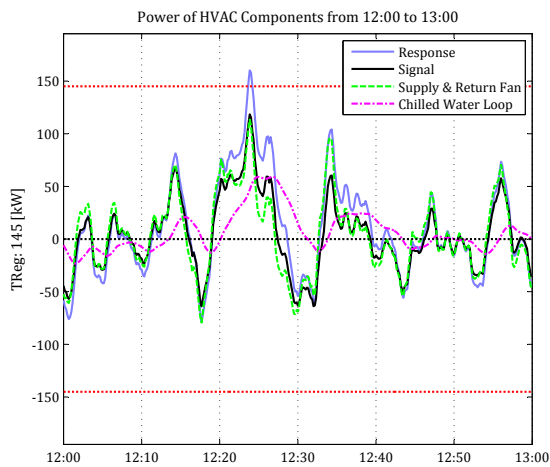
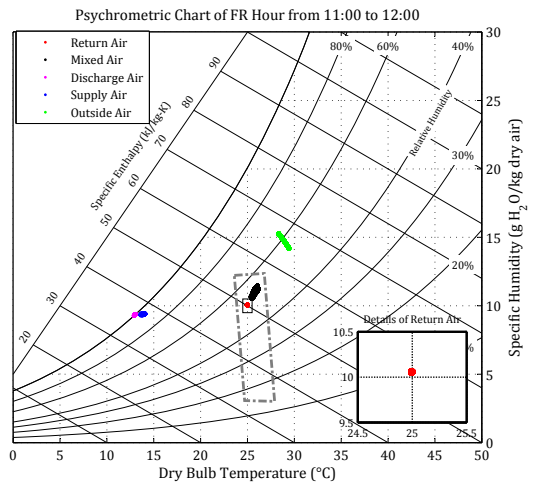
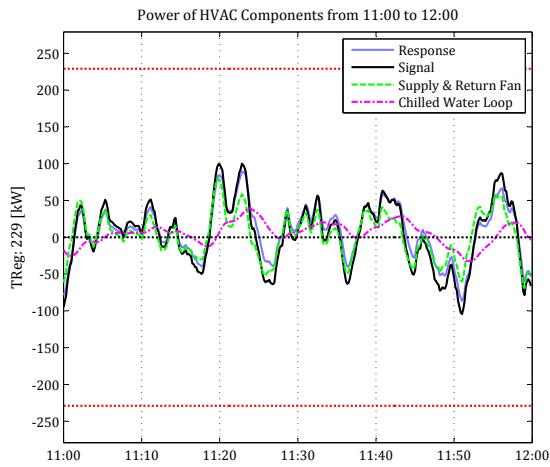
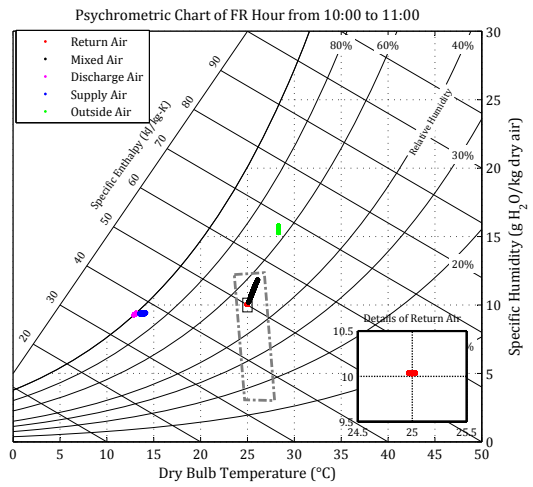
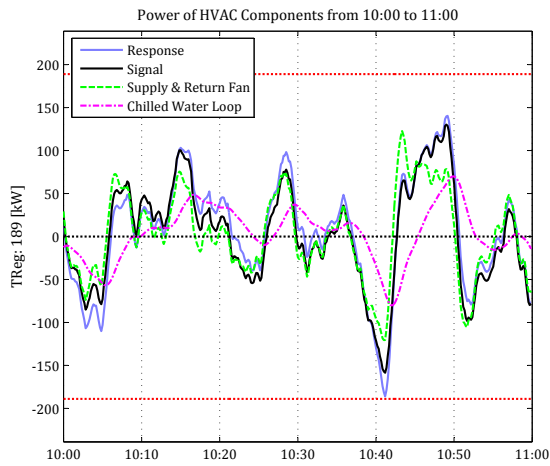


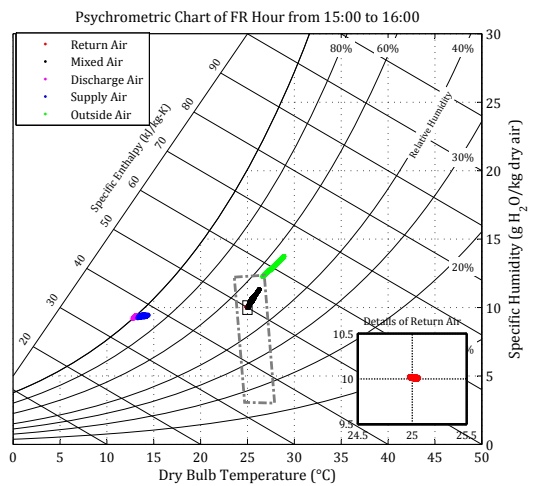
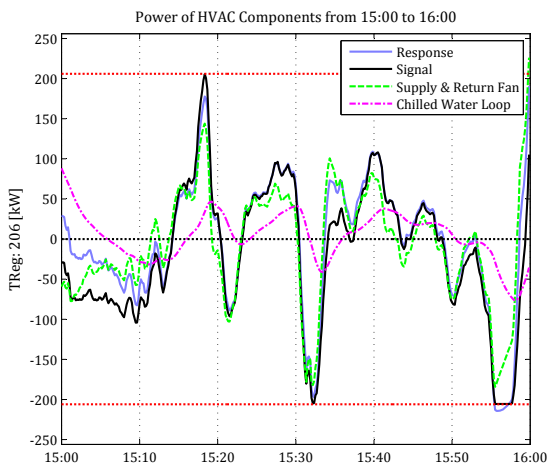
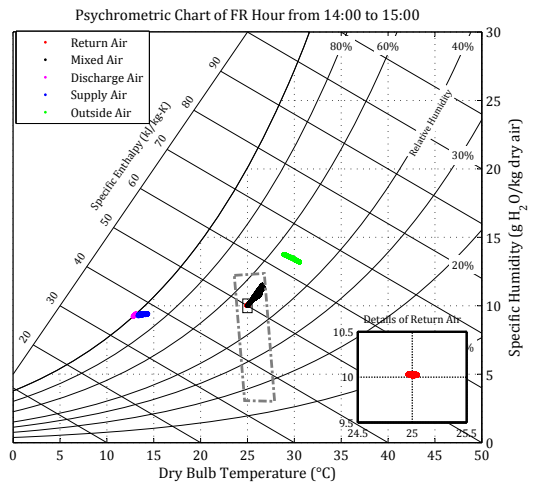
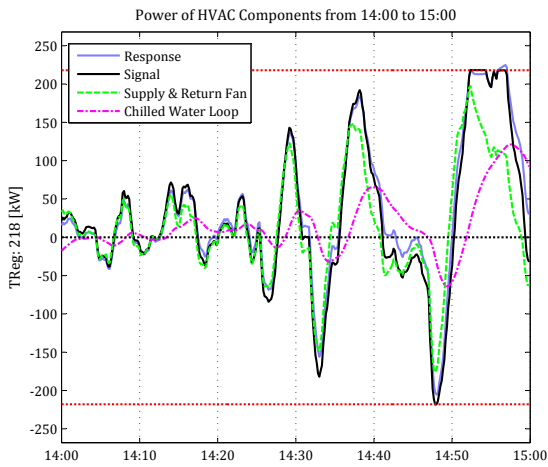
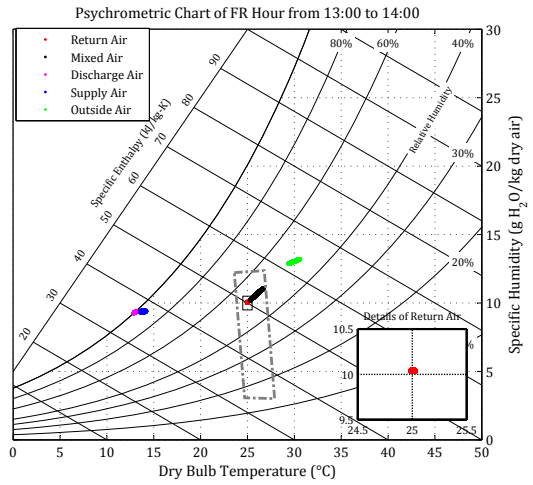
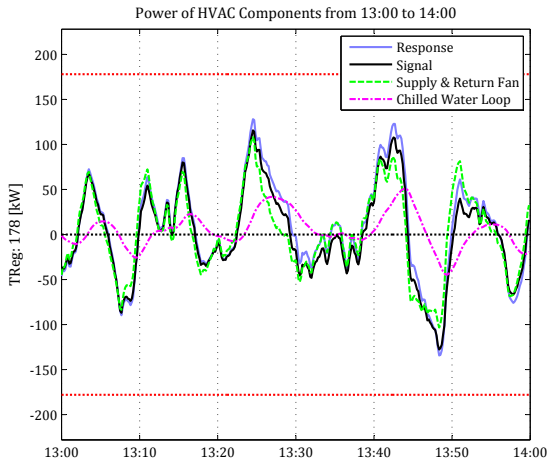


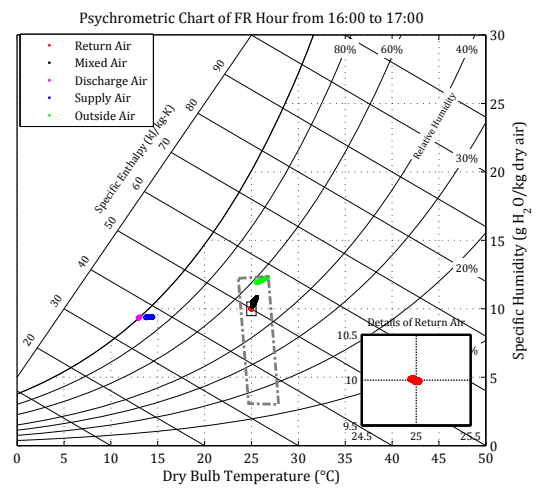
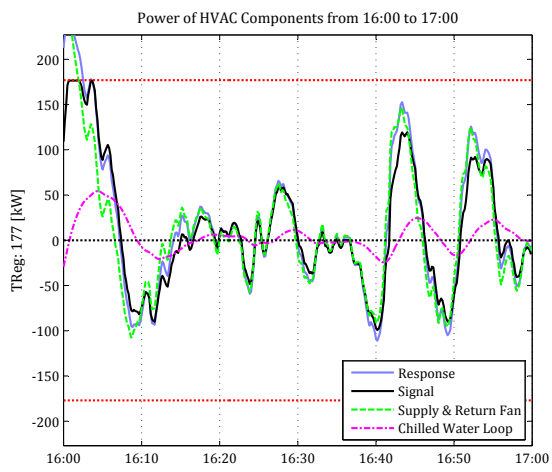
## Appendix G

### Results of Combined Injection: $P_{static}$ Setpoint and OAF



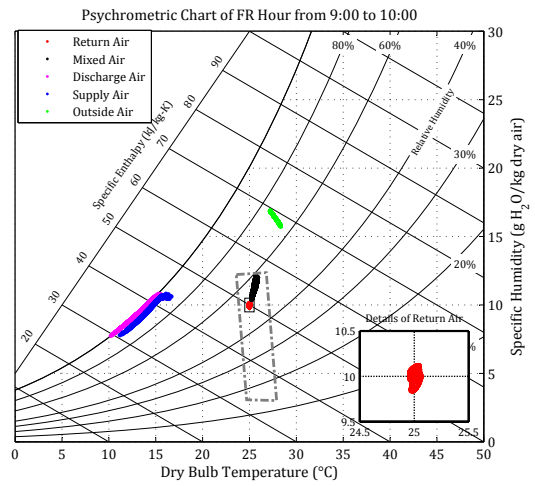
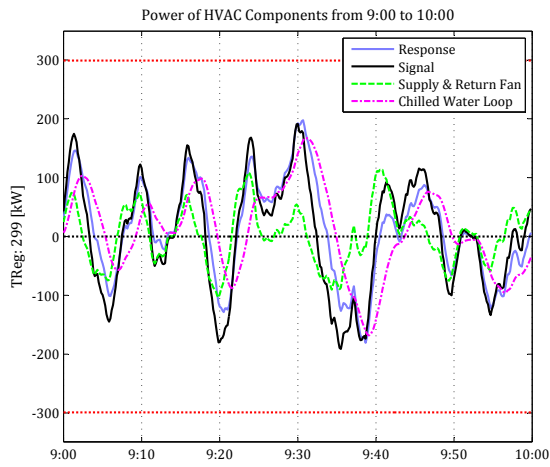


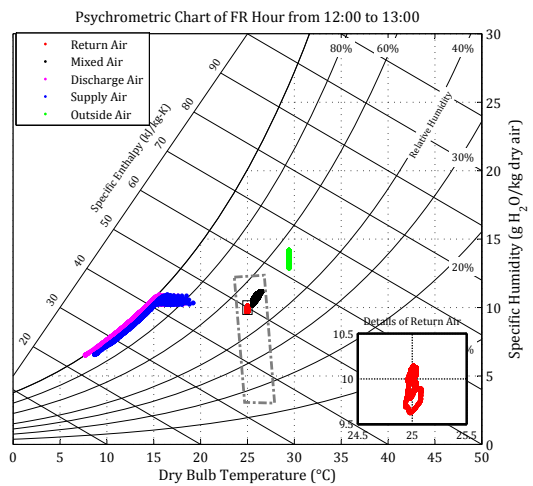
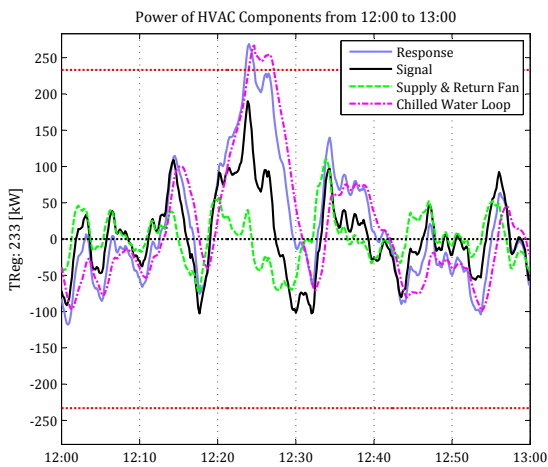
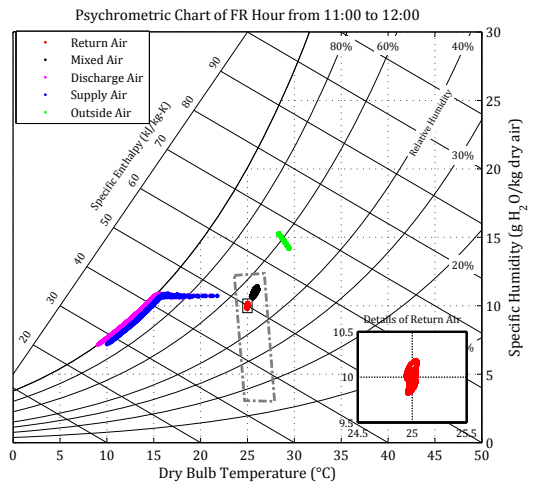
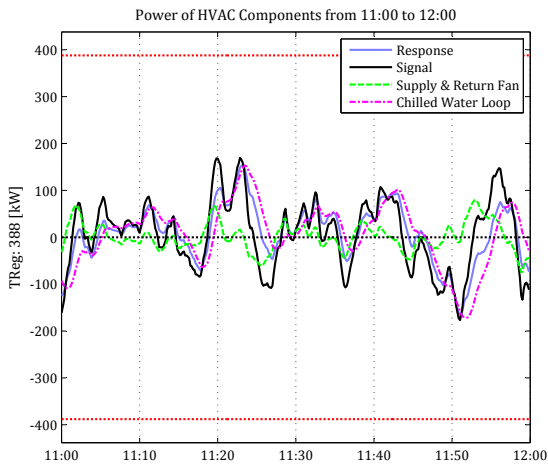
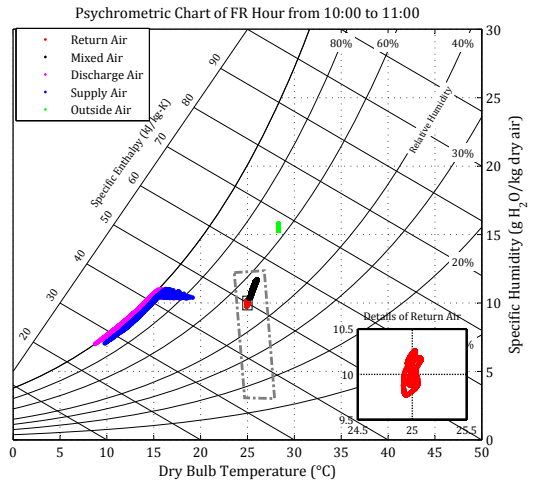
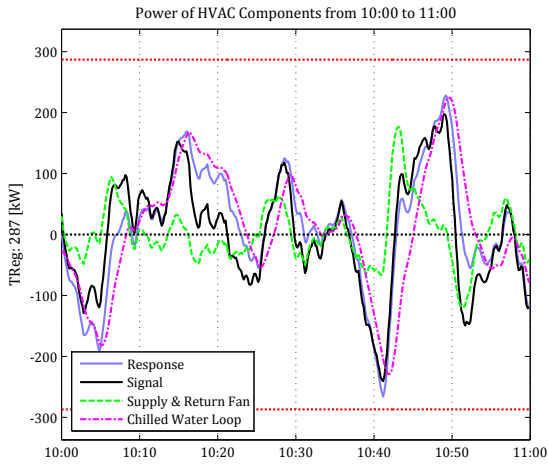


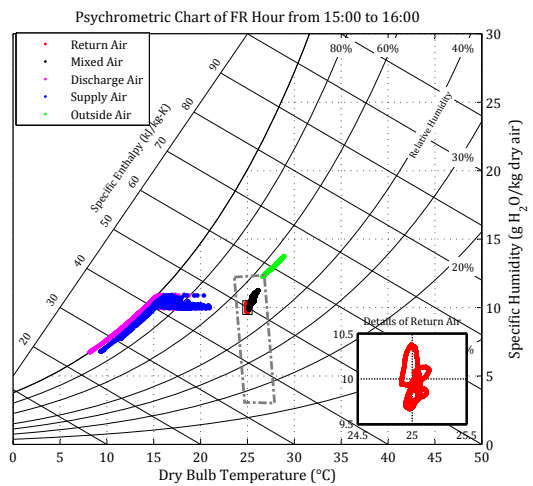
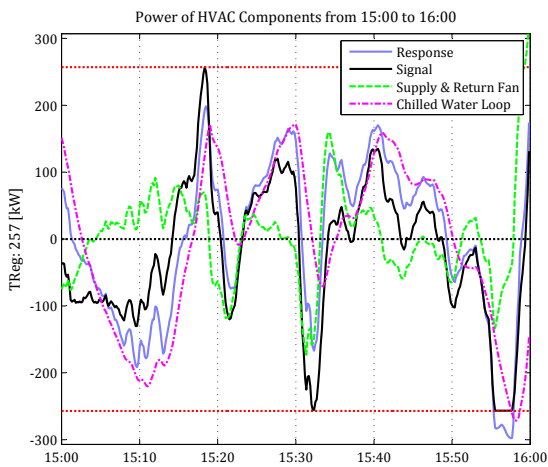
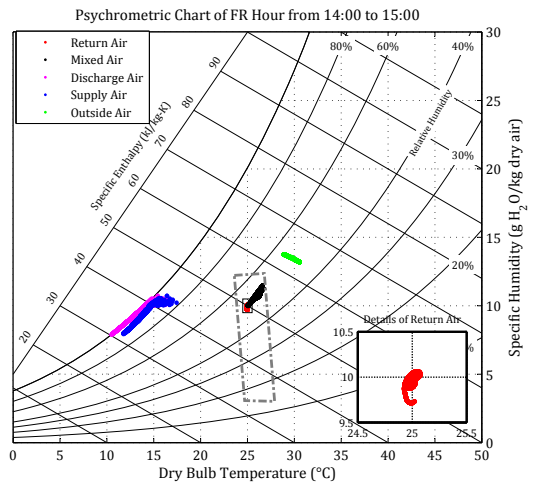
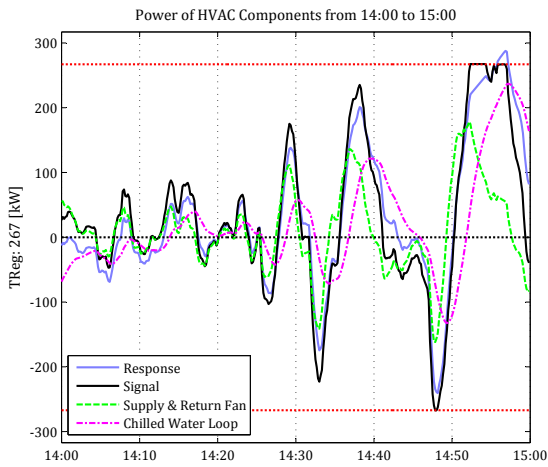
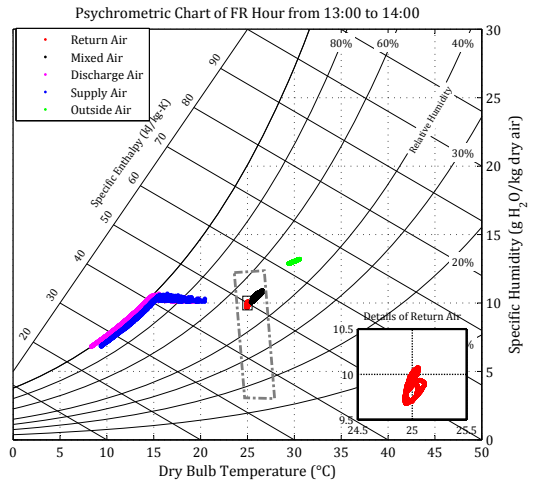
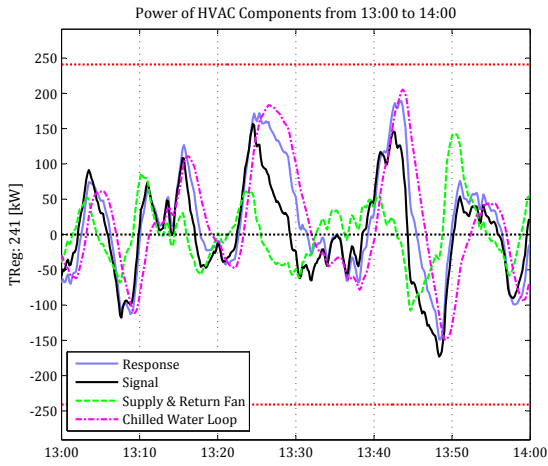


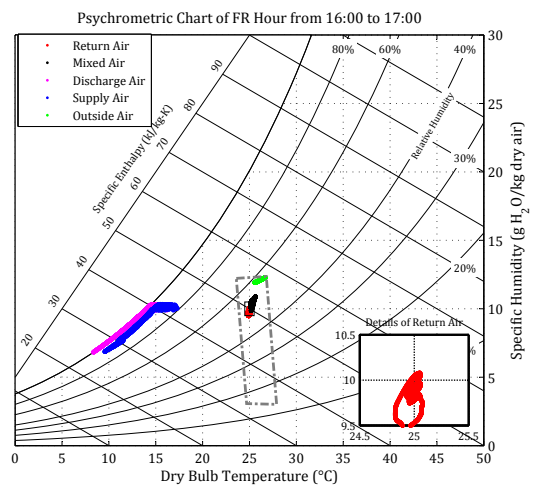
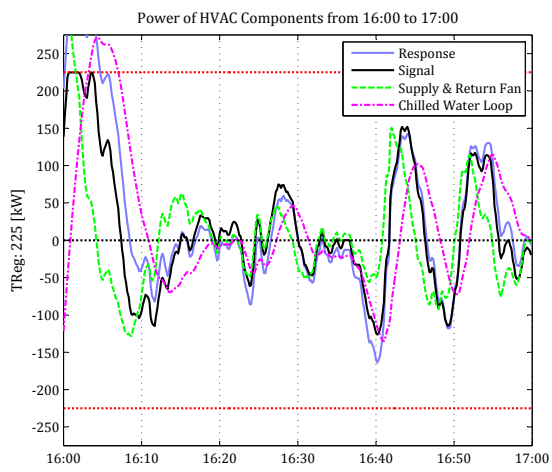
## Appendix H

### Results of Combined Injection: $P_{\text{static}}$ Setpoint, $T_{\text{DA}}$ Setpoint and OAF









# Appendix I

## Results of Combined Injection: All Four Methods Combined

